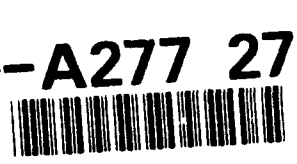

DEVELOPMENT OF AN ADVANCED CONTINUUM THEORY FOR COMPOSITE LAMINATES

Final Report

Volume II

December 1993

Prepared by:

Berkeley Applied Science and Engineering Inc.
5 Third St., Suite 530
San Francisco, CA 94103
Phone (415) 543-1600

REPORT DOCUMENTATION PAGE

Form Approved
OMB No. 0704-0188

1. AGENCY USE ONLY (Leave blank)	2. REPORT DATE	3. REPORT TYPE AND DATES COVERED
	93Dec31	Technical-91Jan01 through 93Dec31

4. TITLE AND SUBTITLE

Development of an Advanced Continuum Theory for Composite Laminates. Phase II Final Report.

5. FUNDING NUMBERS

F49620-91-C0043

6. AUTHOR(S)

M. Panahandeh
A. Masud
G.R. Ghanimati

7. PERFORMING ORGANIZATION NAME(S) AND ADDRESS(ES)

Berkeley Applied Science and Engineering, Inc.
5 Third Street, Suite 530
San Francisco, CA 94103-3206
Phone (415) 543-1600

8. PERFORMING ORGANIZATION REPORT NUMBER

AFOSR-TR- 0043

9. SPONSORING/MONITORING AGENCY NAME(S) AND ADDRESS(ES)

Air Force Office of Scientific Research
110 Duncan Ave., #B115
Bolling AFB, DC 20332-0001

10. SPONSORING/MONITORING AGENCY REPORT NUMBER

11. SUPPLEMENTARY NOTES

12a. DISTRIBUTION/AVAILABILITY STATEMENT

Unlimited

12b. DISTRIBUTION CODE

13. ABSTRACT *(Maximum 200 words)*

A continuum theory with a micro-macro structure was developed for composite laminates that satisfies the traction and displacement continuity requirements at interfaces. The interlaminar stresses were included in the model in a natural way and without any ad hoc assumptions. The built-in micro-structure of the continuum model can account for the effects of curvature and geometric nonlinearity. A set of constitutive relations in terms of material properties of individual constituents was developed which is capable of modeling fiber orientation and stacking sequence. The theory was further expanded to include the effects of temperature where a set of coupled thermo-mechanical field equations with corresponding constitutive relations were derived. Development of the theory for cylindrical and spherical geometries was completed and wave motions in flat and curved geometries was studied. A layerwise shear-deformable multi-director C^0 finite element formulation for the theory was developed which accounts for 3-D effects, allows thickness variation, and permits the warping of the deformed normal, while satisfying all continuity requirements.

14. SUBJECT TERMS	15. NUMBER OF PAGES
composite laminates, thick sections, micro-structure, interlaminar stress, thermo-mechanical, layerwise, multi-director, Finite Element	16. PRICE CODE

17. SECURITY CLASSIFICATION OF REPORT	18. SECURITY CLASSIFICATION OF THIS PAGE	19. SECURITY CLASSIFICATION OF ABSTRACT	20. LIMITATION OF ABSTRACT
UNCLASSIFIED	UNCLASSFIED	UNCLASSIFIED	UL(Unlimited)

BASE

DEVELOPMENT OF AN ADVANCED CONTINUUM THEORY FOR COMPOSITE LAMINATES

Final Report

Volume II

Prepared for:

AIR FORCE OFFICE OF SCIENTIFIC RESEARCH

Contract # F49620-91-C-0019

Prepared by:

M. Panahandeh
A. Masud
G. R. Ghanimati

Berkeley Applied Science and Engineering Inc.
5 Third St., Suite 530
San Francisco, CA 94103
Phone (415) 543-1600

December 1993

ACKNOWLEDEMENT

The present research was sponsored by the Air Force Office of Scientific Research (AFOSR) under contract No. F49620-91-C-0019. The financial support of AFOSR is gratefully acknowledged. The authors are indebted to Dr. Walter F. Jones, the program manager in AFOSR for his encouragement and interest in the work. The helpful discussions with Professor Robert L. Taylor of the University of California at Berkeley and Professor Juan C. Simo of Stanford University are gratefully acknowledged.

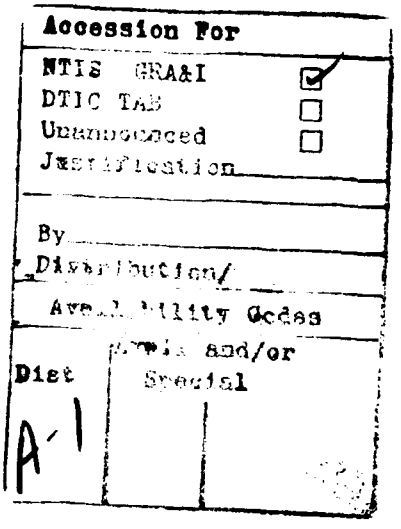

Table of Contents

VOLUME II

13.0 FINITE ELEMENT FORMULATION OF THE LAYER-WISE SHEAR DEFORMABLE COMPOSITE SHELL THEORY

13.1 Introduction

Present Composite Shell Technology and its Limitations

13.1.1 Classical lamination theories

Plate and Shell structures made of laminated composite materials are often modeled as an equivalent single layer using classical laminate theory (C.L.T.) in which the thickness stress components are ignored. The classical laminate theory is a direct extension of classical plate and shell theory in which the well known Kirchhoff-Love kinematic hypothesis is enforced. This theory is adequate when the thickness (relative to side or radius) is small so that the variation of the field variables through the thickness direction is minimal. However, laminated plates and shells made of advanced filamentry composite materials are succeptible to thickness effects because their effective transverse moduli are significantly smaller than the effective elastic modulus along the fiber direction. Furthermore, the classical theory of plates which assumes that the normals to the midplane before deformation remain straight and normal to the plane after deformation, underpredicts deflections and overpredicts natural frequencies and buckling loads. These discrepancies are due to the neglect of transverse shear strains. The errors in deflection, stresses, natural frequencies, and buckling loads are even higher for plates made of advanced composite. The range of applicability of the C.L.T. solution has been well established for laminated flat plates by Pagano [see Pagano 1989]. These analyses have indicated that a theory which accounts for the transverse shear deformation effects would be adequate to predict the gross behavior of the laminate.

13.1.2 Shear deformation theories

In order to overcome these deficiencies in C.L.T., refined laminate theories have been proposed. These are single layer theories in which the transverse shear stresses are taken into account. They provide improved global response estimates for deflections, vibration frequencies

and buckling loads of moderately thick composites when compared to the classical laminate theory. A Mindlin type first-order transverse shear deformation theory (S.D.T.) was first developed by Whitney and Pagano [1970] for multilayered anisotropic plates, and by Dong and Tso [1972] for multilayered anisotropic shells. Both of these approaches (C.L.T. and S.D.T.) considered all layers as one equivalent single anisotropic layer; thus these approaches are inadequate to model the warpage of cross-sections, that is, the distortion of the deformed normal due to transverse shear stresses. Furthermore, the assumption of nondeformable normal results in incompatible shearing stresses between every two adjacent layers. Also the latter approach requires the introduction of an arbitrary shear correction factor which is dependent on the lamination parameters for obtaining accurate results.

13.1.3 3-D Anisotropic elasticity

In another class of composite problems, i.e., for composite structures with a thick cross-section, two-dimensional plate analyses are inadequate because through-thickness stresses (interlaminar and normal stresses) are comparable in magnitude to the other stress components. Thus a *three-dimensional finite element analysis* is necessary in order to calculate the through-thickness stresses accurately. Since material properties vary from layer to layer due to the change of the ply orientation, finite element modeling for very thick composites throughout the thickness becomes extremely difficult and expensive. Traditional, three-dimensional finite element methods, based on one layer per element, are not computationally efficient for analysis.

New Directions in Composite Shell Technology

The exact analyses performed by Pagano [1989] on the composite flat plates have indicated that the distortion of the deformed normal is dependent not only on the laminate thickness, but also on the orientation and the degree of orthotropy of the individual layers. Therefore the hypothesis of nondeformable normals, while acceptable for isotropic plates and shells is often quite unacceptable for multilayered anisotropic plates and shells with very large ratio of Young's

modulus to shear modulus, even if they are relatively thin. Thus a transverse shear deformation theory which also accounts for the distortion of the deformed normal is required for accurate prediction of the behavior (deflections, thickness distribution of the in-plane displacements, natural frequencies, etc.) of multilayered anisotropic plates and shells.

In view of these issues a variationally sound theory that

- Accounts for the 3-D effects
- Allows thickness variation, and
- Permits the warping of the deformed normal

is required for refined and sophisticated analysis of thick and thin composites.

The approach proposed in this work utilizes a displacement field which fulfills a priori the static and geometric continuity conditions between contiguous layers. It is worth mentioning that the number of partial differential equations in the resulting system is independent of the number of plies. In addition, the order of the system is the same as in the first-order shear deformation theory. The chief advantage of the assumed displacement field rests on its capability to model the distortion of the deformed normal and to satisfy the contact conditions ab initio, without increasing the number and order of the partial differential equations with respect to the first-order transverse shear deformation theory. Furthermore, it is feasible to employ this formulation for constructing plate and shell finite elements via the finite element displacement method.

13.2 A C^0-continuous Theory for Composite Laminates

The Continuum Theory for Composite Laminates as presented in the previous chapters requires C^1-continuity of shape functions, just as does the classical Poisson-Kirchhoff Plate Theory and the classical Bernoulli-Euler Beam Theory.

From a mathematical viewpoint, if the stiffness integrands involve derivatives of order m, then the requirements for the convergence of the Finite Element Solution to the exact solution with the refinement of the mesh are

i) Shape functions should be smooth to order C^m on each element interior, Ω^e;

ii) Shape functions should be C^{m-1} continuous across each element boundary Γ^e.

iii) Shape functions should be complete.

Finite elements that satisfy these properties are called CONFORMING, or COMPATIBLE elements.

Continuous (i.e., C^0) finite element interpolations are easily constructed. The same cannot be said for multidimensional C^1-interpolations [Hughes, 87]. Furthermore, there has been an increasing trend in the literature to go towards elements based upon theories which accommodate transverse shear strains and require only C^0-continuity [Hughes, 87]. Although this approach is not without its own inherent difficulties, it opens the way to a greater variety of interpolatory schemes.

13.3 New Ideas Proposed in the Present Theory

In the following section we present a Finite Element Shear Deformable Theory for thick as well as thin composites. The proposed theory has a number of noteworthy attributes which directly address the technical drawbacks present in most of the theories that have been proposed for composite analysis to date.

- The displacement field proposed in this work is continuous in 3-D where as the rotation field is layer wise continuous (in 2-D) and can be discontinuous across the finite element layers through the thickness direction.
- The displacement field fulfills a priori the static and geometric continuity conditions between contiguous layers.
- The **novel idea** in the assumed displacement field lies in its *capability to model the distortion of the deformed normal*, without increasing the number and order of the partial differential equations with respect to the first-order transverse shear deformation theory.
- Another **new idea** in the theory is its *3-D feature*, thereby modeling the interlaminar conditions and predicting the 3-D edge effects more accurately.
- A salient feature of the proposed theory is that, *at most, only first derivatives of displacement and rotation fields appear in the variational equations*. The practical consequence of this fact is that only C^0 continuity of finite element functions is required which is readily satisfied by the family of Lagrange elements.
- The number of partial differential equations in the resulting system is *independent of the number of plies and their orientations in the composite*.
- Another advantage of the proposed composite shell theory lies in the *greater flexibility in the specification of the boundary conditions*.
- The theory covers a wide range in the sense that in one limit case when there is only one layer of proposed elements through the thickness, one recovers the features of the standard Shear Deformation Theories (S.D.T.). However the added advantage in the present case lies in the 3-D feature of the theory which controls the variation in the thickness via the Poisson terms rather than ad hoc mathematical tricks as done in the literature.
- In another limit case, one can model the composite with one element per ply through

the composite thickness, a procedure that is typically done while using the standard 3-D anisotropic elasticity elements. The added advantage of the proposed theory in this limit case is that because of the shear deformation capability of the proposed elements, they model the warping of the deformed normal more accurately, thereby improving the bending behavior.

- From a practical design point of view it provides the engineer the freedom to determine the precision in analysis. If a general response of the composite structure is required, the composite can be modeled with one element through the thickness. On the other hand, the designer can model the thickness with as many layers of the proposed element as deemed necessary to achieve the required accuracy.
- Furthermore, it is feasible to employ this formulation for constructing plate and shell finite elements via the *finite element displacement method.*

13.4 Main Assumptions of the Plate/Shell Theories

1. The domain Ω is of the following special form:

$$\Omega = \{(x,y,z) \in \mathbb{R}^3 \mid z \in [-\frac{t}{2}, \frac{t}{2}] \ , \ (x,y) \in A \subset \mathbb{R}^2\} \qquad (13.4.1)$$

where t is the plate or the shell thickness and A is the area of the reference surface.

2. $\sigma_{33} = 0$

$\Rightarrow$ plane stress hypothesis (see Hughes, 87, p. 311).

3. $U_\alpha(x,y,z) = -z\theta_\alpha(x,y)$

This assumption implies that plane sections remain plane. θ_α is interpreted as the rotation of a fiber initially normal to the plate reference surface.

4. $U_3(x,y,z) = W(x,y)$

This means that the transverse displacement w does not vary through the thickness.

13.5 Main Assumptions of the Layer-wise Shear Deformable Shell Theory

1. The domain Ω is of the following special form:

$$\Omega = \left\{ (x,y,z) \in \mathbb{R}^3 \mid z^{(l)} \in \left[\frac{-t}{2}, \frac{t}{2} \right]^{(l)} , \; T = \sum_l z^{(l)}, (x,y)^{(l)} \in A^{(l)} \subset \mathbb{R}^2 \right\} \qquad (13.5.1)$$

i.e., there are l layers of finite elements in the thickness direction, and $A^{(l)}$ is the area of the reference surface for that layer and T is the total thickness T of the composite shell.

2. The displacement field is assumed to take the following form

$$U_\alpha^{(l)}(x,y,z) = u_\alpha^{(l)}(x,y,z) - z^{(l)}\zeta\theta_\alpha^{(l)}(x,y) \qquad (13.5.2)$$

here $u_\alpha^{(l)}(x,y,z)$ are the displacements and $\theta_\alpha^{(l)}(x,y)$ are the fiber rotations for the l^{th} layer reference surface and $\zeta \in [0,1]$ is a parameter that establishes the position of a point from the reference surface in the thickness direction.

3. The displacement field in the thickness direction is assumed to be a function of z

$$U_3^{(l)} = u_3(x,y,z) \qquad (13.5.3)$$

By this assumption the transverse displacement, u_3 does vary through the thickness thereby producing through the thickness strains which result in thickness variation in the shell.

4. As a consequence of the above relaxation

$$\sigma_{33} \neq 0$$

i.e., we do not invoke the plane stress hypothesis.

5. We know from the elasticity theory that the displacements and stresses at the interface between l^{th} and $(l+1)^{th}$ bounded layers must satisfy the following contact conditions

$$U_\alpha^{(l)} = U_\alpha^{(l+1)} \tag{13.5.4a}$$

$$U_3^{(l)} = U_3^{(l+1)} \tag{13.5.4b}$$

In addition, continuity of stress tractions requires that the following stress conditions at the interface of layers be satisfied

$$\tau_{\alpha 3}^{(l)} = \tau_{\alpha 3}^{(l+1)} \tag{13.5.5a}$$

$$\tau_{33}^{(l)} = \tau_{33}^{(l+1)} \tag{13.5.5b}$$

A consequence of the second assumption above, (13.5.2), is that each finite element layer is associated with non-normal cross-sectional rotations which are assumed to be the same for all representative elements or plies in the finite element layer in accordance with the Mindlin kinematic assumption. Another consequence of the second assumption is that it results in independent shear deformation of the director in each layer and allows the warping of the composite cross-section. It also results in discontinuous strain fields across the different material sets, thereby creating the provision of stress continuity across the material interfaces. Consequently, the fifth assumption is inherently satisfied.

The proposed theory goes one step further than the present shear deformable theories for composite laminates in that the non-normal cross-sectional rotations may or may not be the same from one finite element layer to the other. This allows warping or deformation of the normal, thus producing a higher order displacement field through the thickness direction. Consider the interface between l^{th} and $(l+1)^{th}$ finite element layers and impose the continuity of the tangential

components of the displacement field via

$$U_\alpha^{(l)} = U_\alpha^{(l+1)}$$

therefore

$$u_\alpha^{(l)}(x,y,z) + z^{(l)}\zeta\theta_\alpha^{(l)}(x,y) = u_\alpha^{(l+1)}(x,y,z) + z^{(l+1)}\zeta\theta_\alpha^{(l+1)}(x,y) \tag{13.5.6}$$

for the interface between l and $(l+1)^{th}$ layer

$$\zeta = +1 \text{ for } l^{th} \text{ layer}$$

$$\zeta = 0 \text{ for } (l+1)^{th} \text{ layer}$$

Substituting in Eq. (13.5.6)

$$u_\alpha^{(l+1)}(x,y,z) - u_\alpha^{(l)}(x,y,z) = z^{(l)}\theta_\alpha^{(l)}(x,y)$$

$$\theta_\alpha^{(l)}(x,y) = \frac{1}{z^{(l)}}\left[u_\alpha^{(l+1)}(x,y,z) - u_\alpha^{(l)}(x,y,z)\right] \tag{13.5.7}$$

It implies that in a discrete sense

$$\theta_1^{(l)}(x,y) = u_{1,3}^{(l)}(x,y,z) \tag{13.5.8a}$$

$$\theta_2^{(l)}(x,y) = u_{2,3}^{(l)}(x,y,z) \tag{13.5.8b}$$

So when we substitute these in $\gamma_{\alpha 3}$ expressions we obtain the modified shear strain expression.

Furthermore, in examining $U_\alpha^{(l)}$ and $U_3^{(l)}$ in assumptions 2 and 3, it is easy to realize that the displacement field assumed is a continuous function of z coordinate for all values of $u^{(l)}(x,y,z)$ and $\theta^{(l)}(x,y)$. Consequently, the requirement of continuity of the displacement field is automatically satisfied.

13.6 Geometric Representation

13.6.1 Proposed Composite Shell Element

Figure 13.1 shows a typical configuration of a doubly curved composite shell. It can be made of numerous plies with variable material properties, reinforcement fiber orientations and ply thicknesses. For all practical purposes, these plies are stacked on top of each other in a certain predefined sequence. We call this sequence which repeats itself in the thickness direction as a "representative element." In our mathematical modeling of the mechanics of shell, no such assumption has been made which limits the number of individual plies, ply thicknesses, their orientation or their stacking sequence to join a representative element. At the same time, there is no limitation on the number of such representative elements in the thickness of the composite shell. Consequently the finite element model developed can be applied, with the same ease, both at the individual laminate level (i.e., the microstructure level) or the representative element level (i.e., the macrostructure level) or even to a congregate of representative elements.

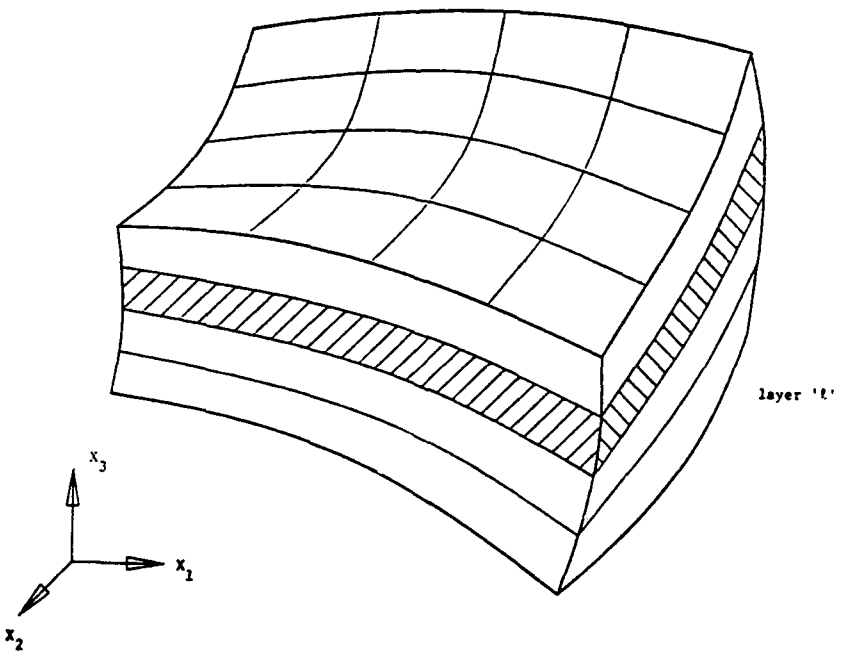

Fig. 13.1a

As shown in Fig. 13.1, the composite is discretized via four finite element layers through the thickness. As noted previously, each of these layers could be representing either the micro or the macro structure of the composite.

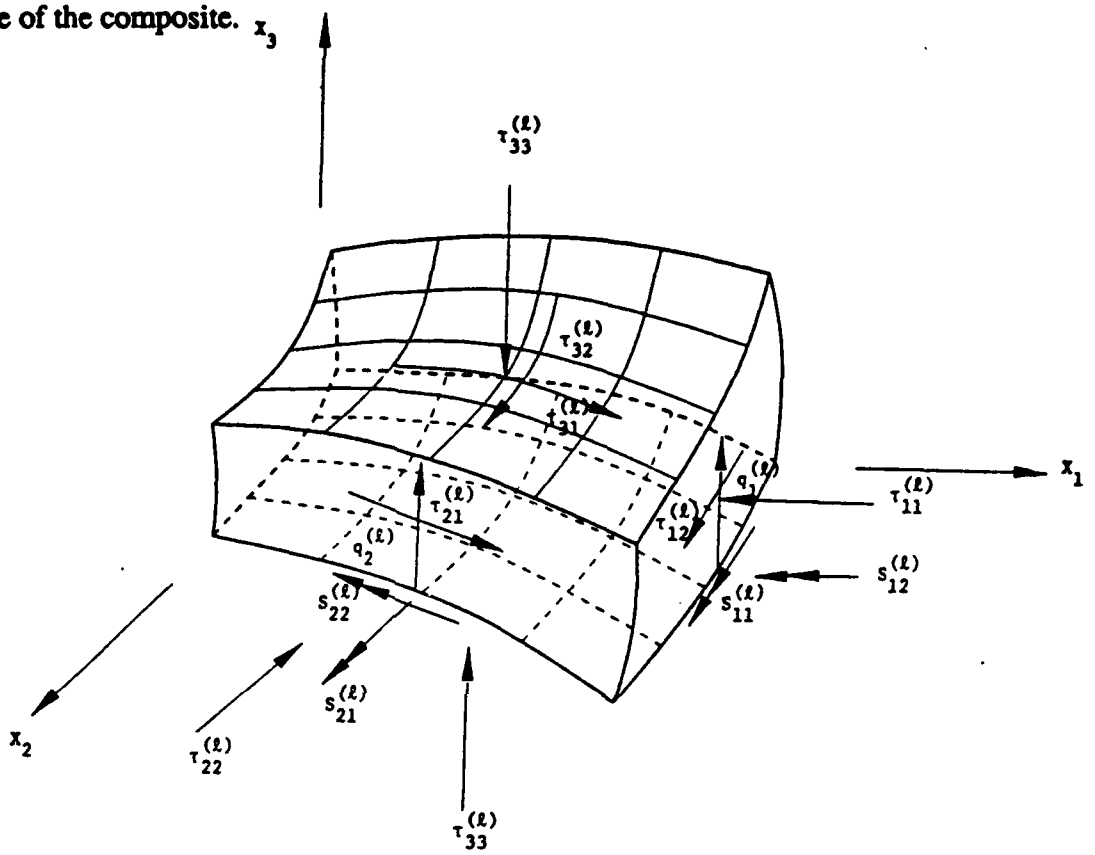

Fig. 13.1b
Stress representation on a typical finite element layer

Let us concentrate our attention to the case in which the composite is composed of four laminates, each being modeled via a finite element layer. A typical such layer is shown via the shaded region in Fig. 13.1a. The stresses and stress couples acting on this layer are shown in Fig. 13.1b. Figure 13.2 shows a schematic diagram of the geometry of the layer with the reference surface associated with the bottom surface of the layer. In our presentation, a typical composite shell element has its reference surface associated with its lower face as shown in Fig. 13.2.

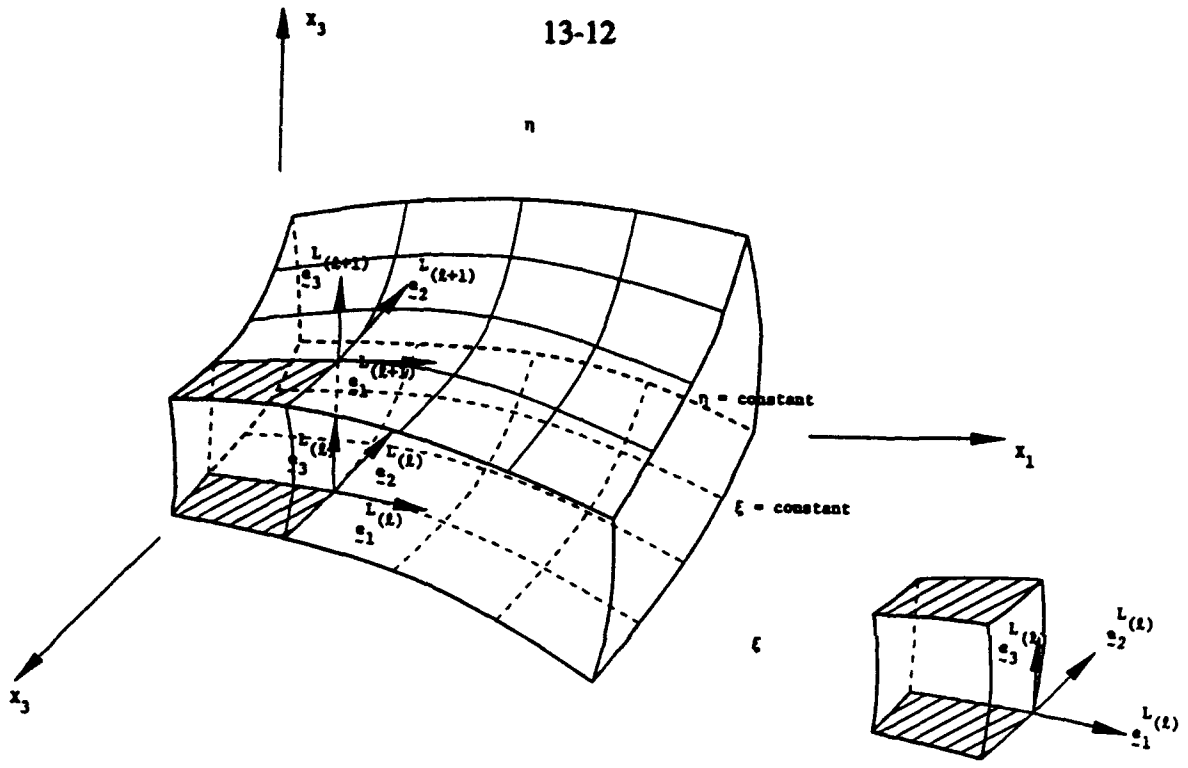

Fig. 13.2

A more detailed account of the nodal degrees of freedom and stresses and stress resultants at the finite element level is shown in Fig. 13.3.

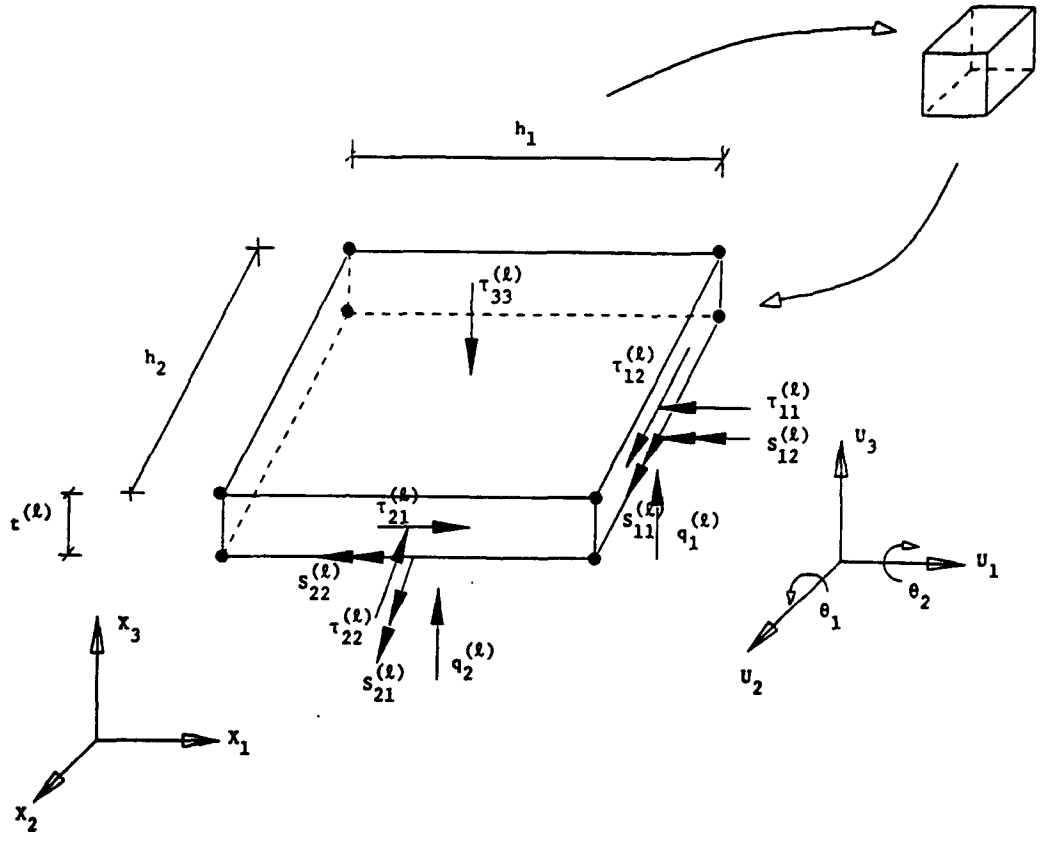

Fig. 13.3

13.6.2 Kinematics of the Deformation Through the Thickness

Figure 13.4 shows a thick composite laminate with "m" number of representative elements, each containing "n" different layers. In the "Layerwise Shear Deformable Finite Element Theory for Composite Shells" that we are presenting in this work, the total thickness T is divided into $\hat{L}$ finite elements through the thickness. Each layer of finite elements through the thickness is associated with a reference surface which is coincident with the lower surface of that layer. The total thickness is given by

$$t_1 + t_2 + \cdots + t_{\hat{L}} = T \tag{13.6.1}$$

and reference surface of 1st layer lies at

$$t = 0$$

Reference surface for the second layer of finite elements lies at

$$t = t_1$$

Similarly for the 3rd layer

$$t = (t_1 + t_2)$$

It is very important to note that the normal fiber rotation (i.e. θ_α) and the slope (i.e., $u_{3,\alpha}$) are not necessarily the same and thus transverse shear strains are accommodated. This is to be contrasted with the classical lamination theories (C.L.T.) in which $\theta_\alpha = w_{,\alpha}$ and consequently the transverse shear strains are zero.

Within each layer (of finite elements), the normal to the reference surface for that layer, rotates by θ_α^I, thereby generating shear strain $\gamma_{\alpha 3}$. Consequently, in the deformed configuration, node 2 (through the thickness, see fig. 13.4) moves to the location 2′.

Now, the normal to the undeformed reference surface in the second layer rotates by an angle θ_α^l, generating shear strain $\gamma_{\alpha 3}$. (Here $l = 2$, i.e., finite element layer #2). Because of the continuity of the displacement field in the thickness direction we obtain the new locations of finite element nodal points as 1′, 2′, 3′ and 4′, shown in the deformed configuration. It should be noted that this new location of points produces a higher order variation of strains through the thickness direction. This is a very important feature that precludes the need for introducing *ad hoc* polynomial expressions to model the higher order variation of displacement field through the thickness.

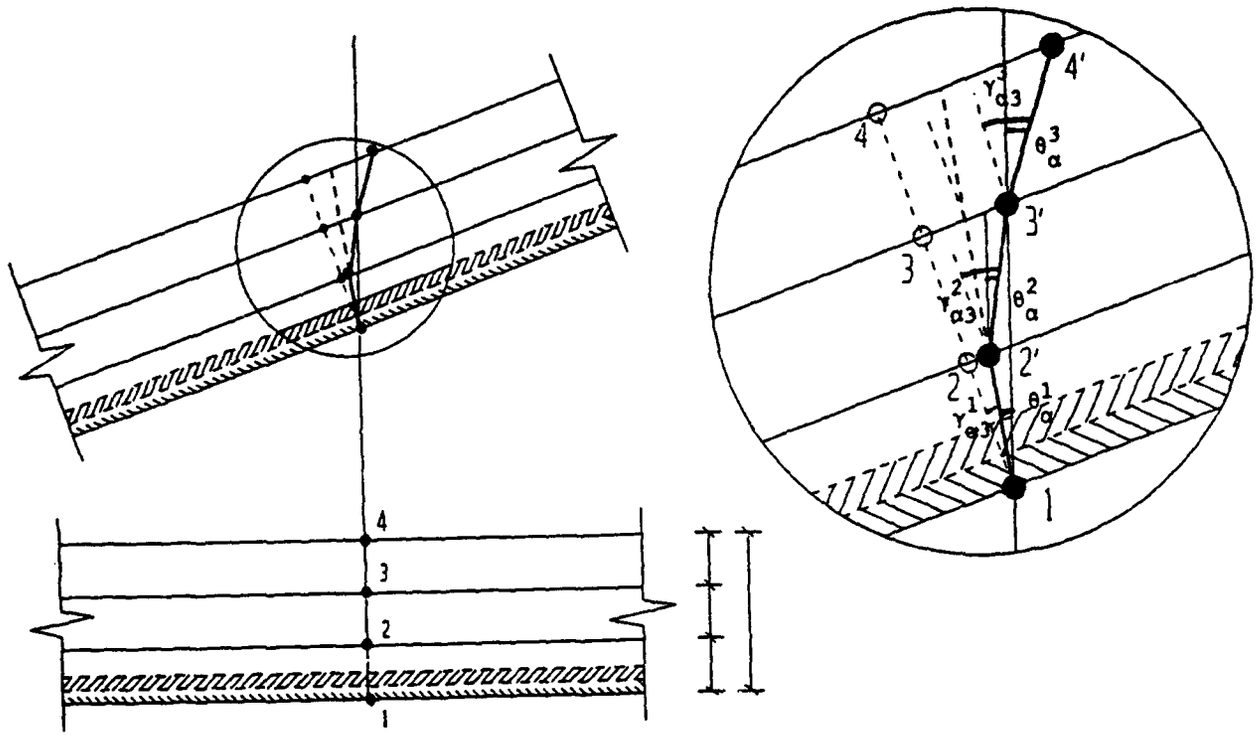

Fig. 13.4 Shell Kinematics. Variation of Transverse Shear Strains Through the Thickness

13.7 Finite Element Description of the Thick Composite Shell

13.7.1 Doubly curved composite shells in 3-D

The geometry of a typical quadrilateral shell element is defined by the following relations

$$\mathbf{x}^{(l)}(\xi,\eta,\zeta) = \bar{\mathbf{x}}^{(l)}(\xi,\eta) + \mathbf{X}^{(l)}(\xi,\eta,\zeta) \tag{13.7.1}$$

$$\bar{\mathbf{x}}^{(l)}(\xi,\eta) = \sum_{a=1}^{n_{en}} N_a(\xi,\eta)\bar{\mathbf{x}}_a^{(l)} \tag{13.7.2}$$

$$\mathbf{X}^{(l)}(\xi,\eta,\zeta) = \sum_{a=1}^{n_{en}} N_a(\xi,\eta)\mathbf{X}_a^{(l)}(\zeta) \tag{13.7.3}$$

$$\mathbf{X}_a^{(l)}(\zeta) = Z_a^{(l)}(\zeta)\hat{\mathbf{X}}_a^{(l)} \quad \text{(no sum)} \tag{13.7.4}$$

$$Z_a^{(l)}(\zeta) = N^+(\zeta)Z_a^{(l)+} + N^-(\zeta)Z_a^{(l)-} \tag{13.7.5}$$

$$N^+(\zeta) = \frac{1}{2}(1+\zeta) \tag{13.7.6a}$$

$$N^-(\zeta) = \frac{1}{2}(1-\zeta) \tag{13.7.6b}$$

where

$\mathbf{x}^{(l)}$: the position vector of a generic point of the shell for layer l.

$\bar{\mathbf{x}}^{(l)}$: the position vector of a point in the reference surface, for layer l.

$\mathbf{X}^{(l)}$: the position vector of a generic point relative to $\bar{\mathbf{x}}^{(l)}$ which defines the director through the point for layer l (in computational shell literature, $\mathbf{X}^{(l)}$ is referred to as fiber direction).

$\bar{\mathbf{x}}_a^{(l)}$: the position vector of nodal point "a" in layer l.

N_a: denotes a two-dimensional shape function associated with node "a".

n_{en}: the number of element nodes in the reference surface of layer l.

$\hat{X}_a^{(I)}$: a unit vector emanating from node "a" in the director direction.

Z_a: a "thickness function" associated with node "a", which is defined by the location of the reference surface.

The above relations represent a smooth mapping of the biunit cube into the physical shell domain. For "ζ" fixed, the surface defined by (13.7.1) is called a *lamina* and for "ξ,η" fixed, the line described by (13.7.1) is the director. The directors are, in general, not perpendicular to the laminae. Sometimes the director is referred to as the "pseudonormal."

For a particular choice of two-dimensional shape functions, eqs. (13.7.1)-(13.7.6) are precisely defined upon specification of $\bar{x}_a^{(I)}$, $\hat{X}_a^{(I)}$, $Z_a^{(I)+}$ and $Z_a^{(I)-}$ ($a = 1,2,...n_{en}$). It is convenient in practice to take as input the coordinates of the top and bottom surfaces of the shell along each nodal director ($x_a^{(I)+}$ and $x_a^{(I)-}$, respectively) and a parameter $\bar{\zeta} \in [-1,+1]$, which defines the location of the reference surface. *For example if* $\bar{\zeta} = -1,0,+1$ *(respectively), then the reference surface is taken to be the bottom, middle, top (respectively) of the shell.* From these data we may calculate

$$\bar{x}_a^{(I)} = \frac{1}{2}(1-\bar{\zeta})x_a^{(I)-} + \frac{1}{2}(1+\bar{\zeta})x_a^{(I)+} \tag{13.7.7}$$

$$\hat{X}_a^{(I)} = \frac{x_a^{(I)+} - x_a^{(I)-}}{\| x_a^{(I)+} - x_a^{(I)-} \|} \tag{13.7.8}$$

$$Z_a^{(I)+} = \frac{1}{2}(1-\bar{\zeta}) \| x_a^{(I)+} - x_a^{(I)-} \| \tag{13.7.9a}$$

$$Z_a^{(I)-} = -\frac{1}{2}(1+\bar{\zeta}) \| x_a^{(I)+} - x_a^{(I)-} \| \tag{13.7.9b}$$

where $\| \cdot \|$ denotes the Euclidean norm (i.e., $\| x \| = (x_1^2+x_2^2+x_3^2)^{1/2}$).

Lamina Coordinate Systems

At each integration point in the element a Cartesian reference frame is erected so that two axes are tangent to the lamina through the point. The frame is defined by its orthonormal basis vectors $\mathbf{e}_1^L, \mathbf{e}_2^L, \mathbf{e}_3^L$ in which $\mathbf{e}_3^L$ is perpendicular to the lamina. The basis vectors are calculated as follows

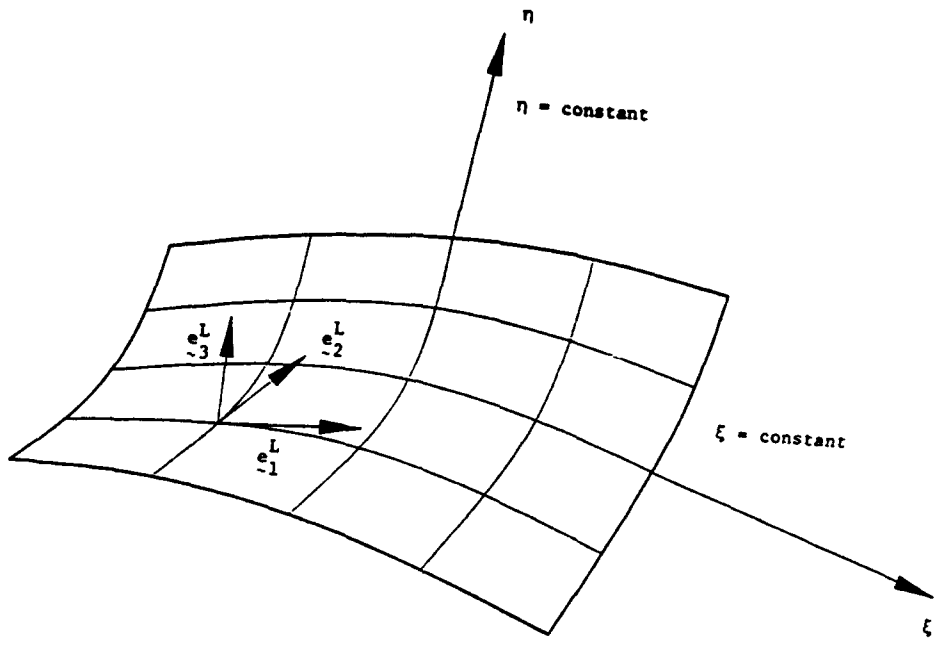

Fig. 13.5 Typical lamina coordinate system (ζ = constant surface)

Construct unit tangent vectors to the ξ– and η– coordinate directions:

$$\mathbf{e}_\xi^{(l)} = \frac{\mathbf{x}_{,\xi}^{(l)}}{\| \mathbf{x}_{,\xi}^{(l)} \|} \tag{13.7.10a}$$

$$\mathbf{e}_\eta^{(l)} = \frac{\mathbf{x}_{,\eta}^{(l)}}{\| \mathbf{x}_{,\eta}^{(l)} \|} \tag{13.7.10b}$$

Consequently

$$\mathbf{e}_3^L = \frac{\mathbf{e}_\xi^{(l)} \times \mathbf{e}_\eta^{(l)}}{\| \mathbf{e}_\xi^{(l)} \times \mathbf{e}_\eta^{(l)} \|} \tag{13.7.11}$$

The vectors tangent to the lamina are selected so that the angle between $\mathbf{e}_1^L$ and $\mathbf{e}_\xi^{(l)}$ is the same

as the angle between $\mathbf{e}_\eta^{(l)}$ and $\mathbf{e}_2^L$ and so that the $\mathbf{e}_1^L,\mathbf{e}_2^L$-basis is as "close" as possible to the $\mathbf{e}_\xi^{(l)},\mathbf{e}_\eta^{(l)}$ basis. Thus

$$\mathbf{e}_1^L = \frac{\sqrt{2}}{2}(\mathbf{e}_\alpha^{(l)} - \mathbf{e}_\beta^{(l)}) \tag{13.7.12a}$$

$$\mathbf{e}_2^L = \frac{\sqrt{2}}{2}(\mathbf{e}_\alpha^{(l)} + \mathbf{e}_\beta^{(l)}) \tag{13.7.12b}$$

where

$$\mathbf{e}_\alpha^{(l)} = \frac{\frac{1}{2}(\mathbf{e}_\xi^{(l)} + \mathbf{e}_\eta^{(l)})}{\| \frac{1}{2}(\mathbf{e}_\xi^{(l)} + \mathbf{e}_\eta^{(l)}) \|} \tag{13.7.13a}$$

$$\mathbf{e}_\beta^{(l)} = \frac{\mathbf{e}_3^L \times \mathbf{e}_\alpha^{(l)}}{\| \mathbf{e}_3^L \times \mathbf{e}_\alpha^{(l)} \|} \tag{13.7.13b}$$

Furthermore, we also define the orthogonal matrix to transform quantities from the global coordinate system to the lamina system

$$\mathbf{q} = [q_{ij}] = [\mathbf{e}_1^L\ \mathbf{e}_2^L\ \mathbf{e}_3^L]^T \tag{13.7.14}$$

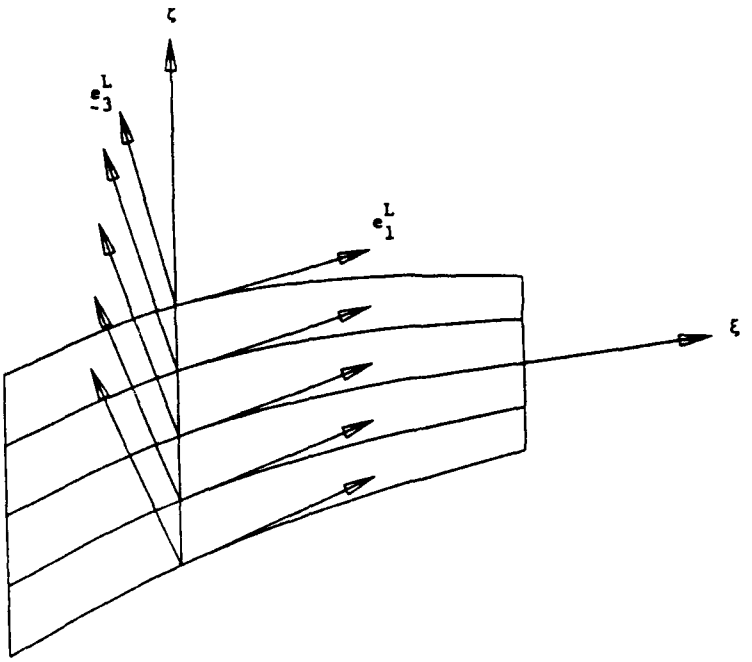

Fig. 13.6 η = constant surface

For the present case

$$\mathbf{e}_1^L = \mathbf{A}_1 \quad , \quad \mathbf{e}_2^L = \mathbf{A}_2 \quad , \quad \mathbf{e}_3^L = \mathbf{D} \tag{13.7.15}$$

When specialized to flat geometries these become

$$\mathbf{e}_1^L = \mathbf{A}_1 = \mathbf{E}_1 = \begin{Bmatrix} 1 \\ 0 \\ 0 \end{Bmatrix} \tag{13.7.16a}$$

$$\mathbf{e}_2^L = \mathbf{A}_2 = \mathbf{E}_2 = \begin{Bmatrix} 0 \\ 1 \\ 0 \end{Bmatrix} \tag{13.7.16b}$$

$$\mathbf{e}_3^L = \mathbf{D} = \mathbf{E}_3 = \begin{Bmatrix} 0 \\ 0 \\ 1 \end{Bmatrix} \tag{13.7.16c}$$

where $\mathbf{E}_1$, $\mathbf{E}_2$, $\mathbf{E}_3$ are unit vectors in the Cartesian frame.

Fiber Coordinate System

A unique coordinate system is erected at the nodes on the reference surface for each layer and is used as a reference frame for rotations. One of the directions of this frame is required to be coincident with the director direction. This one condition is not sufficient to define the frame. The following algorithm [Hughes 1987] can be employed to define this frame.

Let $\hat{\mathbf{X}}$ denote the unit basis vector in the director direction and $\mathbf{e}_1,\mathbf{e}_2,\mathbf{e}_3$ denote the global Cartesian basis, i.e.,

$$\mathbf{e}_1 = \begin{Bmatrix} 1 \\ 0 \\ 0 \end{Bmatrix} \ , \ \mathbf{e}_2 = \begin{Bmatrix} 0 \\ 1 \\ 0 \end{Bmatrix} \ , \ \mathbf{e}_3 = \begin{Bmatrix} 0 \\ 0 \\ 1 \end{Bmatrix} \ ,$$

The global Cartesian components of $\hat{\mathbf{X}}$ are denoted by $\hat{X}_i$, i = 1,2,3.

Algorithm

1. Let $a_i = |\hat{X}_i|$, i = 1,2,3.
2. j = 1
3. If $a_1 > a_3$, then $a_3 = a_1$, and j = 2.
4. If $a_2 > a_3$, j = 3.
5. $\mathbf{e}_3^f = \hat{\mathbf{X}}$
6. $\mathbf{e}_2^f = (\hat{\mathbf{X}} \times \mathbf{e}_j)/\|\hat{\mathbf{X}} \times \mathbf{e}_j\|$
7. $\mathbf{e}_1^f = \mathbf{e}_2^f \times \mathbf{X}$

The orthonormal fiber basis obtained (i.e., $\mathbf{e}_1^f,\mathbf{e}_2^f,\mathbf{e}_3^f$) satisfies the condition that if $\hat{\mathbf{X}}$ is close to $\mathbf{e}_3$, then $\mathbf{e}_1^f,\mathbf{e}_2^f,\mathbf{e}_3^f$ will be close to $\mathbf{e}_1,\mathbf{e}_2,\mathbf{e}_3$, respectively.

13.7.2 Kinematics in the context of Finite Element Method

The displacement of the shell is assumed to take the following form:

$$\mathbf{u}^{(l)}(\xi,\eta,\zeta) = \bar{\mathbf{u}}^{(l)}(\xi,\eta) + \mathbf{U}^{(l)}(\xi,\eta,\zeta) \tag{13.7.17}$$

$$\bar{\mathbf{u}}^{(l)}(\xi,\eta) = \sum_{a=1}^{n_{en}} N_a(\xi,\eta)\bar{\mathbf{u}}_a^{(l)} \tag{13.7.18}$$

$$\mathbf{U}^{(l)}(\xi,\eta,\zeta) = \sum_{a=1}^{n_{en}} N_a(\xi,\eta)\mathbf{U}_a^{(l)}(\zeta) \tag{13.7.19}$$

$$\mathbf{U}_a^{(l)}(\zeta) = Z_a^{(l)}(\zeta)\tilde{\mathbf{U}}_a^{(l)} \quad \text{(no sum)} \tag{13.7.20}$$

where

$\mathbf{u}^{(l)}$ is the displacement of a generic point in the shell layer *l*.

$\bar{\mathbf{u}}^{(l)}$ is the displacement of a point on the reference surface of the shell layer *l*.

$\mathbf{U}^{(l)}$ is the "director displacement" for the shell layer *l*.

$$\tilde{\mathbf{U}}_a^{(l)} = \hat{\mathbf{U}}_a^{(l)} + \bar{\mathbf{U}}_a^{(l)}$$

where

$$\bar{\mathbf{U}}_a^{(l)} = (\bar{u}_{ai} - u_{(a+n_{en})i})\mathbf{e}_{ai}^{(l)t}$$

The vector $\hat{\mathbf{U}}_a^{(l)}$ is constructed such that the director may rotate, viz.

$$\hat{\mathbf{U}}_a^{(l)} = \theta_{a2}^{(l)}\mathbf{e}_{a1}^{(l)f} - \theta_{a1}^{(l)}\mathbf{e}_{a2}^{(l)f}$$

The quantities $\theta_{a1}^{(l)}$ and $\theta_{a2}^{(l)}$ represent the rotations of the fiber about the base vectors $\mathbf{e}_{a1}^{(l)f}$ and $\mathbf{e}_{a2}^{(l)f}$, for shell layer *l*, respectively.

13.7.3 Appearance of 3D effects in the theory

Typical shell theories have shell description and parameterization done via a 2D reference surface and a director field which is orthogonal to this surface. Plane stress hypothesis is normally invoked. Based on the assumption that the thickness of the shell is small, some of these theories do not permit the thickness variation thereby making the thickness strains identically equal to zero. In other cases, [Simo and Fox 1988], the variation of the shell thickness is accounted for by associating a parameter with the director field and bounding it so that the thickness does not take unrealistic values. First allowing and then later controlling the thickness variation of shells is an important issue and it arises because of the introduction of engineering approximates to convert a 3D theory, representing 3D phenomenon, to a 2D theory and still expecting it to somehow manifest the effects in the third dimension.

In our description of the shell, there is a third dimension, i.e., through the thickness dimension which permits the development of strain field, and thereby modeling thick laminates in a more realistic way. Furthermore, we do not have to introduce auxiliary functions in the director field to control the shell thickness. In our theory, because of the Poisson effects in the third dimension, strains develop through the thickness and account for the thickness variation.

13.8 Derivation of C matrix for a representative element

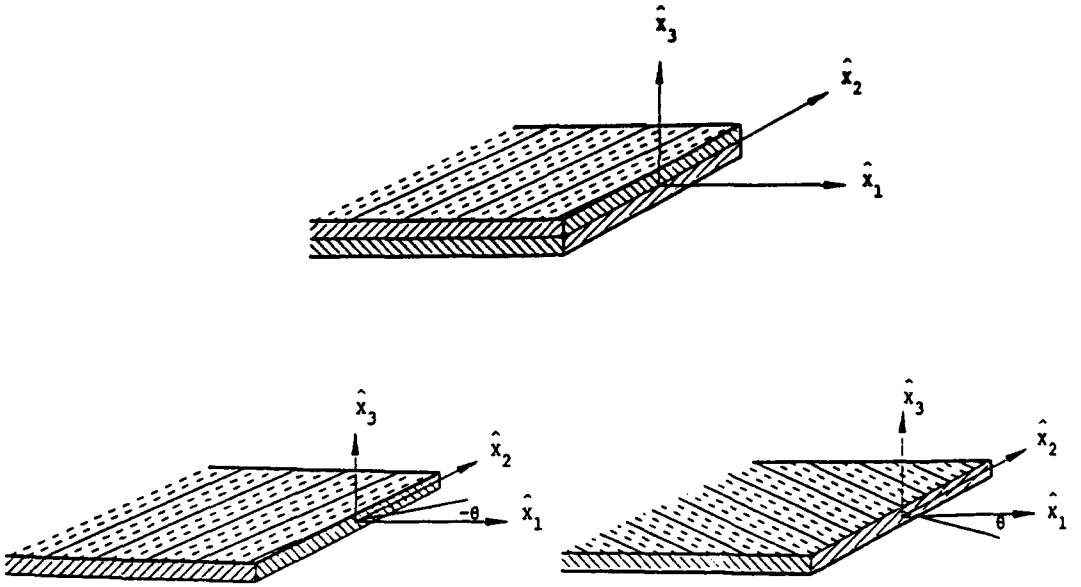

Fig. 13.7 Schematic diagram of a "representative element" and its constituent laminates

Suppose, the representative element is made of two laminates of the same material but with reinforcement fiber orientation at $+\theta$ and $-\theta$ degrees with respect to the extension direction.

Let $C_{(\alpha)}$ (α = 1,...number of plies in representative element) represent the C matrix (constitutive matrix) for the laminate with regard to its mutually perpendicular planes of elastic symmetry. In general it can be written as

$$C_{(\alpha)} = \begin{bmatrix} C_{11} & C_{12} & C_{13} & 0 & 0 & C_{16} \\ C_{12} & C_{22} & C_{23} & 0 & 0 & C_{26} \\ C_{13} & C_{23} & C_{33} & 0 & 0 & C_{36} \\ 0 & 0 & 0 & C_{44} & C_{45} & 0 \\ 0 & 0 & 0 & C_{54} & C_{55} & 0 \\ C_{16} & C_{26} & C_{36} & 0 & 0 & C_{66} \end{bmatrix} \tag{13.8.1}$$

where α represents the number of laminates in a representative element.

Let $\hat{X}_1$ represent the direction along the loading for the composite element and let $\hat{X}_3$ represent its thickness direction. This axis is assumed to be perpendicular to the plane of elastic symmetry. The $C(\alpha)$ for a laminate can be projected from its mutually perpendicular planes of elastic symmetry onto the composite coordinate system $(\hat{X}_1,\hat{X}_2,\hat{X}_3)$ about the $\hat{X}_3$ axis via the following transformation matrix.

$$Q_{(\alpha)} = \begin{bmatrix} C^2 & S^2 & 0 & 0 & 0 & CS \\ S^2 & C^2 & 0 & 0 & 0 & -CS \\ 0 & 0 & 1 & 0 & 0 & 0 \\ 0 & 0 & 0 & C & -S & 0 \\ 0 & 0 & 0 & S & C & 0 \\ -2CS & 2CS & 0 & 0 & 0 & (C^2-S^2) \end{bmatrix} \tag{13.8.2}$$

where $C = \cos\theta$, $S = \sin\theta$.

Then the transformed constitutive matrix is obtained as

$$C'_{(\alpha)} = Q^T_{(\alpha)} C_{(\alpha)} Q_{(\alpha)} \tag{13.8.3}$$

In general, $C'_{(\alpha)}$ will have the following form

$$C'_{(\alpha)} = \begin{bmatrix} C'_{11} & C'_{12} & C'_{13} & 0 & 0 & C'_{16} \\ C'_{12} & C'_{22} & C'_{23} & 0 & 0 & C'_{26} \\ C'_{13} & C'_{23} & C'_{33} & 0 & 0 & C'_{36} \\ 0 & 0 & 0 & C'_{44} & C'_{45} & 0 \\ 0 & 0 & 0 & C'_{45} & C'_{55} & 0 \\ C'_{16} & C'_{26} & C'_{36} & 0 & 0 & C'_{66} \end{bmatrix} \tag{13.8.4}$$

We evaluate the $C_{(rep.\ elem.)}$, i.e., the constitutive relation for the macro element via the expression

$$C_{(rep.\ elem.)} = mC'_{(1)} + (1-m)C'_{(2)} \tag{13.8.5}$$

where $m = \xi_1/\xi_2 < 1$.

Now $C_{(rep.\ elem.)}$ provides us an effective C matrix which repeats itself in the composite in its thickness direction. In other words it represents an effective material in which the effects of various fiber orientations and different material properties have been integrated in a consistent manner.

$$C_{(macro)} = \int_0^{\hat{X}_3^{(max)}} C_{(rep.\ elem.)} dx_3 \tag{13.8.6}$$

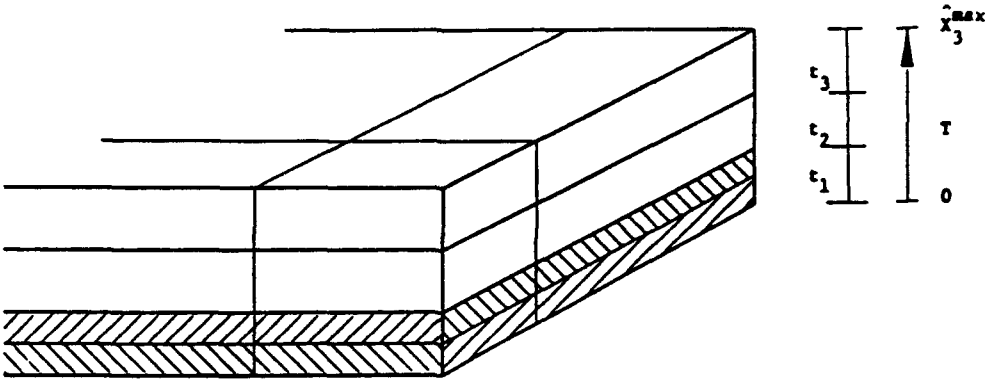

Fig. 13.8 Finite element mesh, through the thickness

Figure 13.8 shows a typical representative element, composed of "n" plies (in this figure, n = 2). There can be "m" such representative elements in the thickness direction.

Now that we have shown a consistent way of arriving at the macro level from the ply level, we are in a position where we can talk about its numerical implementation. There are a number of important factors which have to be considered and are summarized below. These technical issues make the present implementation different from a 3D continuum model and also from the standard 2D shell elements, whether they are based on the degenerated shell approach or the Cosserat surface approach.

From an implementational standpoint, this theory, in effect, combines the 2D shell effects with the 3D continuum effects. It is a well known fact that a shell can be analyzed as a congregate of 3D elements in which the in-plane dimensions of the finite elements are of the order of its thickness dimension. The drawback lies in the tremendous storage requirements and the CPU intensive calculations of the large systems of equations. A shell formulation allows the same engineering accuracy with considerably less elements, thereby making the computations cost effective and economic.

Following is a brief presentation of finite element formulation.

13.9 Finite Element Formulation

13.9.1 Strong Form of the Problem

To the general equilibrium equations we add the boundary conditions

$$u_\alpha = \hat{u}_\alpha \text{ on } \Gamma_u \tag{13.9.1a}$$

$$u_3 = \hat{u}_3 \text{ on } \Gamma_{u_3} \tag{13.9.1b}$$

$$\theta_\alpha = \hat{\theta}_\alpha \text{ on } \Gamma_\theta \tag{13.9.1c}$$

In addition

$$\tau^{\alpha\beta} n_\beta = \bar{\bar{\tau}}^\alpha \text{ on } \Gamma_\tau^\alpha \tag{13.9.1d}$$

$$q^\alpha n_\alpha = \bar{\bar{q}} \text{ on } \Gamma_q \tag{13.9.1e}$$

$$S^{\alpha\beta} n_\beta = \bar{\bar{S}}^\alpha \text{ on } \Gamma_s \tag{13.9.1f}$$

where $\Gamma_u \cup \Gamma_{u_3}$ corresponds to the boundary where displacement type boundary conditions are applied; $\Gamma_\tau^\alpha \cup \Gamma_q$ corresponds to the boundary where traction type conditions are applied; Γ_θ corresponds to the boundary with prescribed rotation; Γ_s corresponds to the portion of boundary with applied moments.

As usual

$$\mathbf{n} = n_\alpha \mathbf{E}_\alpha \equiv n_\alpha \mathbf{A}_\alpha \tag{13.9.2}$$

denotes the unit outward normal to the boundary $\partial\Omega$ of domain Ω.

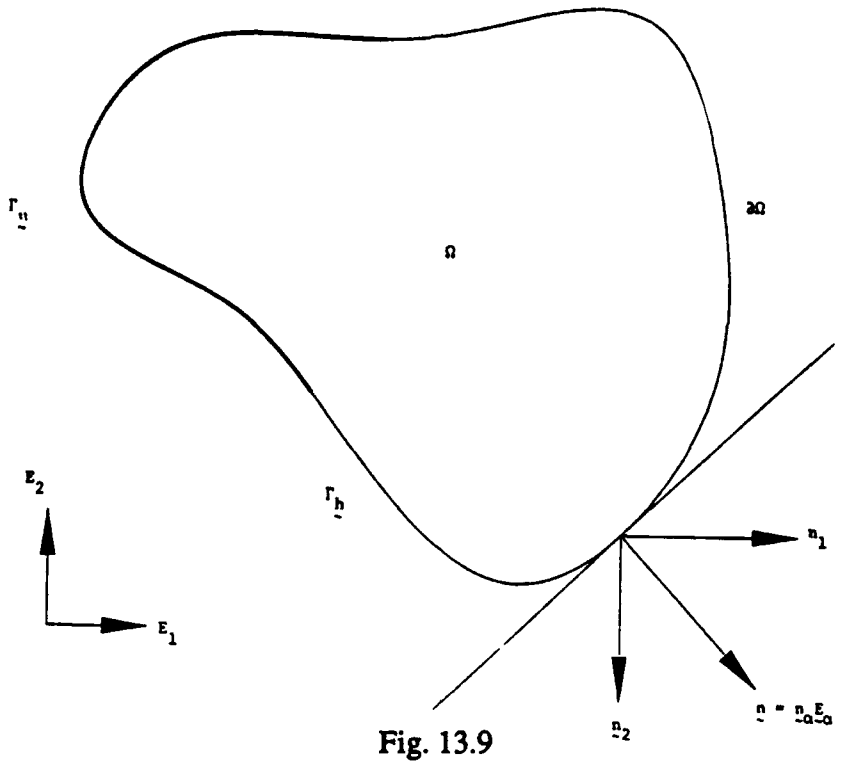

Fig. 13.9

13.9.2 The Weak Form of the Equations

Multiplying the strong form of the problem with the admissible variations, integrating by parts and using the prescribed essential and the natural boundary conditions we arrive at the weak form of the problem.

The spaces relevant to the problem are

$$S = \{(\mathbf{u},u_3,\theta) \mid (\mathbf{u},u_3,\theta) \in H^1(\Omega)\ ,\ (\mathbf{u},u_3,\theta) : S \to \mathbf{R}\times\mathbf{R}\times\mathbf{R}\ ,\ \text{s.t. } \mathbf{u} = \hat{\mathbf{u}} \text{ on } \Gamma_u\ ,$$

$$u_3 = \hat{u}_3 \text{ on } \Gamma_{u_3}\ ,\ \theta_\alpha = \hat{\theta}_\alpha \text{ on } \Gamma_\theta\} \tag{13.9.3}$$

where S is the space of trial displacements and trial rotations, respectively.

The associated space of weighting functions is

$$V = \{(\bar{\mathbf{u}},\bar{u}_3,\bar{\theta}) \mid (\bar{\mathbf{u}},\bar{u}_3,\bar{\theta}) \in H^1_0(\Omega)\ ,\ (\bar{\mathbf{u}},\bar{u}_3,\bar{\theta}) : S \to \mathbf{R}\times\mathbf{R}\times\mathbf{R}\ ,\ \text{s.t. } \bar{\mathbf{u}} = 0 \text{ on } \Gamma_u\ ,$$

$$\bar{u}_3 = 0 \text{ on } \Gamma_{u_3}\ ,\ \bar{\theta} = 0 \text{ on } \Gamma_\theta\} \tag{13.9.4}$$

where $H^1(\Omega)$ denotes the space of square-integrable functions along with their generalized derivatives defined over Ω, and $H_o^1(\Omega)$ is the subset of $H^1(\Omega)$ whose members satisfy zero essential boundary conditions.

13.9.3 Finite Element Nomenclature

Summary of Composite Laminate C^o-Theory Notation

$u^{(l)} = \langle u_1, u_2, u_3 \rangle^{(l)T}$	displacement vector
$\theta^{(l)} = \theta_\alpha^{(l)} = \langle \theta_1, \theta_2 \rangle^{(l)T}$	rotation vector
$\kappa_{\alpha\beta}^{(l)} = \delta_{(\alpha,\beta)}^{(l)} = \theta_{(\alpha,\beta)}^{(l)}$	curvature tensor
$\gamma_{3\alpha}^{(l)} = u_{3,\alpha}^{(l)} - \delta_\alpha^{(l)} = u_{3,\alpha}^{(l)} - \theta_\alpha^{(l)}$	shear strain vector
$S_{\alpha\beta}^{(l)} = \frac{1}{\hat{X}_3^m} \int_o^{\hat{X}_3^{max}} \tau_{\alpha\beta}^{(l)} \xi \, d\xi$	moment (stress couple) tensor
$q_\alpha^{(l)} = \int_o^{\hat{X}_3^{max}} \tau_{\alpha 3}^{(l)} d\xi$	shear force vector
$\hat{u}_\alpha$	prescribed boundary displacement
$\hat{\theta}_\alpha$	prescribed boundary rotations

The variational equation for the Composite Laminate Theory for Shells is derived from the variational equation of the three-dimensional theory by making use of the preceding relations.

Let $\Omega \subset R^{n_{sd}}$ be a bounded open set with piecewise smooth boundary Γ; $n_{sd} \geq 1$ denotes the number of spatial dimensions. Γ admits the following decomposition

$$\Gamma_g \cup \Gamma_h = \Gamma \qquad (13.9.5a)$$

$$\Gamma_g \cap \Gamma_h = \phi \tag{13.9.5b}$$

where Γ_g and Γ_h are the portions of the boundary with prescribed essential and natural boundary conditions, defined as

$$\Gamma_g = \Gamma_u \cup \Gamma_\theta \tag{13.9.6a}$$

$$\Gamma_h = \Gamma_\tau \cup \Gamma_q \cup \Gamma_s \tag{13.9.6b}$$

1. The domain Ω is of the following special form

$$\Omega = \{(x,y,z) \in \mathbb{R}^3 \mid z \in [0,\hat{X}_3^{max}] \, , (x,y) \in A \subset \mathbb{R}^2\} \tag{13.9.7}$$

2. The integrals appearing in the three dimensional variational equations are replaced by

$$\int_\Omega \cdots \, d\Omega = \int_A \int_0^{\hat{X}_3^{max}} \cdots \, dx_3 \, dA \tag{13.9.10}$$

$$\int_{\Gamma_h} \cdots \, d\Gamma = \int_A <\cdots> dA + \int_{\partial A} \int^{\hat{X}_3^{max}} \cdots \, dx_3 \, ds \tag{13.9.11}$$

where ds is measured along the perimeter of A.

13.9.4 Finite Element Stiffness Matrix and Load Vector

The finite element stiffness matrix and load vector may be obtained directly from the matrix form of the variational equation. The finite element approximations for $\mathbf{u},\bar{\mathbf{u}},\theta$ and $\bar{\theta}$ are denoted by $\mathbf{u}^h,\bar{\mathbf{u}}^h,\theta^h$ and $\bar{\theta}^h$, respectively.

In a typical element, possessing n_{en} nodes,

$$\mathbf{u}^h = \sum_{a=1}^{n_{en}} N_a \, \mathbf{u}_a^h \tag{13.9.12a}$$

$$\bar{\mathbf{u}}^h = \sum_{a=1}^{n_{en}} N_a \bar{\mathbf{u}}_a^h \tag{13.9.12b}$$

$$\boldsymbol{\theta}^h = \sum_{a=1}^{n_{en}} N_a \boldsymbol{\theta}_a^h \tag{13.9.13a}$$

$$\bar{\boldsymbol{\theta}}^h = \sum_{a=1}^{n_{en}} N_a \bar{\boldsymbol{\theta}}_a^h \tag{13.9.13b}$$

where N_a is the shape function associated with node "a", $\mathbf{u}_a^h$, $\bar{\mathbf{u}}_a^h$, $\boldsymbol{\theta}_a^h$, and $\bar{\boldsymbol{\theta}}_a^h$ are the a^{th} nodal values of $\mathbf{u}^h$, $\bar{\mathbf{u}}^h$, $\boldsymbol{\theta}^h$ and $\bar{\boldsymbol{\theta}}^h$, respectively. It is not necessary to assume that $\boldsymbol{\theta}^h$ and $\mathbf{u}^h$ be defined in terms of the same shape functions and nodal patterns. However, for the present implementation, this will be the case.

13.9.5 Nodal Degrees of Freedom

$$\mathbf{d}^e = \{d_p^e\} \tag{13.9.14a}$$

$$\bar{\mathbf{d}}^e = \{\bar{d}_p^e\} \tag{13.9.14b}$$

$$d_p^e = \begin{Bmatrix} u_{1a}^h \\ u_{2a}^h \\ u_{3a}^h \\ \theta_{1a}^h \\ \theta_{2a}^h \end{Bmatrix} \tag{13.9.14c}$$

$$\bar{d}_p^e = \begin{Bmatrix} \bar{u}_{1a}^h \\ \bar{u}_{2a}^h \\ \bar{u}_{3a}^h \\ \bar{\theta}_{1a}^h \\ \bar{\theta}_{2a}^h \end{Bmatrix} \tag{13.9.14d}$$

where p is the local equation number at the element level.

13.9.6 Matrix Expressions

Stress Vectors

The resultant stress vectors for an element which has the 3D-effects of an elasticity element and 2D effects of a shell like element are:

$$\hat{\tau} = \left\{ \begin{array}{c} \tau_{11}^{(l)} \\ \tau_{22}^{(l)} \\ \tau_{12}^{(l)} \end{array} \right\} \quad \text{inplane} \tag{13.9.15a}$$

$$\hat{q} = \left\{ \begin{array}{c} q_1^{(l)} \\ q_2^{(l)} \end{array} \right\} \quad \text{shear} \tag{13.9.15b}$$

$$\hat{\sigma} = \left\{ \begin{array}{c} \sigma_{11}^{(l)} \\ \sigma_{22}^{(l)} \\ \sigma_{12}^{(l)} \end{array} \right\} \quad \text{bending} \tag{13.9.15c}$$

$$\overset{v}{\tau} = \{\tau_{33}^{(l)}\} \quad \text{through-the-thickness} \tag{13.9.15d}$$

Strain Vectors

The strain vectors corresponding to the stress vectors are

$$\hat{\varepsilon} = \left\{ \begin{array}{c} \gamma_{11}^{(l)} \\ \gamma_{22}^{(l)} \\ 2\gamma_{12}^{(l)} \end{array} \right\} \quad \text{inplane} \tag{13.9.16a}$$

$$\hat{\delta} = \left\{ \begin{array}{c} \gamma_{13}^{(l)} \\ \gamma_{23}^{(l)} \end{array} \right\} \quad \text{shear} \tag{13.9.16b}$$

$$\hat{\kappa} = \left\{ \begin{array}{c} \kappa_{11}^{(l)} \\ \kappa_{22}^{(l)} \\ 2\kappa_{12}^{(l)} \end{array} \right\} \quad \text{bending} \tag{13.9.16c}$$

$$\overset{v}{\varepsilon} = \{\gamma_{33}^{(l)}\} \quad \text{through-the-thickness} \tag{13.9.16d}$$

We can combine the strain vector for inplane effects with the strain vector for through-the-thickness effects to yield a vector that incorporates 3D effects

$$\varepsilon = \begin{Bmatrix} \gamma_{11}^{(l)} \\ \gamma_{22}^{(l)} \\ \gamma_{33}^{(l)} \\ 2\gamma_{12}^{(l)} \end{Bmatrix} \tag{13.9.17}$$

13.9.7 Matrix Differential Operators

The strain vectors can be written in terms of differential operators as follows

$$\varepsilon = \begin{Bmatrix} \mathbf{A}_1^T \partial/\partial X^1 \\ \mathbf{A}_2^T \partial/\partial X^2 \\ \mathbf{D}^T \partial/\partial X^3 \\ \mathbf{A}_1^T \partial/\partial X^2 + \mathbf{A}_2^T \partial/\partial X^1 \end{Bmatrix} \mathbf{u} \tag{13.9.18}$$

For the case of flat geometry and linear analysis

$$\mathbf{A}_1 = \begin{Bmatrix} 1 \\ 0 \\ 0 \end{Bmatrix}, \quad \mathbf{A}_2 = \begin{Bmatrix} 0 \\ 1 \\ 0 \end{Bmatrix}, \quad \mathbf{D} = \begin{Bmatrix} 0 \\ 0 \\ 1 \end{Bmatrix},$$

The matrix differential form for the modified membrane effect then becomes

$$\mathbf{B}_m = \begin{Bmatrix} \partial/\partial X^1 \\ \partial/\partial X^2 \\ \partial/\partial X^3 \\ \partial/\partial X^2 + \partial/\partial X^1 \end{Bmatrix} \tag{13.9.19}$$

Similarly, for the shear operator

$$\overset{s}{\delta}_\alpha = \gamma_{\alpha 3} = \frac{1}{2}(u_{3,\alpha} - \delta_\alpha) = \frac{1}{2}(u_{3,\alpha} - \theta_\alpha)$$

Remark: Note the introduction of the rotation field in the above strain-displacement relation

$$\delta_\alpha = [D^T \partial/\partial X^\alpha \quad A_\alpha^T] \begin{Bmatrix} u \\ \theta \end{Bmatrix} \tag{13.9.20}$$

Therefore transverse shear strain vector δ is

$$\delta = [\tilde{B}_{sm} \quad B_{sb}] \begin{Bmatrix} u \\ \theta \end{Bmatrix}$$

where

$$\tilde{B}_{sm} = \begin{bmatrix} D^T \partial/\partial X^1 \\ D^T \partial/\partial X^2 \end{bmatrix} \; ; \; B_{sb} = \begin{bmatrix} A_1^T \\ A_2^T \end{bmatrix}$$

for flat geometries:

$$B_s = [\tilde{B}_{sm} \quad B_{sb}] = \begin{bmatrix} \partial/\partial X^1 & A_1^T \\ \partial/\partial X^2 & A_2^T \end{bmatrix} \tag{13.9.21}$$

Following the same lines, the bending strain vector $\hat{S}$ which comprises of the operators (13.9.16c) and bending membrane coupling, can be written in terms of matrix differential operators:

$$\hat{S} = [\tilde{B}_{bm} \quad B_{bb}] \begin{Bmatrix} u \\ \theta \end{Bmatrix}$$

where

$$\tilde{B}_{bm} = \begin{bmatrix} D_{,1}^T \partial/\partial X^1 \\ D_{,2}^T \partial/\partial X^2 \\ D_{,1}^T \partial/\partial X^2 + D_{,2}^T \partial/\partial X^1 \end{bmatrix} \; ; \; B_{bb} = \begin{bmatrix} A_1^T \partial/\partial X^1 \\ A_2^T \partial/\partial X^2 \\ A_1^T \partial/\partial X^2 + A_2^T \partial/\partial X^1 \end{bmatrix} \tag{13.9.22}$$

Specializing for flat geometries

$$\mathbf{D}_{,\alpha} = 0$$

$$\tilde{\mathbf{B}}_{bm} = [0] \ , \ \tilde{\mathbf{B}}_{bb} = \begin{bmatrix} \partial/\partial X^1 \\ \partial/\partial X^2 \\ \partial/\partial X^2 + \partial/\partial X^1 \end{bmatrix}$$

Finally, a total matrix differential operator $\tilde{\mathbf{B}}$ can be defined which produces the total strain vector $\tilde{\boldsymbol{\varepsilon}}$ when applied to the displacement field $\mathbf{u}$ and the rotation field $\boldsymbol{\theta}$:

$$\tilde{\boldsymbol{\varepsilon}} = \tilde{\mathbf{B}} \begin{Bmatrix} \mathbf{u} \\ \boldsymbol{\theta} \end{Bmatrix}$$

where

$$\tilde{\mathbf{B}} = \begin{bmatrix} \mathbf{B}_m & \mathbf{0} \\ \mathbf{B}_{sm} & \mathbf{B}_{sb} \\ \mathbf{B}_{bm} & \mathbf{B}_{bb} \end{bmatrix} \tag{13.9.23}$$

13.9.8 The Strain Displacement Matrices

We can write the matrix differential operators in terms of element shape functions as follows:

$$\mathbf{B}_{m_a} = \begin{bmatrix} N_{a,1} & 0 & 0 & 0 & 0 \\ 0 & N_{a,2} & 0 & 0 & 0 \\ 0 & 0 & N_{a,3} & 0 & 0 \\ N_{a,2} & N_{a,1} & 0 & 0 & 0 \end{bmatrix} \tag{1.3.9.24a}$$

$$\mathbf{B}_{s_a} = \begin{bmatrix} 0 & 0 & N_{a,1} & -N_a & 0 \\ 0 & 0 & N_{a,2} & 0 & -N_a \end{bmatrix} \tag{13.9.24b}$$

$$\mathbf{B}_{b_a} = \begin{bmatrix} 0 & 0 & 0 & N_{a,1} & 0 \\ 0 & 0 & 0 & 0 & N_{a,2} \\ 0 & 0 & 0 & N_{a,2} & N_{a,1} \end{bmatrix} \tag{13.9.24c}$$

where "a" stands for the node number.

$$\bar{B}_a = \begin{bmatrix} B_{m_a} \\ B_{s_a} \\ B_{b_a} \end{bmatrix} = \begin{bmatrix} B_{m_a} & 0 \\ B_{sm_a} & B_{sb_a} \\ B_{bm_a} & B_{bb_a} \end{bmatrix}$$

13.9.9 Stiffness Matrix

Using the finite element assembly operator, the stiffness matrix is obtained as

$$K = \sum_{l=1}^{L} \sum_{e=1}^{n_{el}} K^e \tag{13.9.25}$$

where L is the total number of finite element layers through the thickness and "n_{el}" is the total number of elements in each layer.

We can also write k as

$$K = A_{e=1}^{n_{el}} [k_{memb}^{e(l)} + k_{thick}^{e(l)} + k_{bending}^{e(l)} + k_{shear}^{e(l)}]$$

$$= A_{e=1}^{n_{el}} [\hat{k}_{memb}^{e(l)} + k_{bending}^{e(l)} + k_{shear}^{e(l)}] \tag{13.9.26}$$

where we have combined the inplane membrane effects with through the thickness effects to engender the modified $\hat{k}^e_{memb}$.

Let us consider each of the stiffness contributions one by one.

- **Modified membrane stiffness**

$$\underset{5_{nen} \times 5_{nen}}{\hat{k}_{memb}^{e(l)}} = [\hat{k}_{ab_{(memb)}}^{e(l)}]$$

where

$$\underset{5\times5}{\hat{\mathbf{k}}^{e(l)}_{ab_{(membr)}}} = \int_{\square} \int_{0}^{(\frac{\hat{X}_3^{max}}{L})} \underset{5\times4}{\mathbf{B}^{T}_{m_a}} \underset{4\times4}{\mathbf{C}^{(l)}_{m}} \underset{4\times5}{\mathbf{B}_{m_b}} j d\zeta d\square \qquad (13.9.27)$$

where $\mathbf{C}^{(l)}_{m}$ is the constitutive matrix for membrane effects for layer *l*, L denotes the total number of finite element layers and

$$\int_{\square} d\square = \int_{-1}^{+1}\int_{-1}^{+1} \cdots d\xi d\eta \quad \text{(lamina integral)}$$

j is the determinant of the Jacobian defined as

$$j = \det \begin{bmatrix} x_{1,\xi} & x_{1,\eta} & x_{1,\zeta} \\ x_{2,\xi} & x_{2,\eta} & x_{2,\zeta} \\ x_{3,\xi} & x_{3,\eta} & x_{3,\zeta} \end{bmatrix}$$

We can write the above equation as

$$\hat{\mathbf{k}}^{e(l)}_{ab} = \sum_{i=1}^{n_{int_{(m)}}} \mathbf{B}^{T}_{m_a} \mathbf{C}^{(l)}_{m} \mathbf{B}_{m_b} j w^{(i)} \qquad (13.9.28)$$

where $n_{int_{(m)}}$ is the integration rule required to exactly evaluate the membrane effects. In this equation we have replaced the integral sign with summation over all the integration points and have also multiplied by the corresponding weight $w^{(i)}$. Since it is a volume integral, so the loop over the nodes covers all the nodal points in the element. Furthermore we need a $2 \times 2 \times 2$ integration rule to evaluate all the monomials in the integral exactly. [Note: $2 \times 2 \times 2$ rule is for an 8-node brick element.] We need to use the appropriate rule for higher order elements.

- **Bending Stiffness**

$$\mathbf{k}_{\text{bend}}^{e(l)} = [\mathbf{k}_{\hat{a}\hat{b}_{(\text{bend})}}^{e(l)}]$$

$$\mathbf{k}_{\hat{a}\hat{b}_{(\text{bend})}}^{e(l)} = \int_{\square} \mathbf{B}_{b_{\hat{a}}}^{T} \mathbf{C}_{b}^{(l)} \mathbf{B}_{b_{\hat{b}}} \tilde{j} \, d\square$$

where $\mathbf{C}_b^{(l)}$ is the constitutive matrix for the bending effects for layer l, and $\tilde{j}$ is the determinant of the 2D reference surface Jacobian defined as

$$\tilde{j} = \det \begin{bmatrix} x_{1,\xi} & x_{1,\eta} \\ x_{2,\xi} & x_{2,\eta} \end{bmatrix}$$

$$\mathbf{k}_{\text{bend}}^{e(l)} = \sum_{i=1}^{n_{\text{int}_b}} \mathbf{B}_{b_{\hat{a}}}^{T} \mathbf{C}_{b}^{(l)} \mathbf{B}_{b_{\hat{b}}} w^{(i)} \tilde{j}$$

The nomenclature used in the proceeding expressions is defined as below.

$\hat{a},\hat{b}$: finite element nodes associated with the reference surface ($1 <= \hat{a}, \hat{b} \le \hat{n}_{en}$).

$n_{int_{(b)}}$: integration rule required to exactly integrate the bending contribution.

$\mathbf{B}_b$: strain displacement matrix associated with bending.

$\hat{n}_{en}$: number of nodes associated with the reference surface.

- **Shear Stiffness**

$$\mathbf{k}_{\text{shear}}^{e(l)} = [\mathbf{k}_{\hat{a}\hat{b}_{(\text{shear})}}^{e(l)}]$$

$$\mathbf{k}_{\hat{a}\hat{b}_{(\text{shear})}}^{e(l)} = \int_{\square} \mathbf{B}_{s_{\hat{a}}}^{T} \mathbf{C}_{s}^{(l)} \mathbf{B}_{s_{\hat{b}}} \tilde{j} \, d\square$$

where $\mathbf{C}_s^{(l)}$ is the constitutive matrix for the shear effects for layer l. Consequently

$$\mathbf{k}_{\text{shear}}^{e(l)} = \sum_{i=1}^{n_{\text{int}_s}} \mathbf{B}_{s_{\hat{a}}} \mathbf{C}^{(l)} \mathbf{B}_{s_{\hat{b}}} \tilde{j} \, w^{(i)} \qquad (13.9.30)$$

13.9.10 Evaluation of Stresses

Let us consider each "layer of finite elements" through the thickness direction. Let $C_b^{(l)}$ and $C_s^{(l)}$ represent the inverse of the in-plane and out-of-plane parts of the compliance matrices for the layers l. As noted previously, we are proposing a "layerwise shear deformable finite element theory for thick composites." Consequently, the bending contribution and the shear contribution to the stiffness matrix are obtained by summing over the corresponding contributions for the individual finite element layers. For each layer l, $C_b^{(l)}$ and $C_s^{(l)}$ are defined as follows:

$$\hat{\sigma}^{(l)}_{\text{bending}} = \begin{Bmatrix} \sigma^{(l)}_{11_{\text{bending}}} \\ \sigma^{(l)}_{22_{\text{bending}}} \\ 2\sigma^{(l)}_{12_{\text{bending}}} \end{Bmatrix} = C_b^{(l)} \begin{Bmatrix} \kappa^{(l)}_{11} \\ \kappa^{(l)}_{22} \\ 2\kappa^{(l)}_{12} \end{Bmatrix} \tag{13.9.31}$$

$$C_b^{(l)} = \begin{bmatrix} C_{11} & C_{12} & C_{16} \\ C_{12} & C_{22} & C_{26} \\ C_{16} & C_{26} & C_{66} \end{bmatrix}^{(l)}$$

Combining the in-plane membrane effect with the through-the-thickness effects in the element

$$\sigma^{\text{mod}(l)}_{\text{memb}} = \begin{Bmatrix} \sigma^{(l)}_{11_{\text{memb}}} \\ \sigma^{(l)}_{22_{\text{memb}}} \\ \sigma^{(l)}_{33(\text{th})} \\ 2\sigma^{(l)}_{12_{\text{memb}}} \end{Bmatrix} = C_m^{(l)} \begin{Bmatrix} u_{1,1} \\ u_{2,2} \\ u_{3,3} \\ u_{1,2}+u_{2,1} \end{Bmatrix} \tag{13.9.32}$$

where $\sigma^{\text{mod}(l)}_{\text{memb}}$ is the modified membrane stress for finite element layer l, and $C_m^{(l)}$ is defined as

$$C_m^{(l)} = \begin{bmatrix} C_{11} & C_{12} & C_{13} & C_{16} \\ C_{12} & C_{22} & C_{23} & C_{26} \\ C_{13} & C_{23} & C_{33} & C_{36} \\ C_{16} & C_{26} & C_{36} & C_{66} \end{bmatrix}^{(l)}$$

Similarly

$$\hat{\sigma}^{(l)}_{shear} = \begin{Bmatrix} \sigma^{(l)}_{13_{shear}} \\ \sigma^{(l)}_{23_{shear}} \end{Bmatrix} = C^{(l)}_s \begin{Bmatrix} \gamma^{(l)}_{13} \\ \gamma^{(l)}_{23} \end{Bmatrix} \tag{13.9.33}$$

$$C^{(l)}_s = \begin{bmatrix} C_{44} & C_{45} \\ C_{45} & C_{55} \end{bmatrix}^{(l)}$$

13.9.11 External Force Vector

Body Force: The element body force vector is given as

$$\underset{5n_{en}\times 1}{\mathbf{f}^{body}} = \{\mathbf{f}^{body}_a\}$$

$$\underset{5\times 1}{\mathbf{f}^{body}_a} = \int_{\square} \int_{0}^{\hat{X}_3^{max}} \mathbf{N}_a^T \mathbf{f}\, j\, d\zeta d\square \tag{13.9.34}$$

where

$$\mathbf{N}_a = \begin{bmatrix} N_a & 0 & 0 & -N_a Z_a e^f_{a_{12}} & N_a Z_a e^f_{a_{11}} \\ 0 & N_a & 0 & -N_a Z_a e^f_{a_{22}} & N_a Z_a e^f_{a_{21}} \\ 0 & 0 & N_a & -N_a Z_a e^f_{a_{32}} & N_a Z_a e^f_{a_{31}} \end{bmatrix}$$

Surface Force: The element surface force vector is defined by

$$\mathbf{f}^{surf} = \{\mathbf{f}^{surf}_a\}$$

$$\mathbf{f}^{surf}_a = \int_{\square} \mathbf{N}_a^T \mathbf{h}\, j_s\, \hat{X}_3\, d\square \quad , \quad \{\hat{X}_3 = \begin{matrix} \hat{X}_3^{max} : \text{Top} \\ 0 \quad : \text{Bottom} \end{matrix} \} \tag{13.9.35}$$

where $\hat{X}_3$ is the thickness parameter, $\mathbf{h}$ is the surface force vector (per unit surface area) and j_s defined as

$$j_s = \| \mathbf{x}_{,\xi} \times \mathbf{x}_{,\eta} \|$$

is the surface Jacobian of the reference surface. The surface force includes both pressure and shear which can be defined as below.

a) *Pressure*: In our case

$$\mathbf{h} = -\hat{X}_3 p \mathbf{n} \quad (\hat{X}_3 = 0 \text{ or } \hat{X}_3 = \hat{X}_3^{max}) \tag{13.9.36}$$

$$\mathbf{n} = \frac{\mathbf{e}_\xi \times \mathbf{e}_\eta}{\| \mathbf{e}_\xi \times \mathbf{e}_\eta \|}$$

where p is the pressure and **n** is the unit normal vector to the composite surface.

b) *Shear*: We assume that the shear is specified in the ξ and η directions on the surface in question. In this case the surface force vector is given by

$$\mathbf{h} = h_\xi \mathbf{e}_\xi + h_\eta \mathbf{e}_\eta \tag{13.9.37}$$

where h_ξ and h_η are the shear in the ξ and η directions, respectively.

Edge Force: Suppose we wish to apply a distributed loading along an η = +1 or -1 edge. Let **h** denote the distributed surface force. The nodal forces are

$$\mathbf{f}_a^{edge} = \int_{-1}^{+1} \int_{0}^{\hat{X}_3^{max}} (N_a^T \mathbf{h}\, j_e) |_{(\eta=+1 \text{ or } -1)} d\zeta\, d\xi \tag{13.9.38}$$

where

$$j_e = \| \mathbf{x}_{,\xi} \times \mathbf{x}_{,\zeta} \| \qquad \text{(edge surface Jacobian)}$$

The case of loading along an ξ = +1 or -1 edge is handled by interchaing ξ and η in the above relations.

Note that when the reference surface is not taken to be the midsurface, nodal moments are produced even when **h** is constant (i.e., in general, $f_{a_4} \neq 0, f_{a_5} \neq 0$). If edge forces or moments are

specified per unit edge length, then nodal forces are computed as explained next. Consider an η = +1 or -1 edge. Let $f_i^{line} = f_i^{line}(\xi)$ denote the edge force and let $m_i^{line} = m_i^{line}(\xi)$ denote the edge moment. The nodal forces are then given by

$$f_a^{edge} = \int_{-1}^{+1} N_a|_{(\eta=+1 \text{ or } -1)} \begin{Bmatrix} f_1^{line} \\ f_2^{line} \\ f_3^{line} \\ \text{-----} \\ m_1^{line} \\ m_2^{line} \end{Bmatrix} \| x_{,\xi} \| d\xi \qquad (13.9.39)$$

Note that m_1^{line} and m_2^{line} must have the same sense as θ_1 and θ_2. The result is made applicable to an ξ = +1 or -1 edge if ξ and η are interchanged in the above relation.

The element external force vector is thus defined by adding all the preceding force vectors as follows

$$f^{ext} = f^{body} + f^{surf} + f^{edge} \qquad (13.9.40)$$

13.9.12 Boundary Conditions

It is important to realize that the boundary conditions in the present theory are not always the same as those for the classical thin plate theory. The differences occur in the specification of the "simply supported" case. In the modified theory, there are two ways of going about this, depending on the actual physical constraints. See Hughes 1987, p. 324-327 for the necessary details.

14.0 NUMERICAL SIMULATIONS

14.1 Introduction

The finite element formulation presented in the previous section was implemented in the computer program FEAP and several test problems were analyzed. These included various composite laminates with flat and curved geometries. The results of these analyses are presented in this section. For each simulation the geometry, the material properties, the boundary conditions, loadings, and the finite element discretization were discussed and various results of the simulation were presented at the end of this section.

Simulation #1

14.1.1 Free Edge Boundary-value Problem [45,-45]s

The first numerical simulation is a prismatic symmetric laminate having traction-free edges at $x = \pm$ a and surfaces $z = \pm$ h, and loaded by strain applied only on its ends at y = constant. Each layer is composed of unidirection fiber-reinforced material such that the fiber direction is defined by its angle θ with the y-axis.

The elastic properties of various composite materials used in this numerical simulation have been taken from N. J. Pagano [p. 4, Pagano 1989]. These material properties are E_L = 137.9 GPa, $E_T = E_z$ = 14.48 GPa, $G_{LT} = G_{LZ} = G_{TZ}$ = 5.86 GPa, $\nu_{LT} = \nu_{LZ} = \nu_{TZ}$ = 0.21 where subscript L denotes the direction parallel to the fibers, T denotes the in-plane direction perpendicular to the fibers, and the subscript Z denotes the out-of-plane direction.

In this example a laminate consisting of four unidirectional fibrous composite layers, two with their axis of elastic symmetry (fiber direction) at +45 and two at -45 to the longitudinal laminate axis was considered. Figure 14.1 shows the laminate geometry and the coordinate system. 1% strain in opposite directions is applied at $y = 0$ and $y = L$, respectively, while it is restrained to move in the axial, lateral and thickness directions at the xz plane passing through $y = L/2$. In

order to solve this problem a finite element mesh comprising 1920 composite shell elements with 2665 nodes was generated. The physical dimensions for the numerical simulation were x = 20, y = 60, z = 2.5, with 12 elements in x direction, 40 elements in the y direction and 4 finite elements through the thickness. For each finite element layer through the thickness, the reference surface was assumed to be associated with the bottom surface of that layer. In the following figures elements 241-280 belong to the bottom layer with +45° ply orientation, elements 721-760 and 1201-1240 belong to the middle two layers with -45° orientation while elements 1681-1720 belong to the top layer with +45° orientation at a section cut at the dashed cross-section in Figure 14.1. In these results, q-1 is the transverse shear stress σ_{yz} and q-2 is the transverse shear stress σ_{xz}. The stress distribution obtained agrees very well with the numerical results by J. N. Pagano for the same physical dimensions of the problem and material properties and rather much refined spatial discretization.

1. Figures 1.1 and 1.2 show the various stress components for $\theta = +45°$ and $\theta = -45°$, respectively. For a deeper insight, please see Fig. 1.3-1.8 and the following explanation.

2. Figure 1.4 shows the inplane shear stress σ_{xy} and is equal in magnitude but opposite in sight for the two material sets. The ratio of σ_{yy} and σ_{xy} agrees closely with that of Pagano's numerical simulation.

3. Figure 1.5 shows the through the thickness stress component σ_{zz}. It shows a sudden increase in value close to the free surface.

4. Figures 1.7 and 1.8 show the transverse shear stresses and Figures 1.9, 1.10 and 1.11 represent the moments generated because of the shearing stresses, thereby giving rise to curvatures near the free edges of the laminate.

5. Figures 1.12, 1.13 and 1.14 represent the displacement fields in the axial, through-thickness and the transverse directions to the applied loading, respectively, whereas Fig.

1.15 represents the distribution of the rotation about the axis of loading. The other rotation component is numerically zero as evidenced by Fig. 1.16. The antisymmetry in the axial displacement plots which is caused by the 3-D nature of the solution close to the free edges is evident in Fig. 1.12.

6. It is important to compare Figures 1.13 and 1.17. Both represent the distribution of the through thickness displacement field, but at $y = L/2$ and $y = L$, respectively. As shown in Fig. 1.17, a twist in the thickness direction takes place, thereby causing the ensuing displacement field become antisymmetric about the symmetry plane which is perpendicular to the thickness direction. Furthermore, at this section, the rotation about the transverse axis also becomes non-zero, and can be seen in Fig. 1.20.

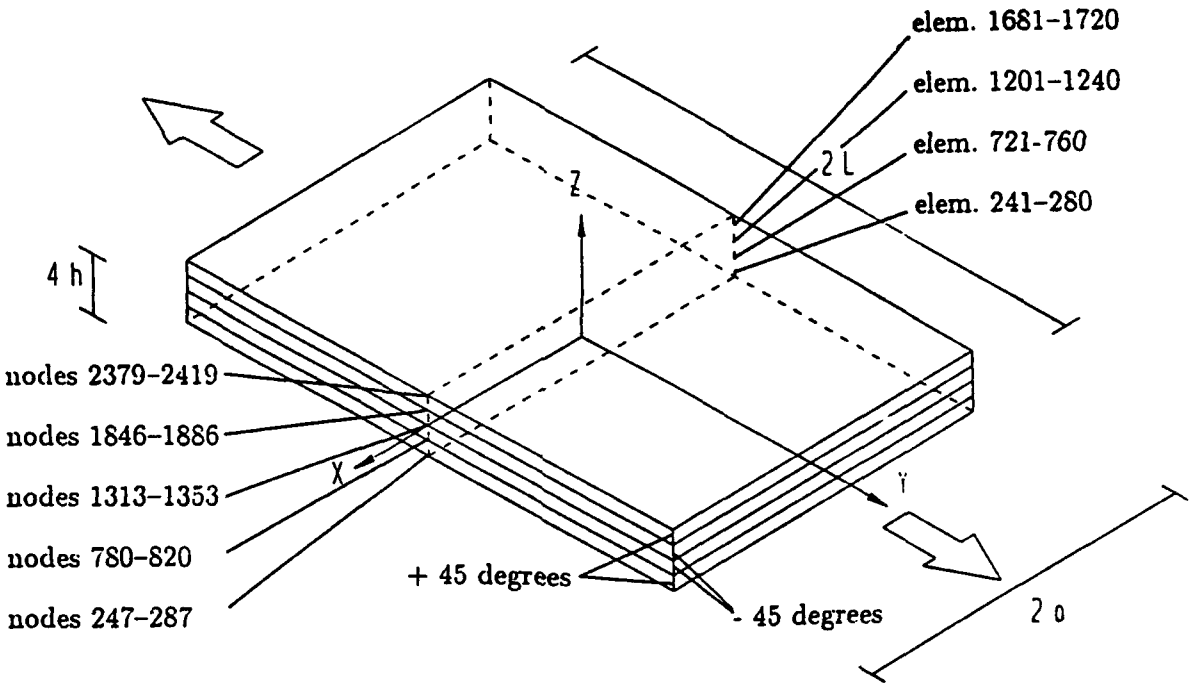

Figure 14.1

Simulation #2

14.1.2 Free Edge Boundary-value Problem with a circular hole [45,-45]s

This numerical simulation is a prismatic symmetric laminate with a circular hole, having traction-free edges at $x = \pm$ a and surfaces $z = \pm$ h, and loaded by strain applied only on its ends at y = constant. The ratio of diameter of the hole to the width of the composite is D/W = 0.1. Each layer is composed of unidirectional fiber-reinforced material such that the fiber direction is defined by its angle θ with the y-axis. The material properties, and the physical dimensions of the composite are the same as in the preceding case, however the computational mesh is quite different. To solve this problem a mesh containing 720 composite elements per finite element layer and with four layers through the thickness was generated. The total number of nodes in this problem is 3780. The unit diameter cylindrical hole has its center point at (0,0,0). No boundary conditions are applied on the surface of the hole, i.e., it is traction free. The block is constrained to move in the axial, transverse or lateral direction by appropriately constraining the nodes along the symmetry lines on the xz section passing through $y = 0$.

1. Figures 2.1 and 2.2 present the various stress components for +45° and -45°, respectively, at a xz plane that passes through $y = 0$.

2. Figure 2.3 shows the axial stress σ_{yy} across the width of the laminate. Elements 521-540 belong to the bottom layer with +45° ply orientation, elements 1241-1260 and 1961-1980 belong to the middle two layers with -45° orientation while elements 2681-2700 belong to the top layer with +45° orientation. Results are shown for the transverse plane along the positive x direction at $y = 0$. Away from the hole the stress distribution obtained agrees very well with the preceding numerical results for the same physical dimensions of the problem and material properties. However a sharp gradient in the stresses can clearly be seen and the value increases to almost two times its value in the region away from the hole or the free edge.

3. Figure 2.4 shows the inplane shear stress σ_{xy} and is equal in magnitude but opposite in sign for the two material sets. Once again close to the hole there is a sudden increase in the value of the stress. The ratio of σ_{yy} and σ_{xy} agrees closely with that of the preceding numerical simulation.

4. Figure 2.5 shows the through the thickness stress component σ_{zz}. Near the hole the value climbs to 12 times its value near the free surface. This shows that if the composite was designed to withhold the through thickness stress of the free edge and a hole was drilled through it, the very high stress concentration that develops around the hole can result in delamination, thereby resulting in a very sharp

5. Figures 2.6 and 2.7 are important in the sense that they show the various stress components along the circumference of the circle for the +45° and the -45° laminates, respectively. These stresses have been evaluated at the Gauss points that are closest to the free edge. The details for the major stresses can be seen in Figs. 2.8-2.10.

6. Figures 2.11-2.14 represent the displacement and rotation fields along the radial distance from the hole in the lateral direction to the applied strain. They should be compared with Figs. 1.12-1.15 of the previous numerical simulation. The difference between the two sets of plots is that in the previous case we had plotted the entire cross section while in the present case only half of the section, i.e., radially out from the center of the hole is shown. It is evident that in the region away from the hole, the numerical results agree closely with that of the simulation without the hole. It shows that the edge effects that arise because of the circular hole are localized in a small region around it. However, the important observation is that although this region is small relative to the entire domain, the gradients in these regions are the steepest, making it more vulnerable to delamination and high stress concentration.

7. Figures 2.15-2.18 provide a deeper insight in the displacement and rotation pattern around the circular hole. Figure 2.15 shows the axial displacement along the circumference of the hole. An antisymmetric deformation can clearly be seen which shows that an analogous 3-D deformation phenomenon takes place at the free edges generated by the hole.

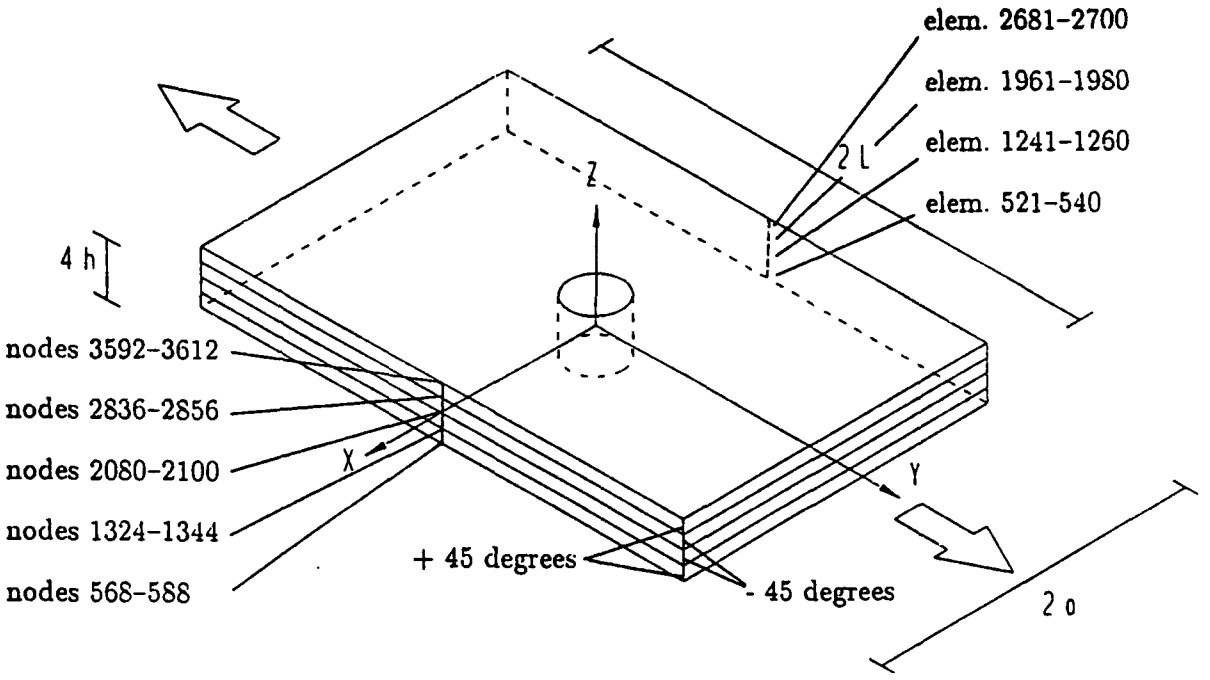

Figure 14.2

Simulation #3

14.1.3 Free Edge Boundary-value Problem [0,90]s

The third numerical simulation is again a prismatic symmetry laminate having traction-free edges at $x = \pm a$ and surfaces $z = \pm h$, and loaded by strain applied only on its ends at y = constant. Each layer is composed of unidirectional fiber-reinforced material such that the fiber direction is defined by its angle θ with the y-axis.

The elastic properties of various composite materials used in this numerical simulation have been taken from N. J. Pagano. In this example a laminate consisting of four unidirectional fibrous composite layers, two with their axes of elastic symmetry (fiber direction) at 0° and two at 90° to the longitudinal laminate axis was considered. Figure 14.1 shows the laminate geometry and the coordinate system. 1% strain in opposite directions is applied at $y = 0$ and $y =$ L, respectively, while it is restrained to move in the axial, lateral and thickness directions by appropriately constraining the nodes along the symmetry lines at $y = L/2$ section. The physical dimensions of the problem, the computational mesh and the boundary conditions are the same as for simulation 1, and therefore are being omitted here.

1. Figures 3.1 and 3.2 show the various stress components for $\theta = 0°$ and $\theta = 90°$, respectively. For a deeper insight into the behavior of these stresses the reader is referred to Figs. 3.3-3.6.

2. Figures 3.7-3.10 represent the displacement and the rotation fields developed at $y = L/2$. In Fig. 3.7, the antisymmetry in the axial displacement, although extremely small, can still be seen which shows that the element is numerically very stable. There is another very important observation that needs to be made at this stage. Unlike the simulation #1 with [45,-45]s laminate (Fig. 1.15) in which the edge at $y = L$ undergoes a twisting deformation, in the [0,90]s laminate, under the same boundary and loading conditions the response in the

through thickness direction still stays symmetric. What is important to note is that whenever one is working with ply orientation which is different from [0,90]s case, there is always going to be a 3-D phenomenon at the edges. So for all practical purposes, in composite design or in the design of engineering components made of composites, if the loading is applied at a certain angle to the ply laminates which is other than 0 degrees or 90 degrees, a computational tool which accounts for 3-D effects is a must.

Simulation #4

14.1.4 Free Edge Boundary-value Problem with a Circular Hole [0,90]s

This numerical simulation is a prismatic symmetric laminate with a circular hole, having traction-free edges at $x = \pm a$ and surfaces $z = \pm h$, and loaded by strain applied only on its ends at y = constant. The diameter to width ratio D/W = 0.1. The material properties, and the physical dimensions of the composite are the same as in the preceding three cases. The computational mesh is identical to the one used in Simulation 2. The difference is that in the present case it is [0,90]s laminate. The unit diameter cylindrical hole has its center point at (0,0,0), see Fig. 14.2. No boundary conditions are applied on the surface of the hole, i.e., it is traction free. The block is constrained to move in the axial, transverse or lateral direction by appropriately constraining the nodes along the symmetry lines at $y = 0$ surface. We have modelled the entire composite without the assumption of symmetry.

1. Figures 4.1 and 4.2 show the relative magnitudes of all the stress components for the layers at 0 degrees and 90 degrees, respectively. As can be seen, the axial stress is orders of magnitude greater than all the other stresses and close to the hole it increases to almost three times its value than in the rest of the domain.

2. Figures 4.3 and 4.4 represent the axial stress σ_{yy} and intermalinar normal stress σ_{zz} at the periphery of the circular hole.

4. Figures 4.5-4.6 and Figs. 4.7-4.9 represent the displacement field along the radial distance from the hole in the transverse direction to the applied loading, and along the circumference of the circular hole, respectively.

Simulation #5

14.1.5 Extension Test; Comparison with J. N. Reddy [45,-45]s

We have selected this numerical from the paper of J. N. Reddy. The same problem with identical boundary conditions, material properties and ply orientations has also been solved by R. M. Jones in his book on *Mechanics of Composite Materials*.

Consider a thick, symmetric, angle-ply laminate [45,-45]s subjected to axial displacements on the ends. The laminate has a length of 2L, width 2W, and thickness 2h, with L = 10W and W = 8h (see Fig. 14.1). Each of the four material layers is of equal thickness h, and is idealized as a homogeneous orthotropic material with the following properties expressed in the material coordinate system:

$$E_L = 20 \times 10^6 \text{ psi} \ , \ E_T = E_z = 2.1 \times 10^6 \text{ psi}$$

$$G_{LT} = G_{LZ} = G_{ZT} = 0.85 \times 10^6 \text{ psi}$$

$$\mu_{LT} = \mu_{LZ} = \mu_{TZ} = 0.21$$

where subscript L denotes the direction parallel to the fibers, subscript T denotes the inplane direction perpendicular to the fibers, and the subscript z denotes the out-of-plane direction. The origin of the global coordinate system coincides with the centroid of the three-dimensional composite laminate. The x-coordinate is taken along the width of the laminate; the y-coordinate is taken along the length of the laminate; and the z-coordinate is taken through the thickness of the laminate. Since the laminate is symmetric about the xy-plane, only the upper half of the laminate is modelled. Thus the computational domain is defined by ($-W \le x \le W$, $-L \le y \le L$, $0 \le z \le 2h$). The displacement boundary conditions for this problem are

$$u_1(0,-L,0) = 0 \quad u_1(0,L,0) = 0$$

$$u_2(x,-L,z) = 0 \quad u_2(x,L,z) = U_o$$

$$u_3(x,y,0) = 0$$

In order to solve this problem a finite element mesh comprising 1920 composite shell elements with 2665 nodes was generated. The physical dimensions for the numerical simulation were L = 200, W = 20, z = 2.5, with 40 elements in x direction, 12 elements in the y direction and 4 composite elements through the thickness.

1. Figures 5.1-5.3 represent the various significant stress components through the composite cross section cut at y = 0, i.e., at midspan of the loading axis. These numerical results are very close to the computed numerical values of J. N. Reddy and R. M. Jones, although both are using a much higher refinement of the mesh in the thickness direction when compared to our spatial discretization.

2. Figures 5.4-5.6 represent the bending stresses. The general behavior is the same as of the previous cases for [45,-45]s.

3. Figures 5.7-5.9 represent the displacement fields as obtained at y = 0 and y = L, respectively. It is interesting to note that the twisting in the through-thickness displacement field that we observed in Simulation 1 is also present in the present simulation.

Simulation #6

14.1.6 Bending Analysis [45,-45,45]s

This simulation presents a bending test involving a square plate with uniformly distributed load. In this simulation the complete plate without the assumption of symmetry was analyzed. The plate is composed of three laminates stacked in 45/-45/45 cross-ply construction with θ measured from the x_1 axis. The material properties of Simulation 1 which were taken from J. N. Pagano have been used in this case as well. The finite element mesh is composed of 675 elements with 225 elements per finite element layer and 3 finite element layers through the thickness. The distribution of elements is $15 \times 15 \times 3$. The total number of nodes is 1024.

In the present numerical simulation the plate is clamped along the boundaries and a uniformly distributed load of intensity q_o is applied in the $+z$ direction. Numerical results are reported for the section cut at $y = b/2$.

1. Figures 6.1 and 6.2 present the various components of stresses for the +45 ply on the tension side and the -45 ply which lies on the axis of symmetry in the z direction, respectively. A detailed analysis of stresses can be seen in Figs. 6.3-6.8. Since the edges are clamped, the stresses have a certain finite value at the boundary.

2. Figures 6.9 and 6.10 present the bending moments.

3. We present the displacement and the rotation fields in Figs. 6.11-6.13.

We would like to mention that bending analysis similar to this simulation has not been reported in the literature.

Figure 6.3 shows bending stresses in x direction (σ_{xx}) for top, center and bottom layers of the plate. For the center layer, the stresses are calculated at the Gaussian integration points

which are located at the neutral axis of the plate and the finite element simulations predict the correct zero values. Stresses for the top and bottom layers are symmetric with regard to the neutral axis but with opposite sign.

Figure 6.4 presents bending stresses in y-y directions for the same cross-section.

Figure 6.5 is the distribution of in-plane shear for the three plies.

Figure 6.6 presents the distribution of transverse normal stress component.

Figures 6.7 and 6.8 show the shear stress components for various layers.

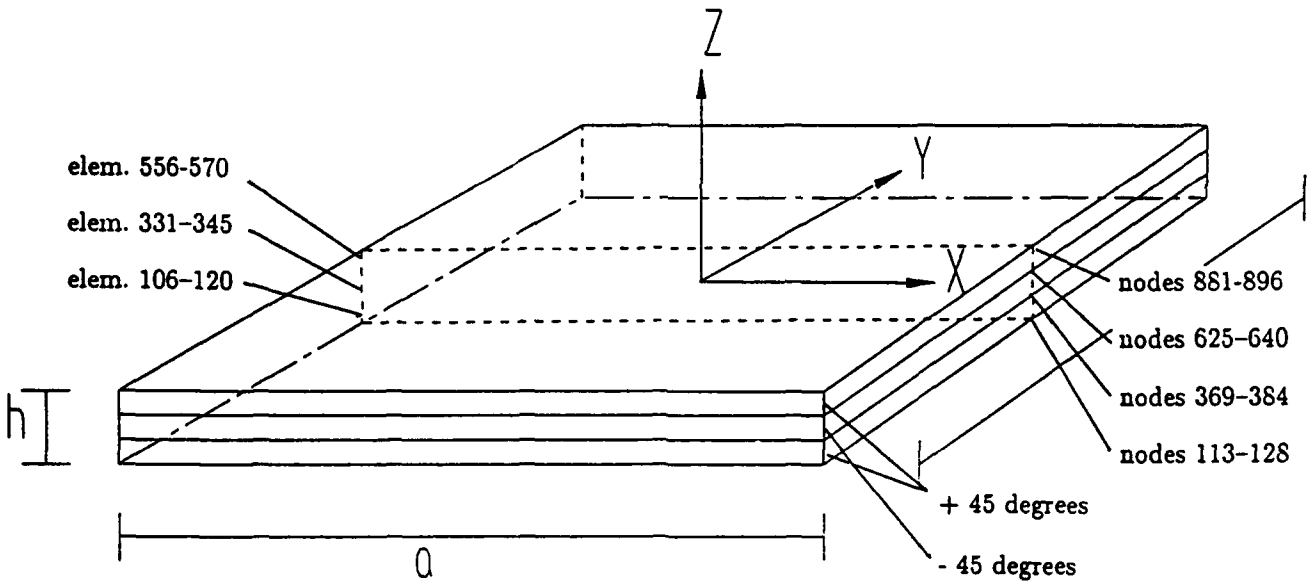

Figure 14.3

Simulation #7

14.1.7 Bending Analysis [45,-45,45]s

This simulation again presents a bending test involving a square plate with uniformly distributed load, but with Simply Supported edges. Once again in this simulation the complete plate without the assumption of symmetry was analyzed. The plate is composed of three laminates stacked in 45/-45/45 cross-ply construction with θ measured from the x_1 axis. The physical dimensions, material properties, loading conditions and the finite element mesh used for analysis remain unchanged from simulation #6.

1. A detailed analysis of stresses can be seen in Figs. 7.1-7.6. Unlike the clamped case, in the simply supported case the stresses tend to vanish at the free edges.

2. Figures 7.7-7.9 present the bending stresses.

3. We present the displacement and the rotation fields in the remaining plots.

Simulation #8

14.1.8 Cylindrical Shell with Free Edge Boundary [45-45]s

The last numerical simulation is a cylindrical shell having traction-free edges at $r = r_1, r_2$, loaded by 1% strain applied in -z direction on its ends at $\theta = 90$ degrees. Each layer is composed of unidirectional fiber-reinforced material such that the fiber direction is defined by its angle θ with the y-axis.

The elastic properties of various composit materials used in this numerical simulation have been taken from N. J. Pagano [p. 4, Pagano 1989]. In this example a laminate consisting of three unidirectional fiberous composite layers, the top and bottom with their axis of elastic symmetry (fiber direction) at +45 while the center one at -45 to the longitudinal laminate was considered. Figure 14.4 shows the laminate geometry and the coordinate system. 1% strain in the -z directions is applied at the cross-section at $\theta = 90$, while it is restrained to move along the cross section at $\theta = 0$. In order to solve this problem a finite element mesh comprising 675 composite shell elements with 1024 nodes was generated. The physical dimensions for the numerical simulation were $r_1 = 20$, $r_2 = 21.5$, $z = 20$, with 15 elements in the θ direction, 15 elements in the y direction and 3 composite elements through the thickness. For each finite element layer through the thickness, the reference surface was assumed to be associated with the bottom surface of the composite shell. We will be looking at a section cut at $Y = 0$ for the displacement and the stress fields.

1. Figure 8.1 shows σ_{xx} across the width of the laminate. Elements 1-15 belong to the bottom layer with +45 ply orientation, elements 226-240 belong to the middle layer with -45 orientation while elements 451-465 belong to the top layer with +45 orientation.

2. Figure 8.2 shows σ_{yy}. Figure 8.3 shows stress component σ_{zz}. At $\theta = 0$ it shows tension on the inner layer and compression on the outer layer with +45 ply orientation.

3. Figures 8.4-8.6 represent the above three stress components at a section cut at y = b/2.

4. Figures 8.6-8.8 represent the displacement field at section y = 0 and Figs. 8.9-8.11 represent the corresponding values at an interior section with y = b/2.

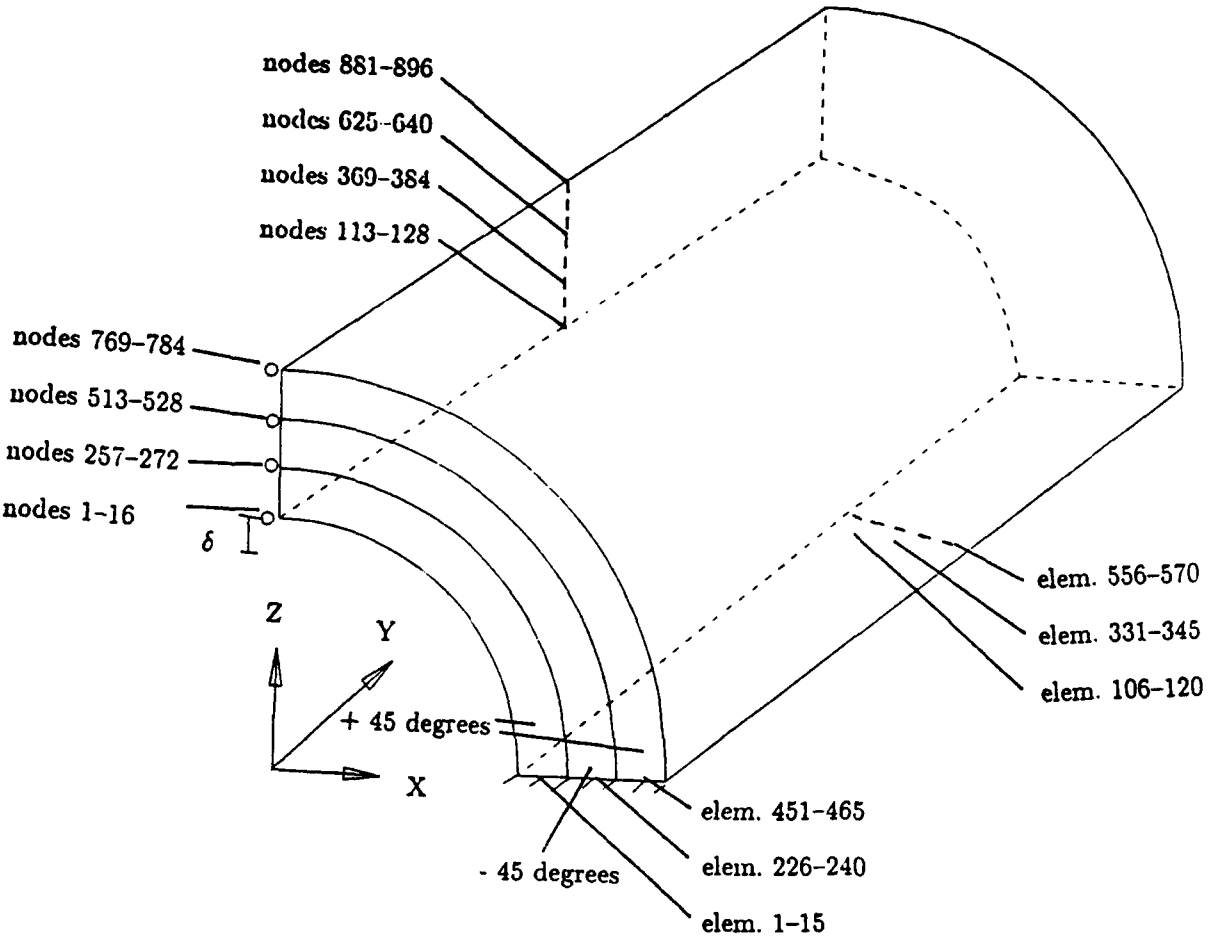

Figure 14.4

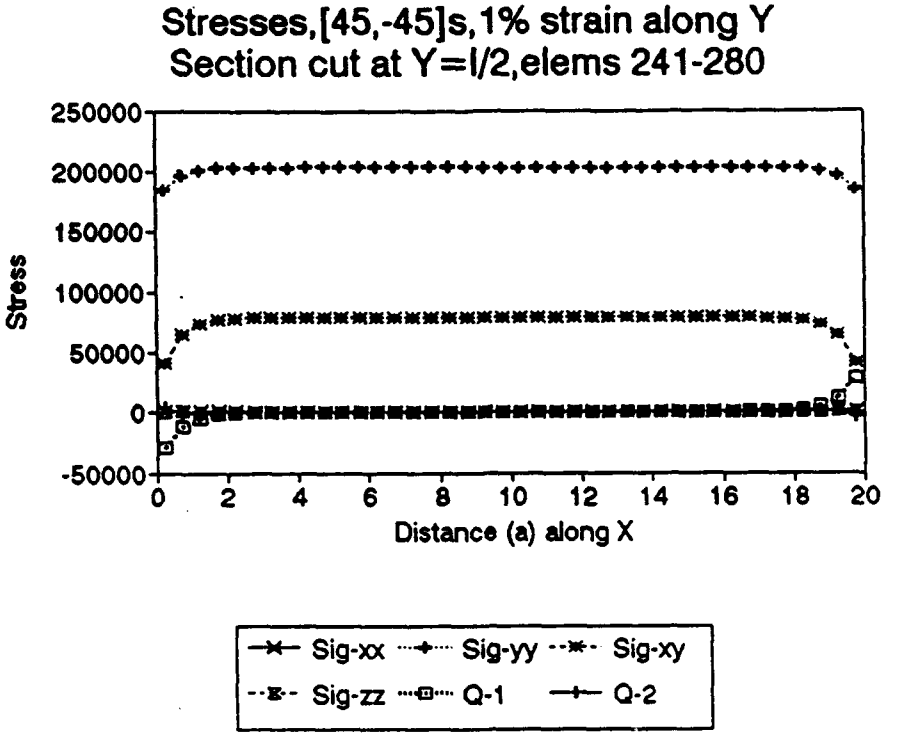

Figure 1.1

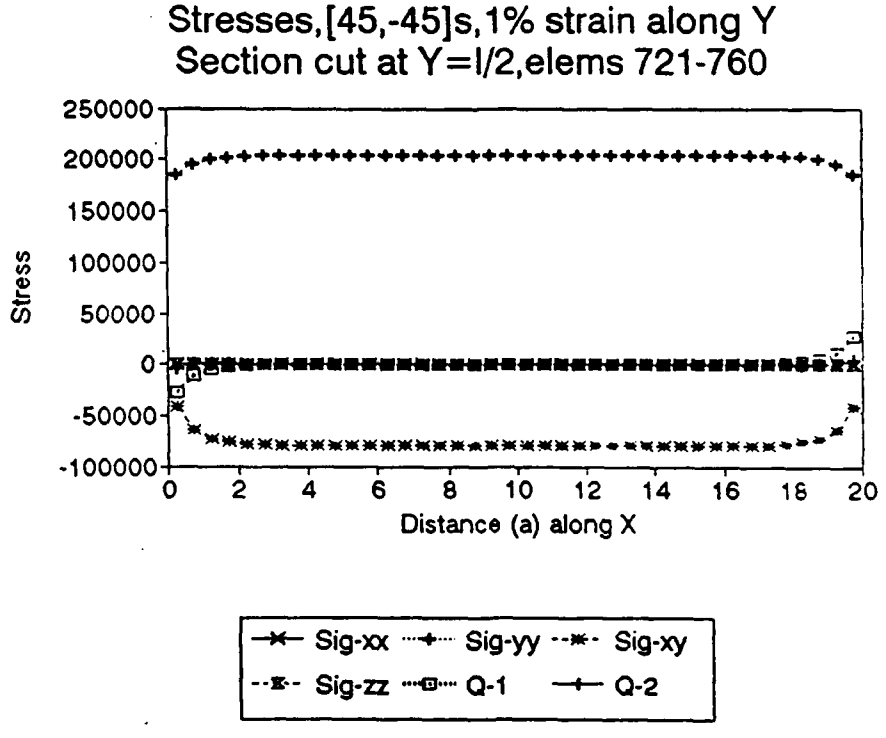

Figure 1.2

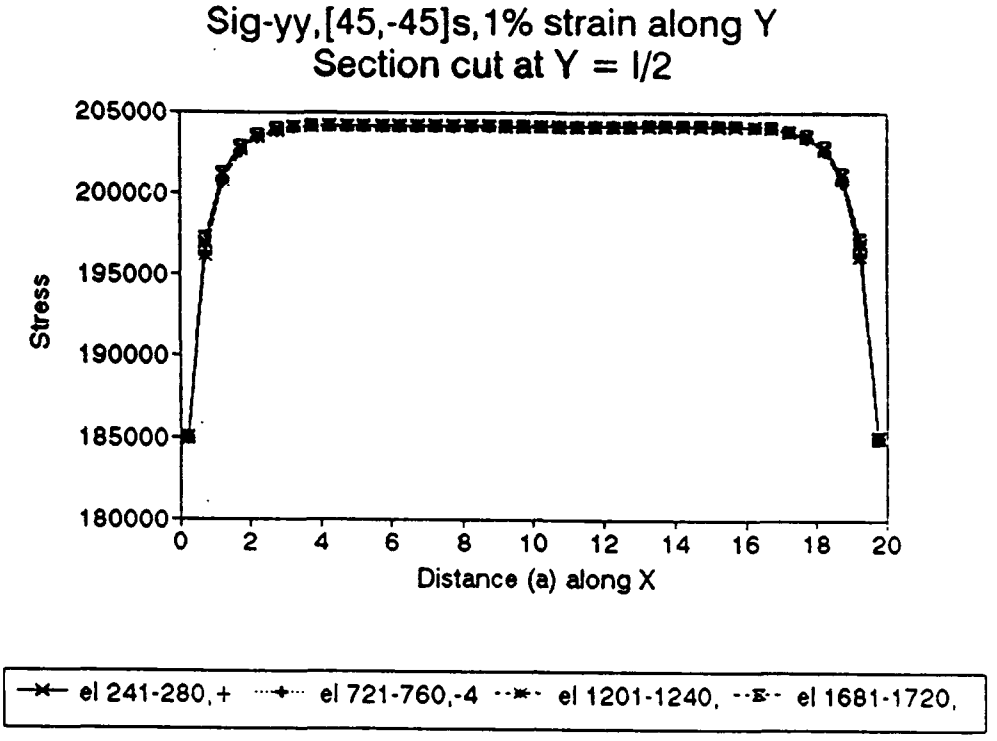

Figure 1.3

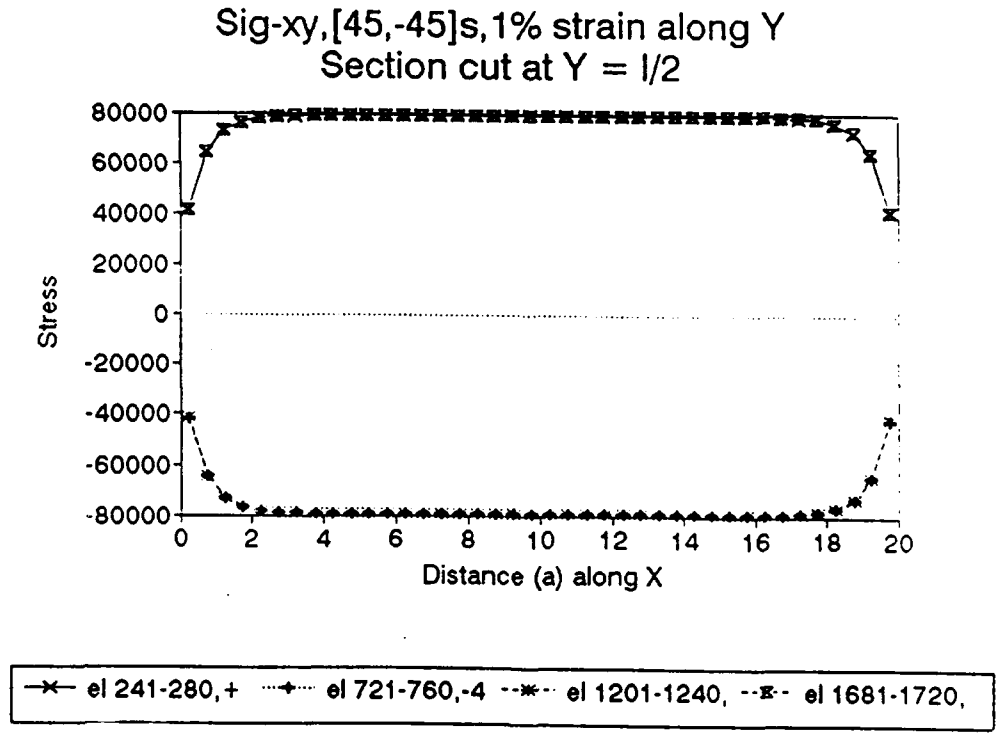

Figure 1.4

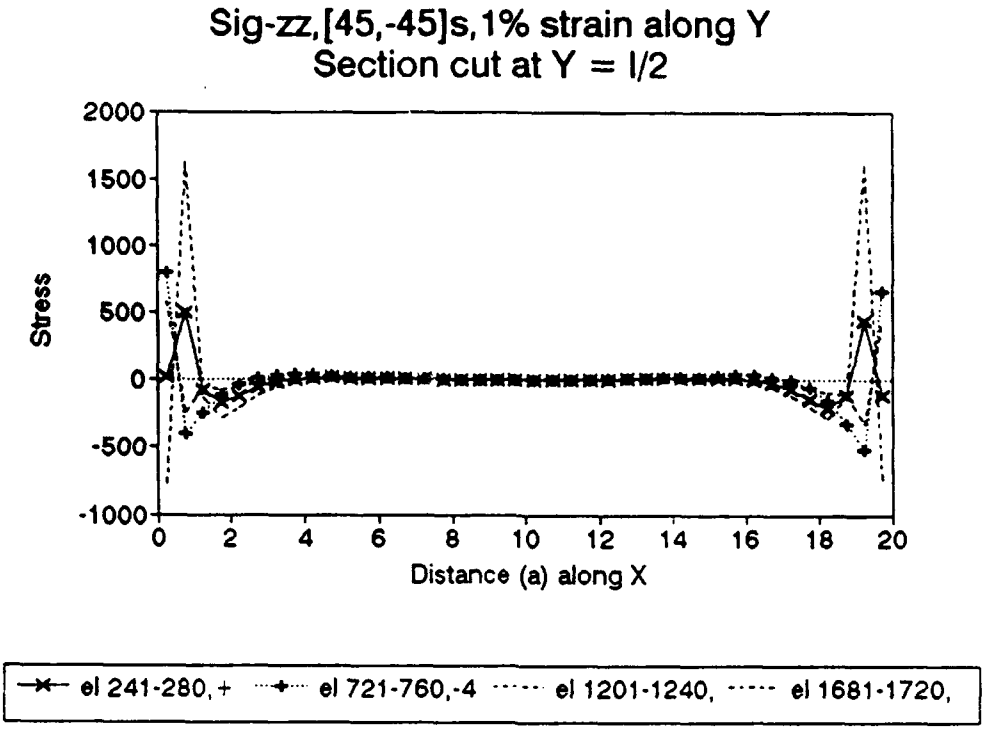

Figure 1.5

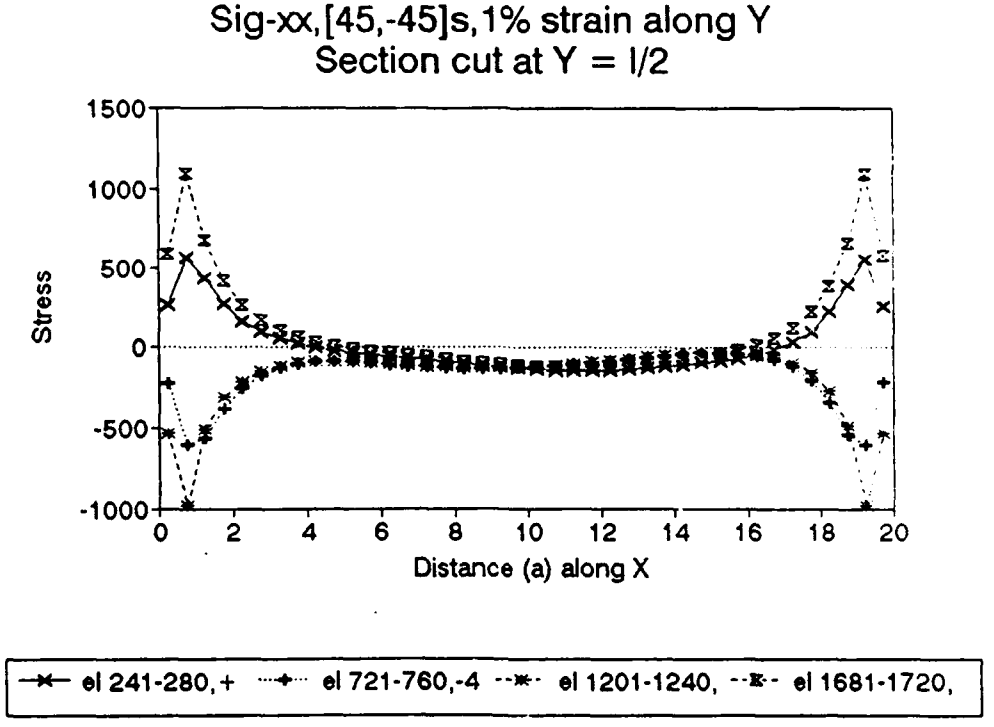

Figure 1.6

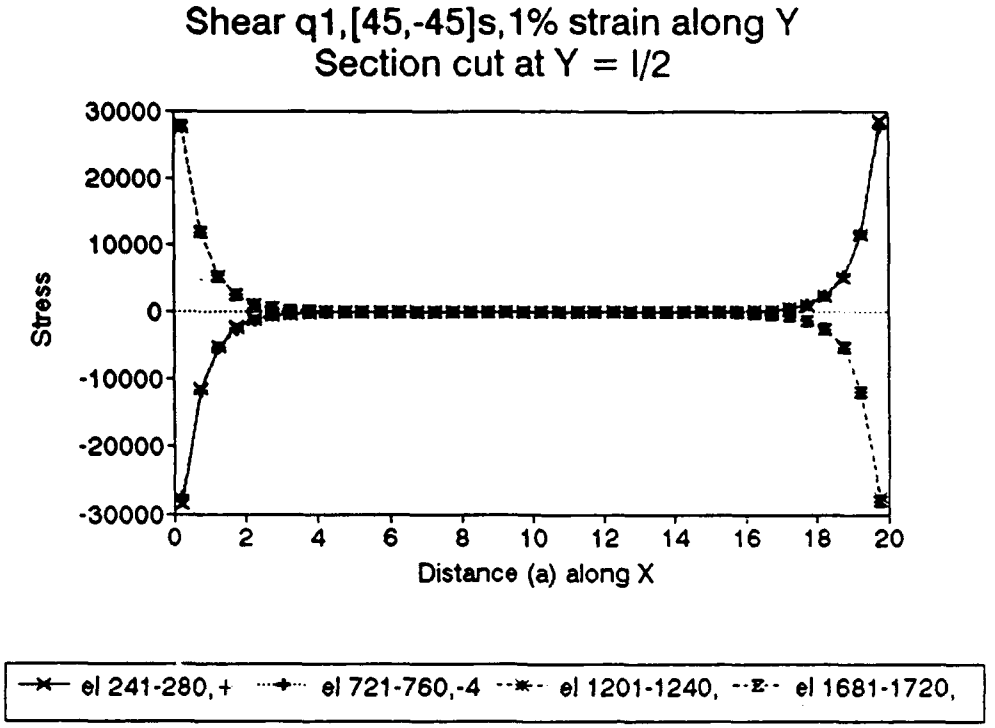

Figure 1.7

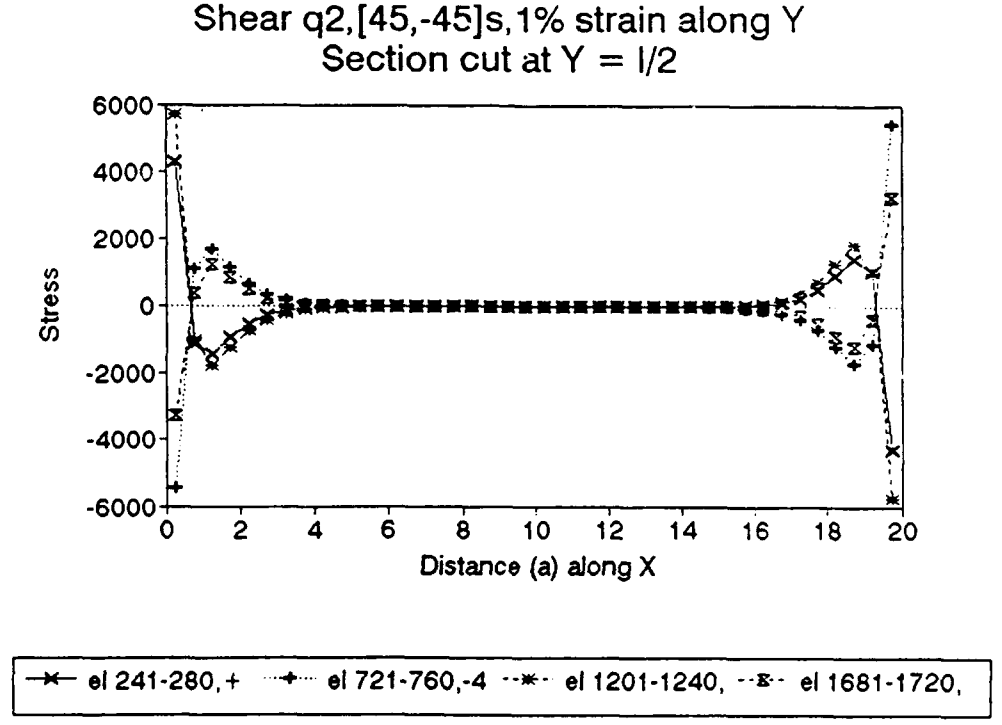

Figure 1.8

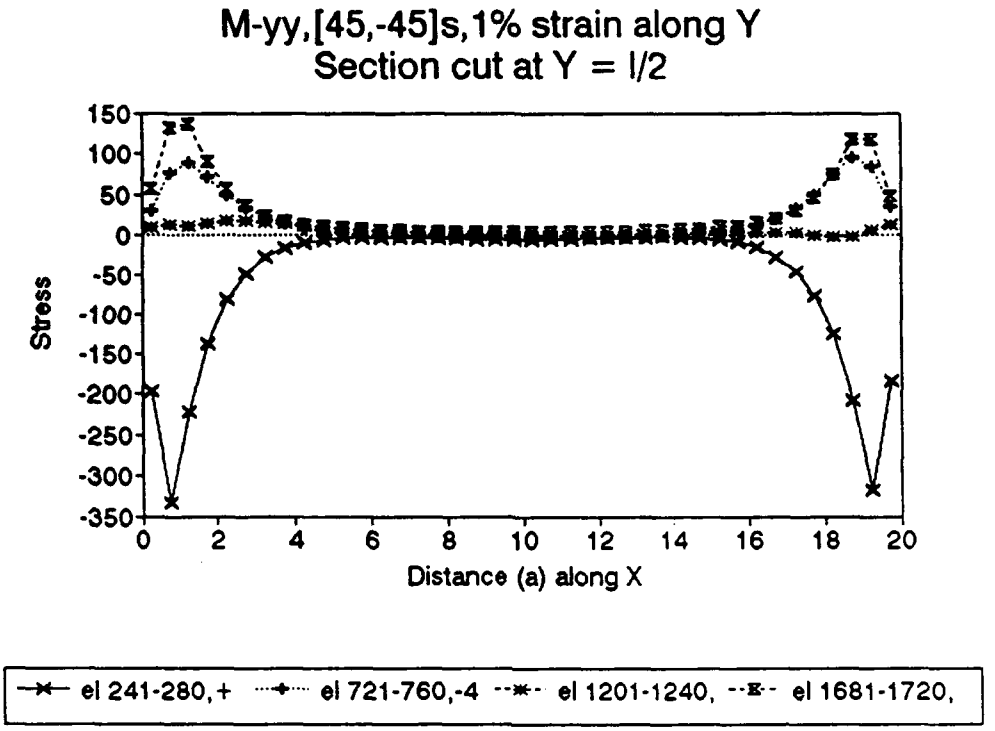

Figure 1.9

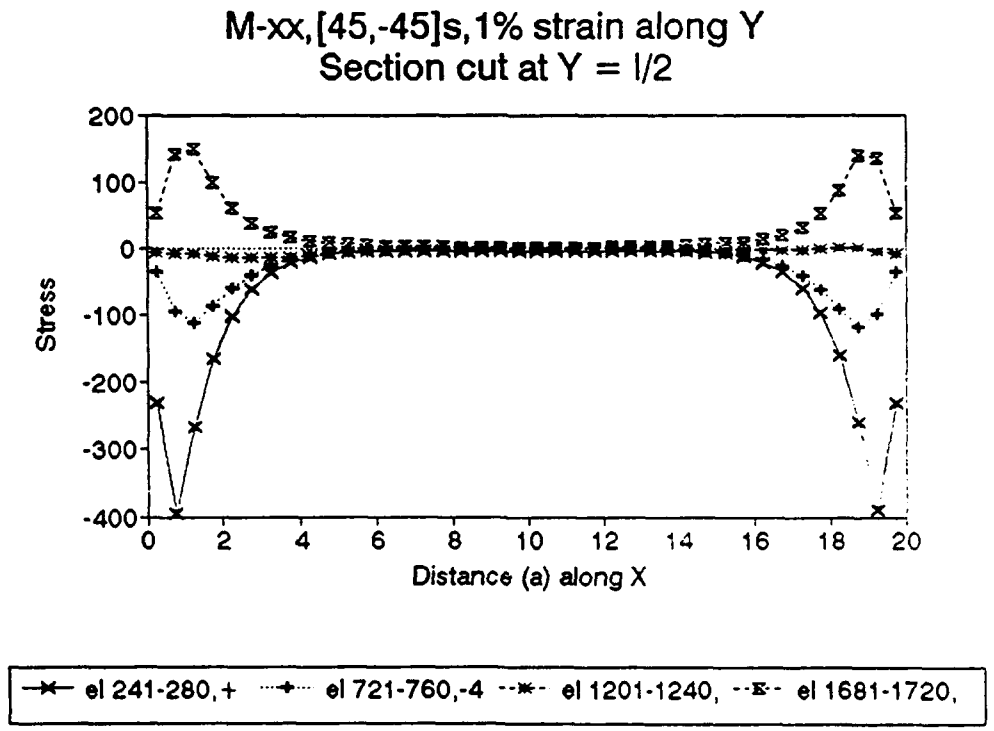

Figure 1.10

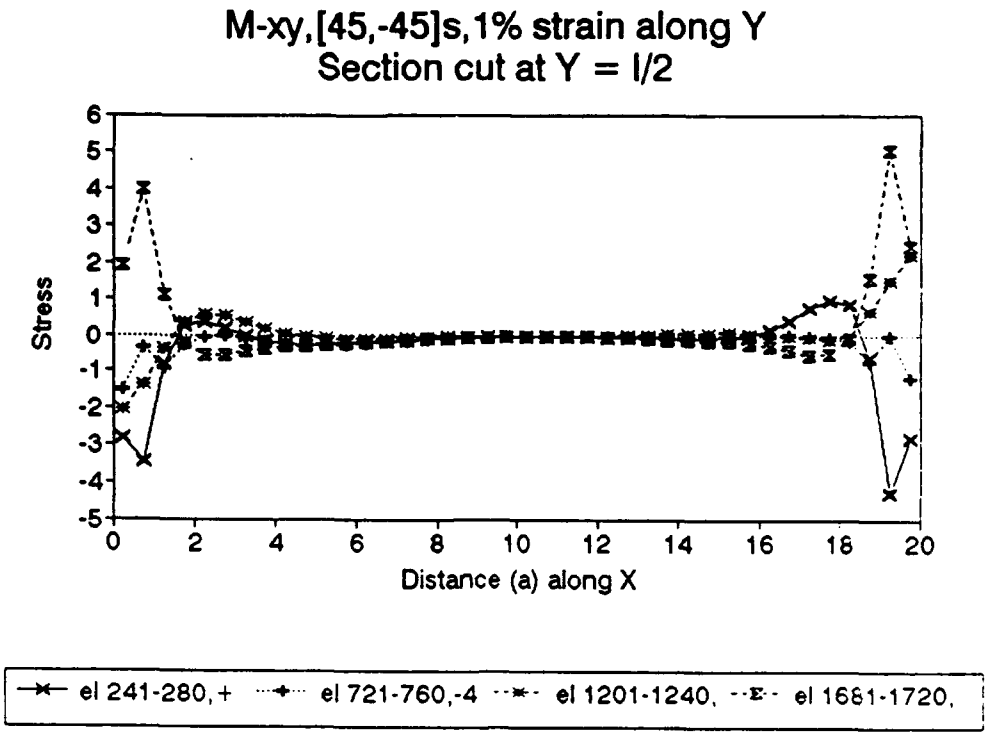

Figure 1.11

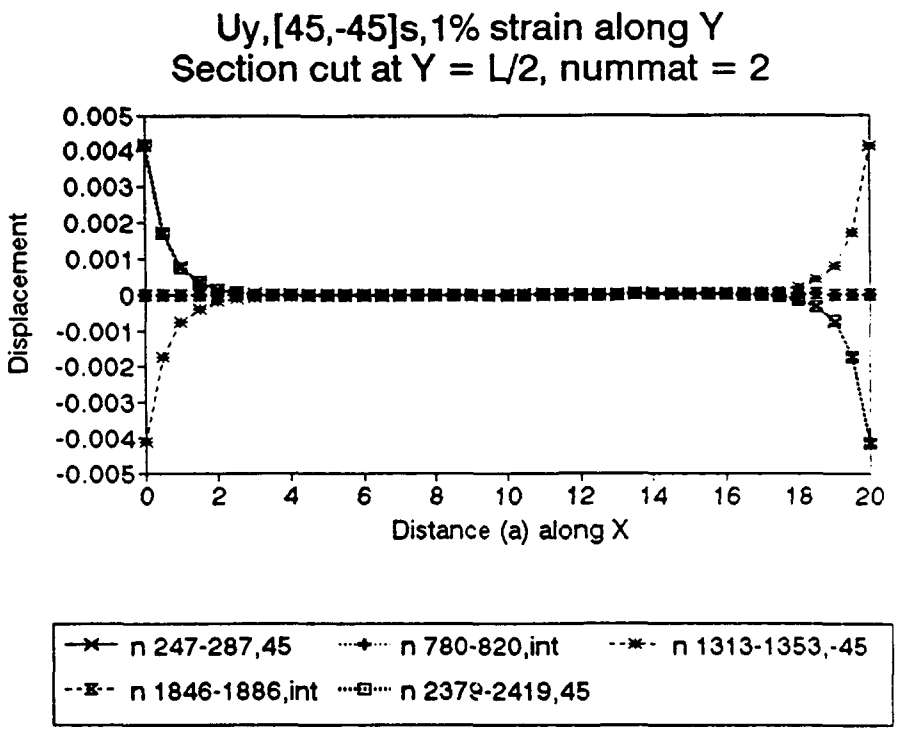

Figure 1.12

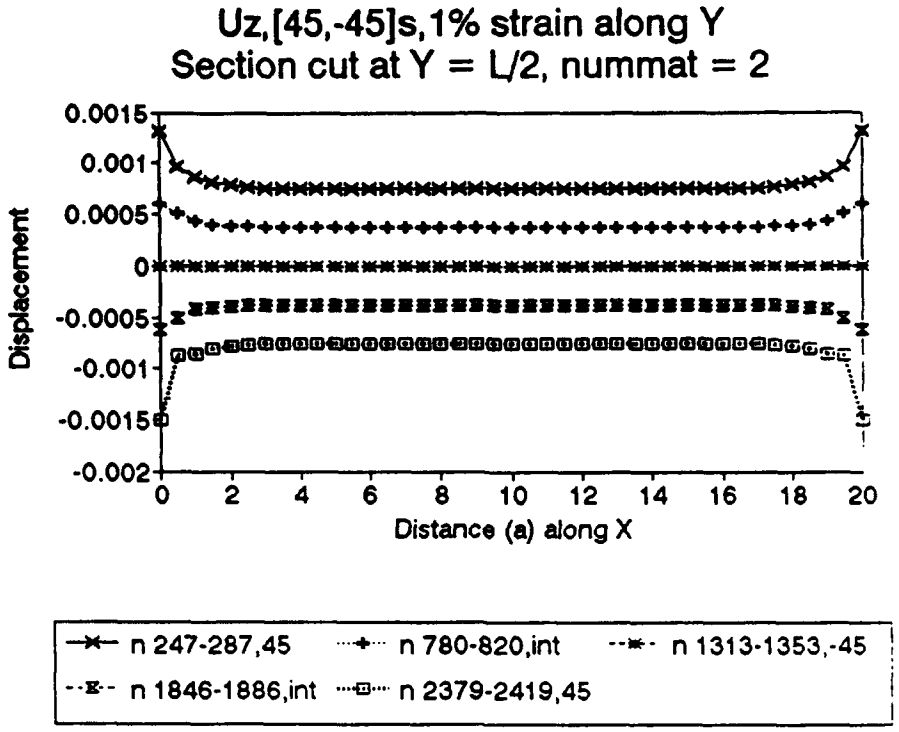

Figure 1.13

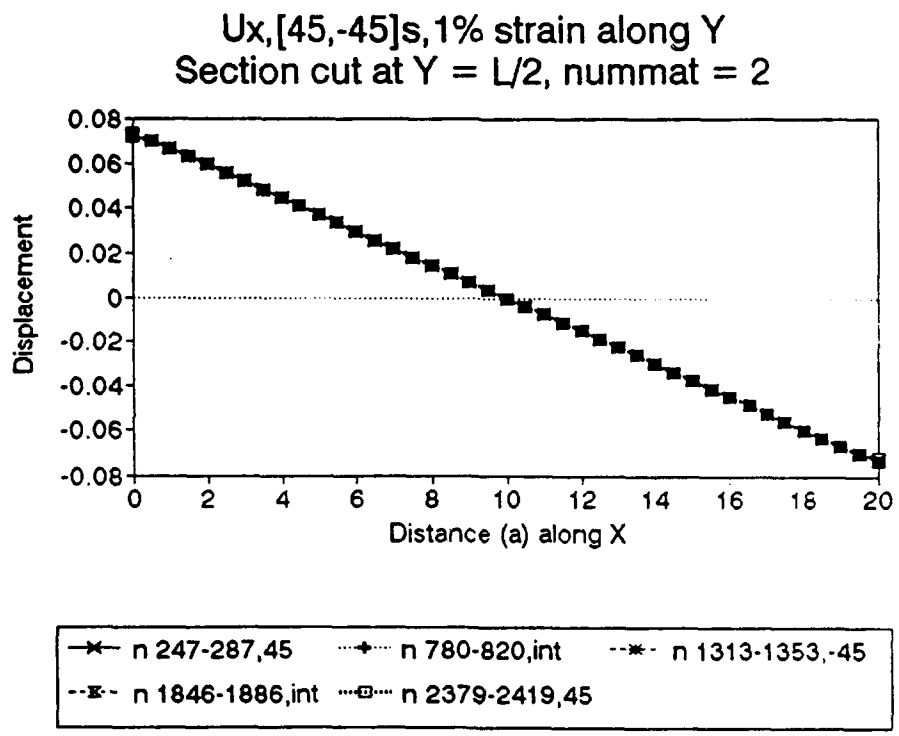

Figure 1.14

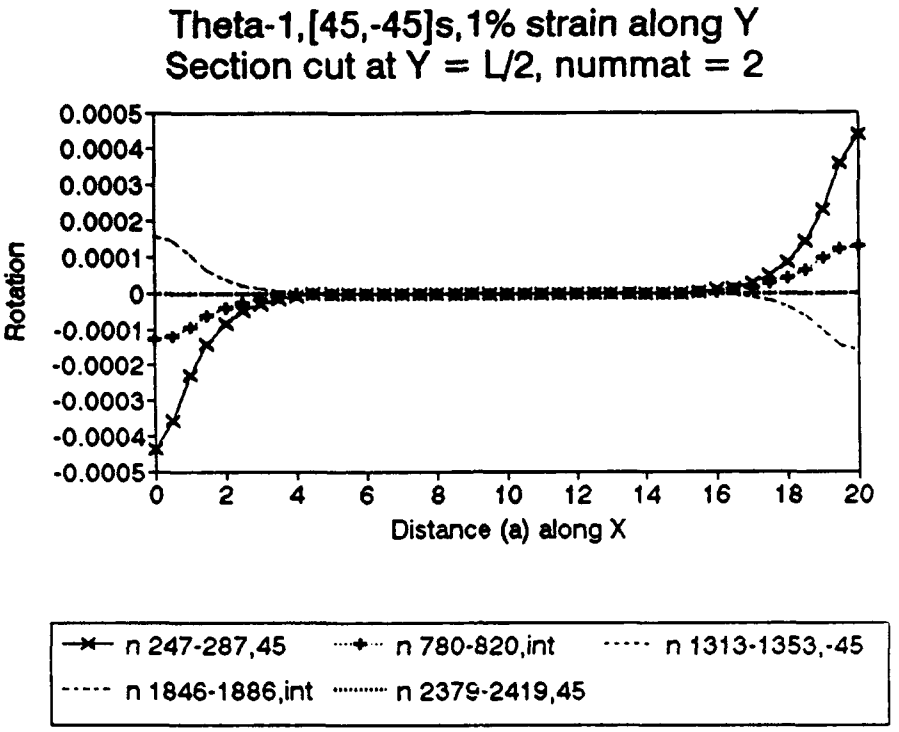

Figure 1.15

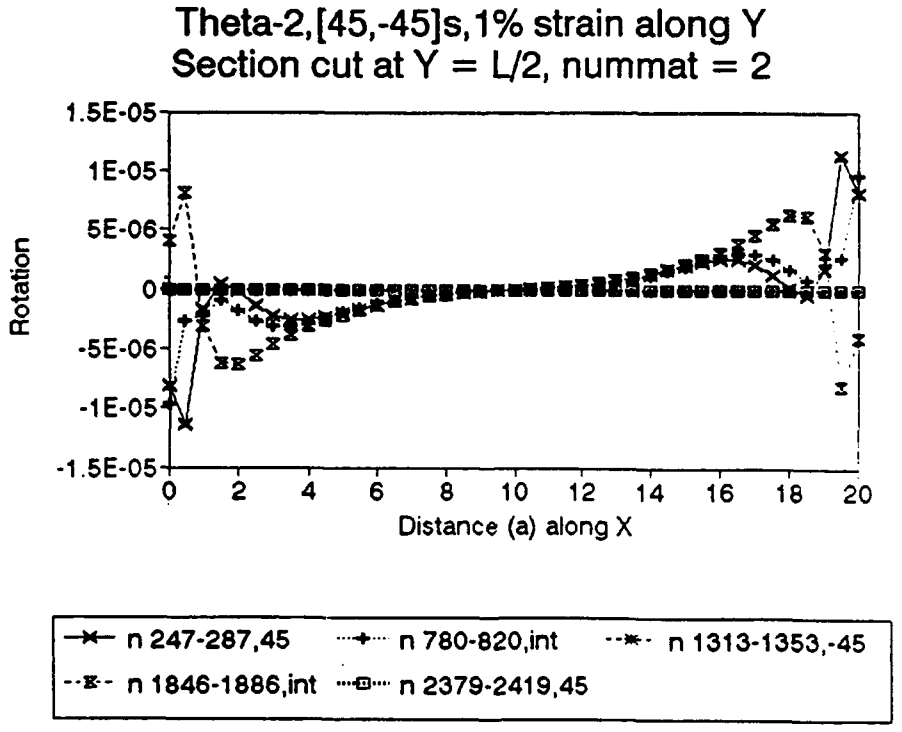

Figure 1.16

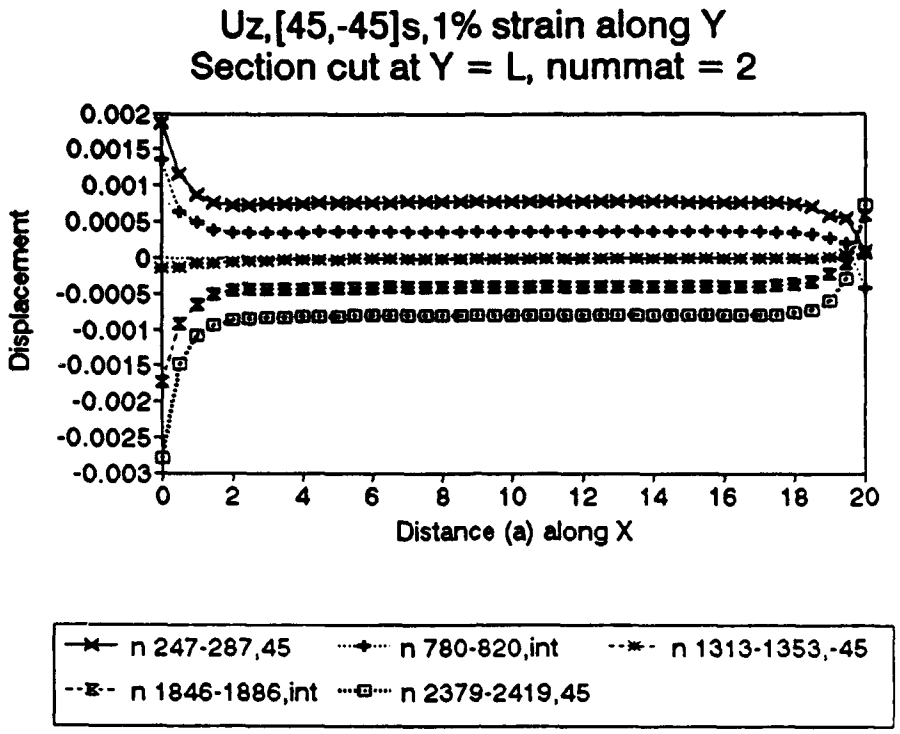

Figure 1.17

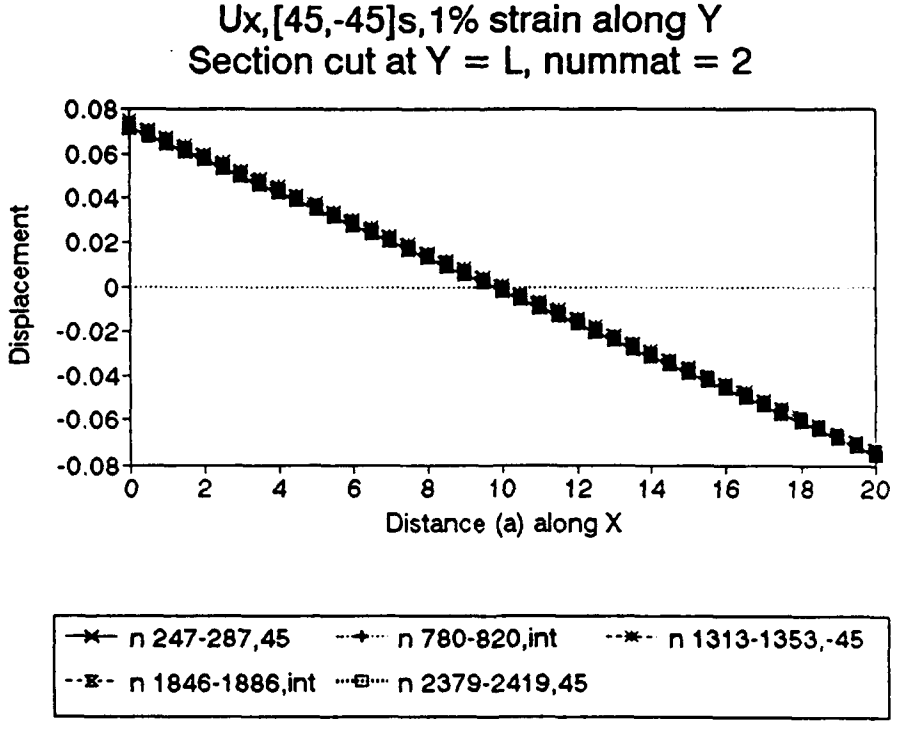

Figure 1.18

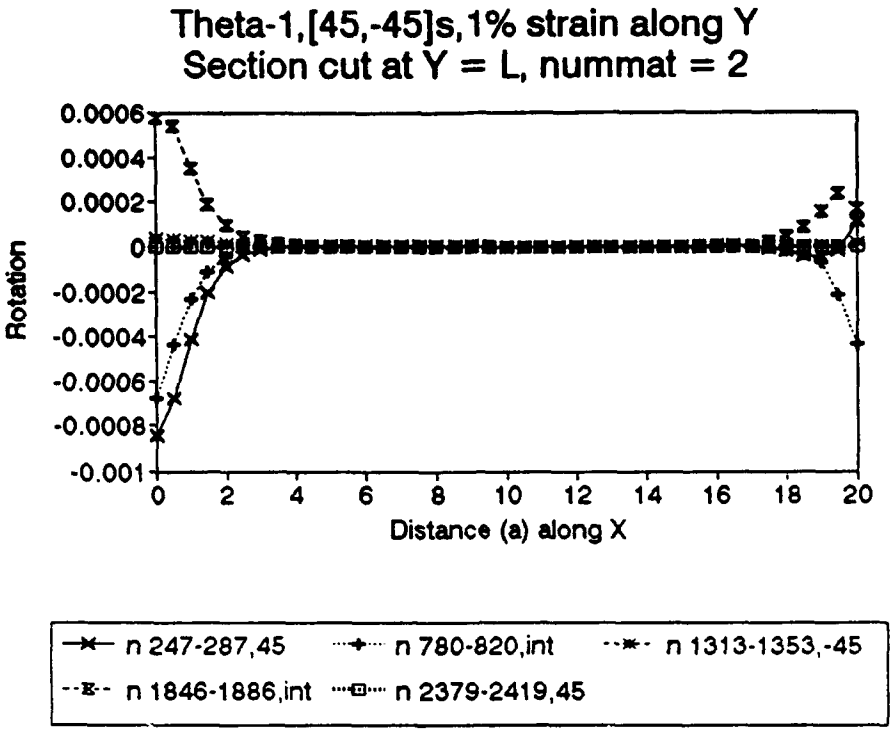

Figure 1.19

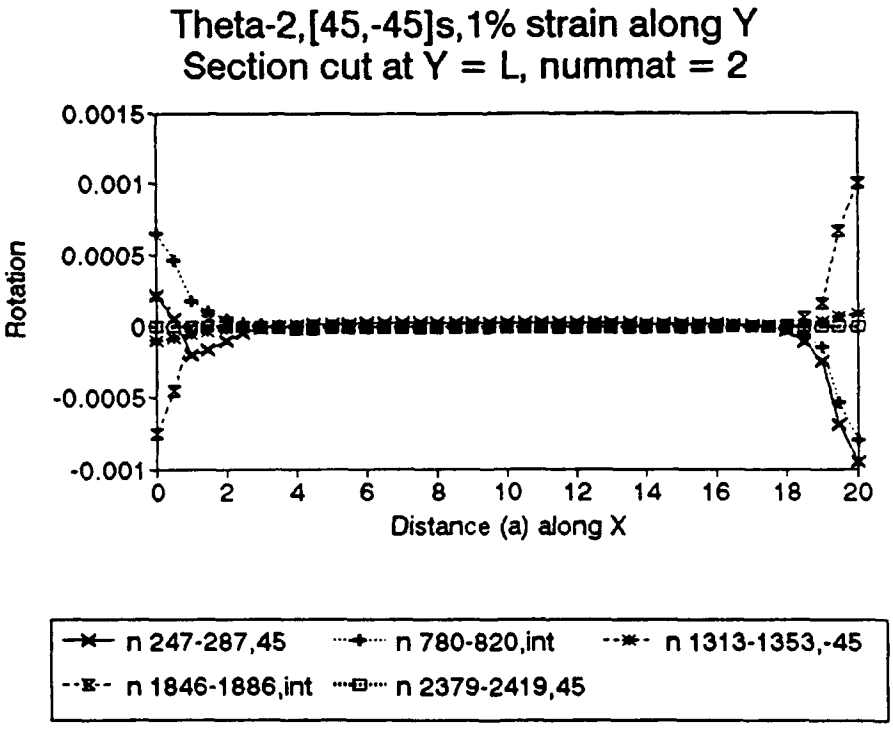

Figure 1.20

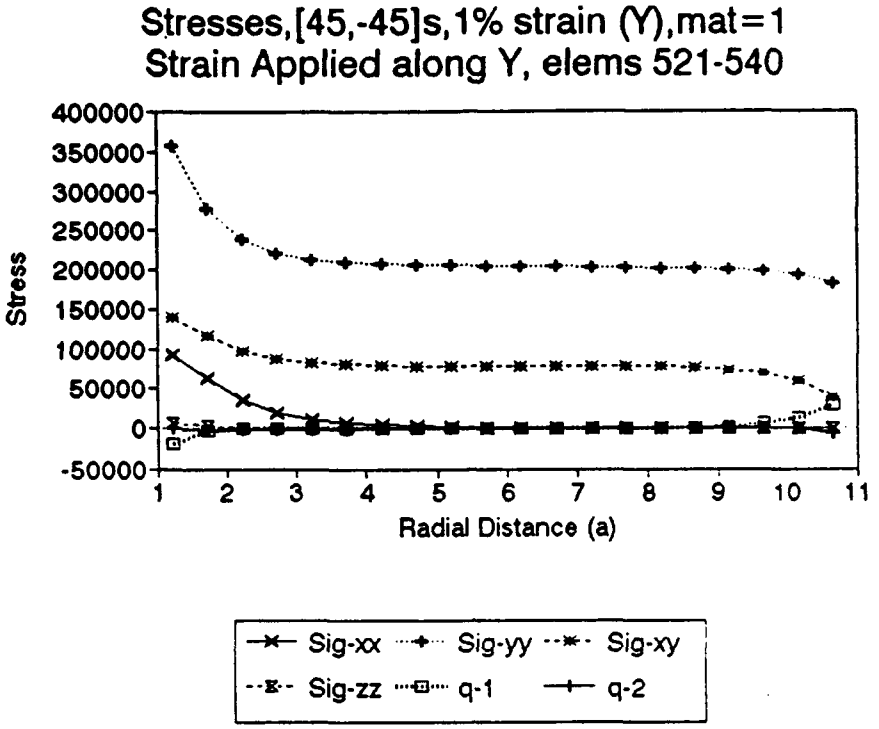

Figure 2.1

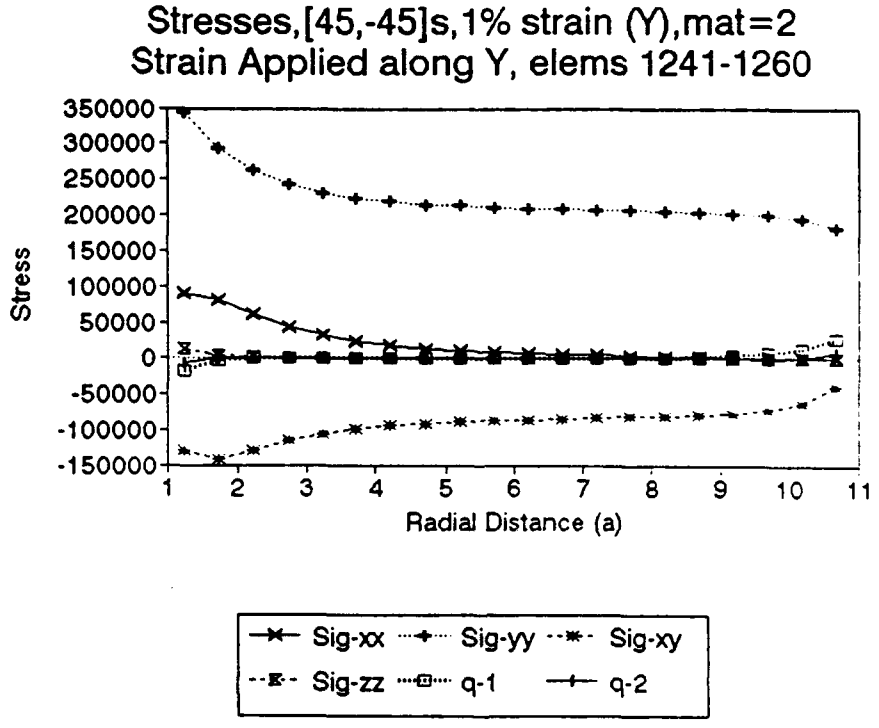

Figure 2.2

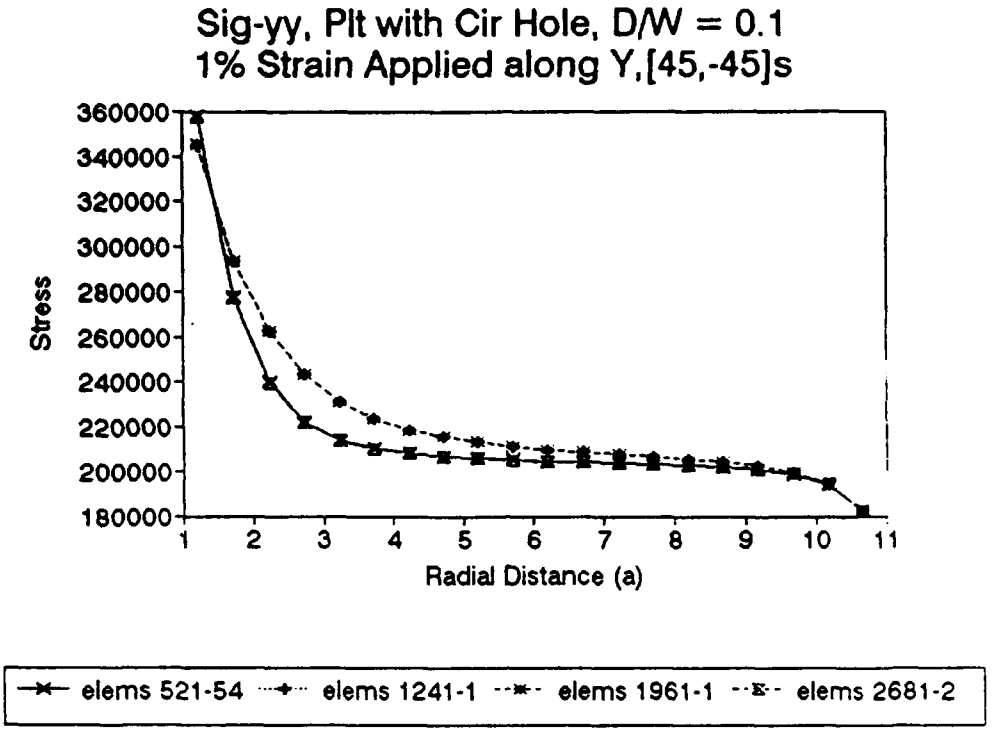

Figure 2.3

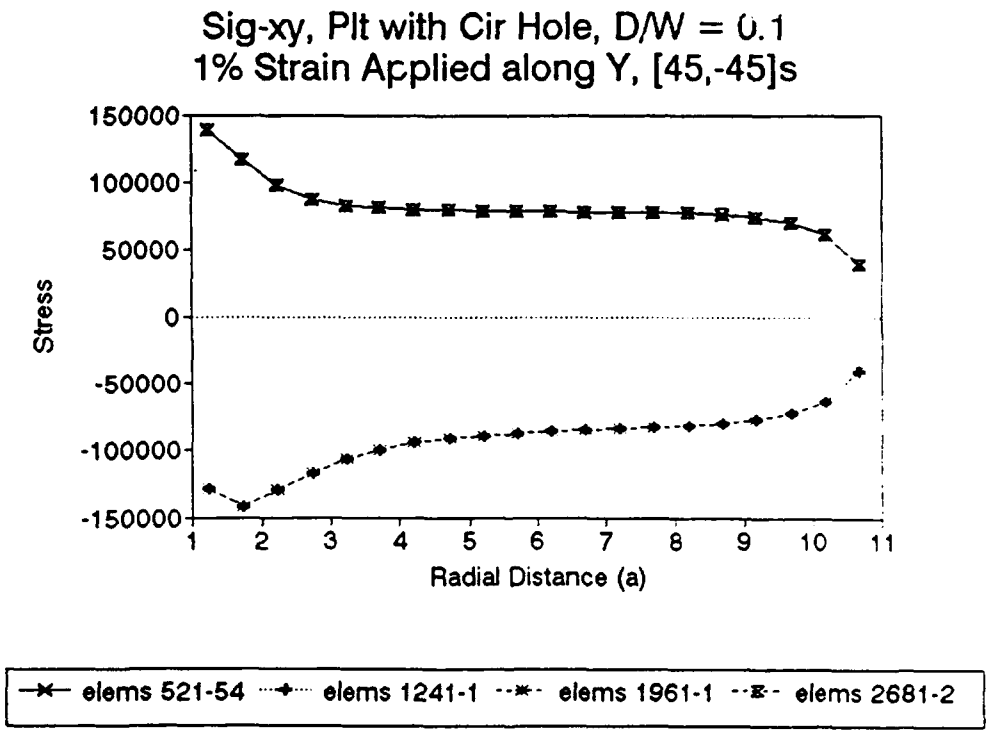

Figure 2.4

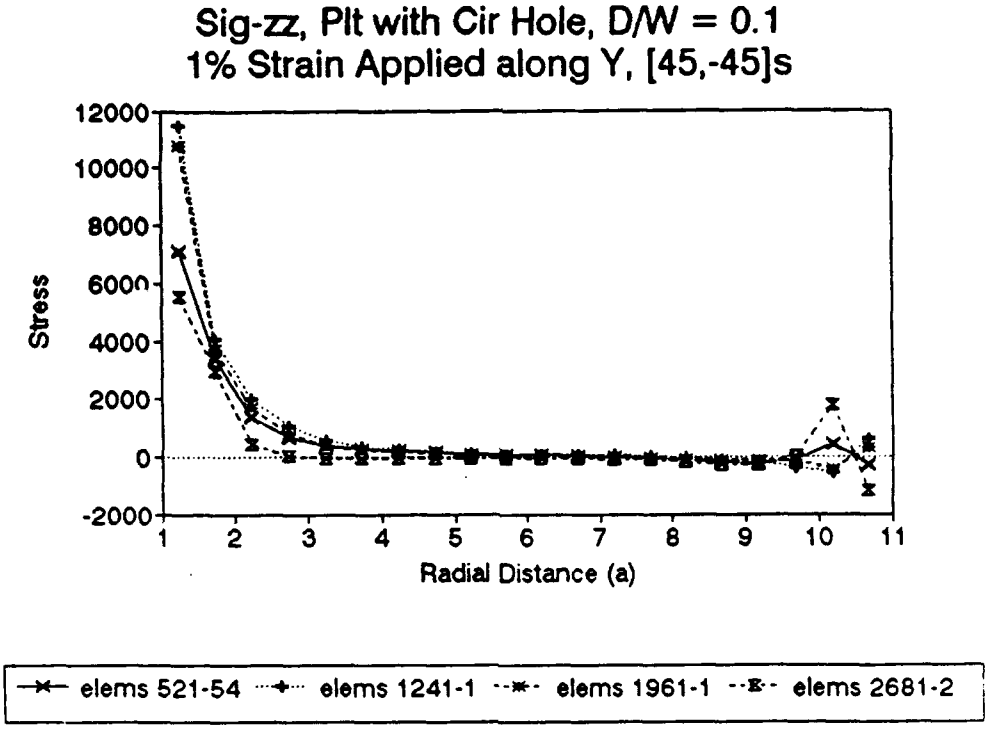

Figure 2.5

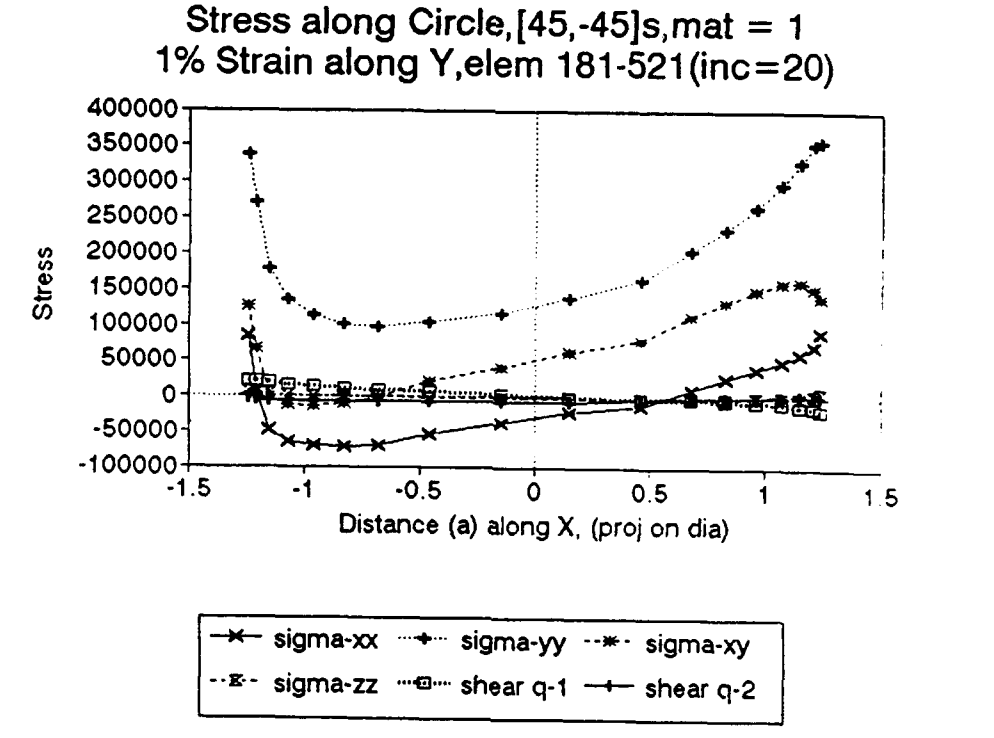

Figure 2.6

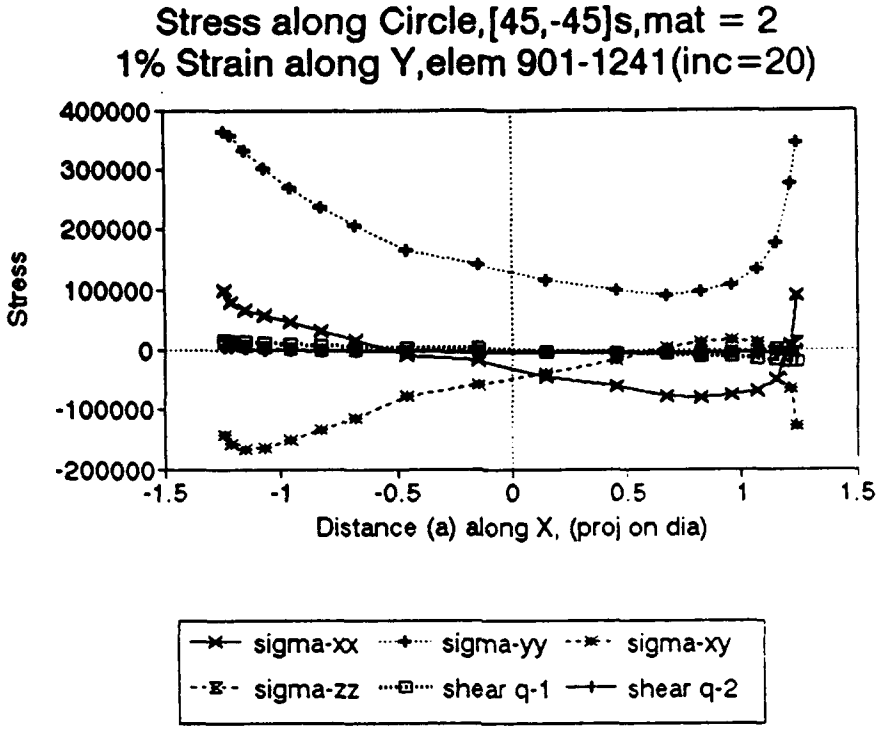

Figure 2.7

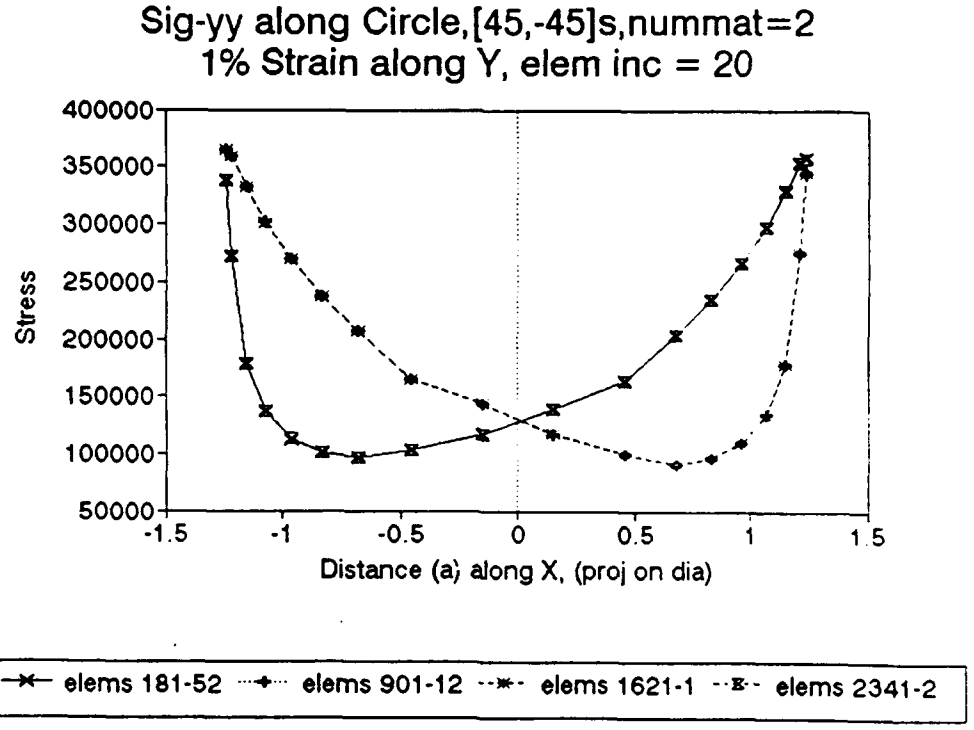

Figure 2.8

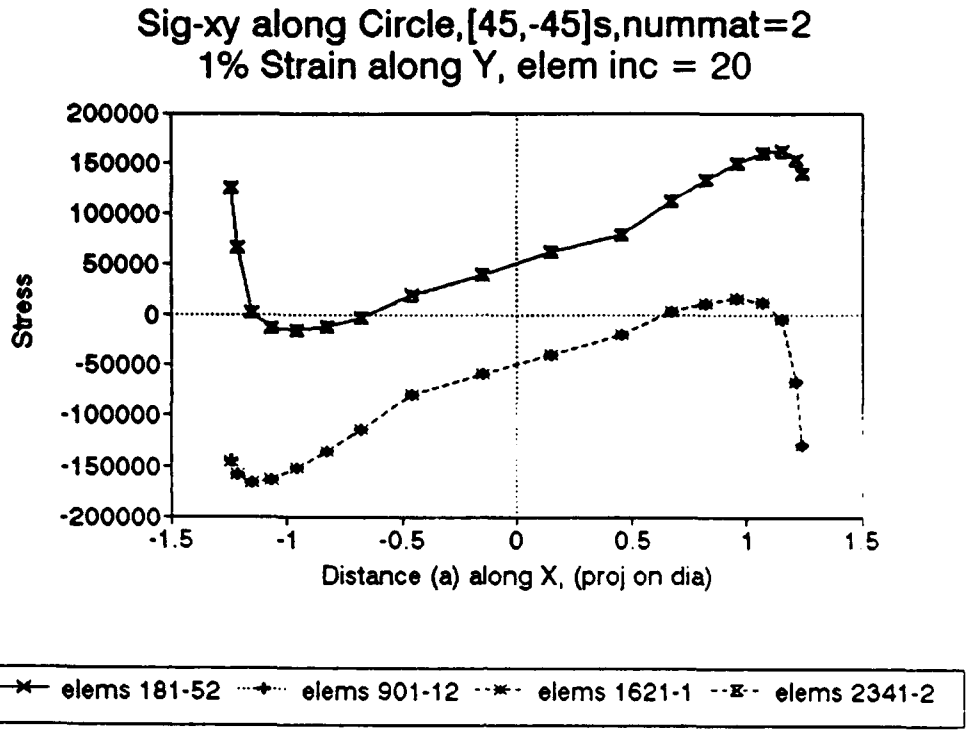

Figure 2.9

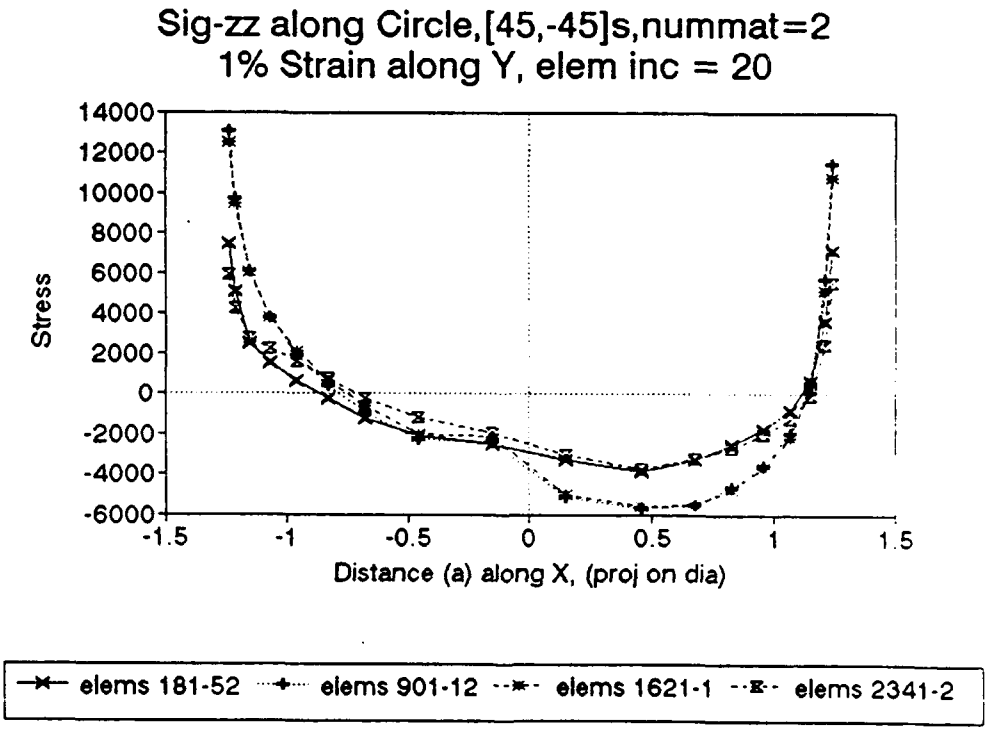

Figure 2.10

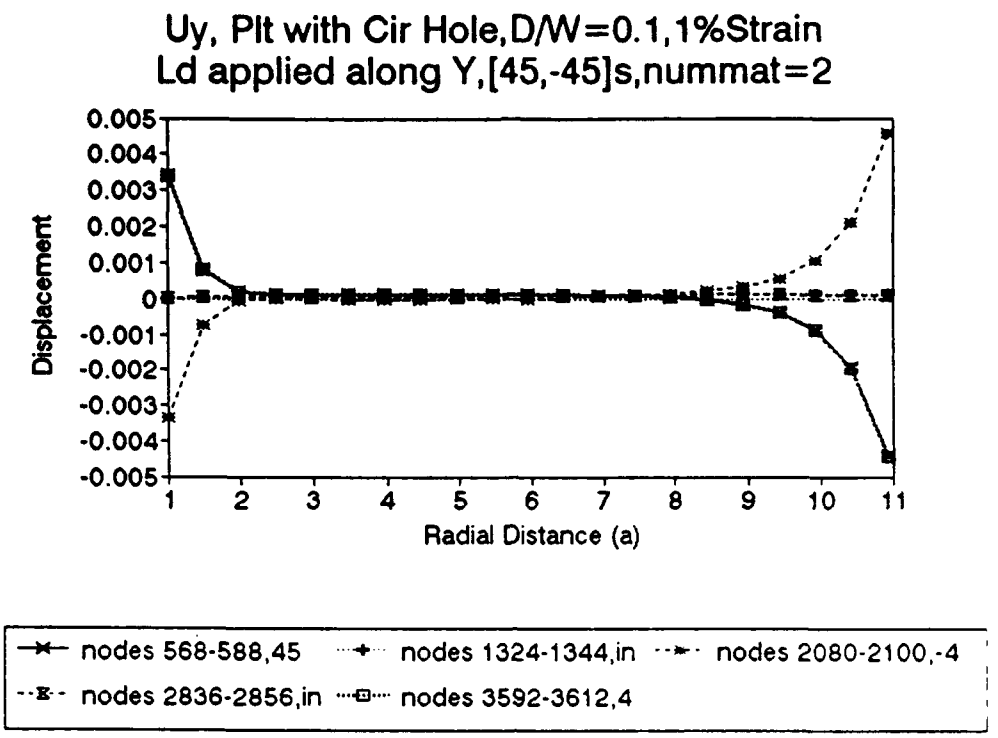

Figure 2.11

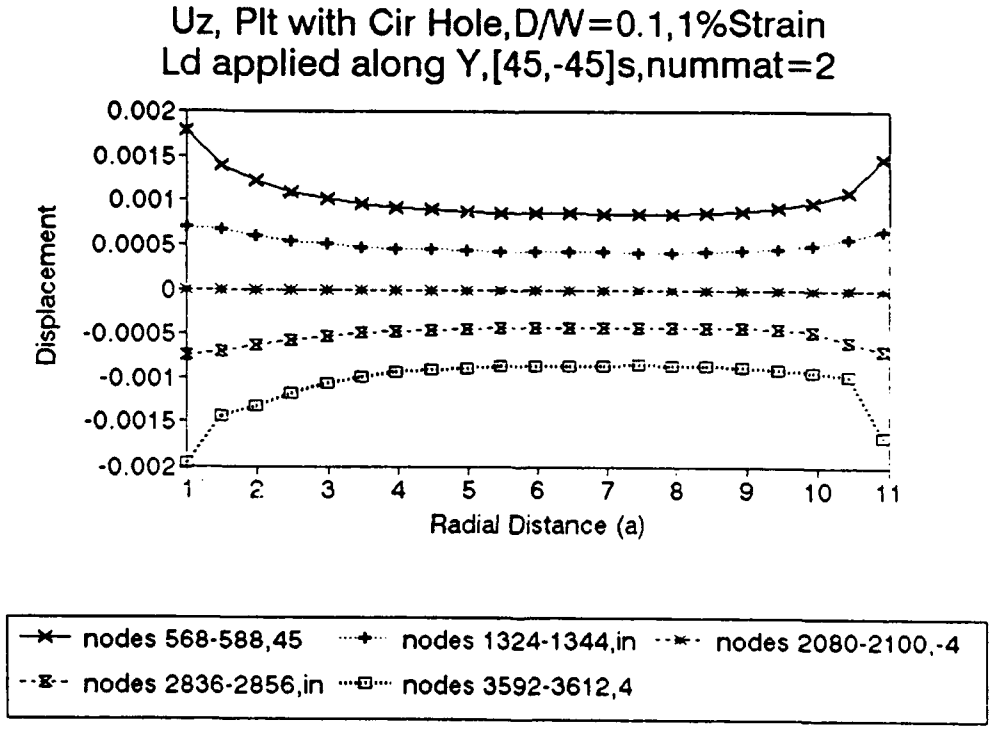

Figure 2.12

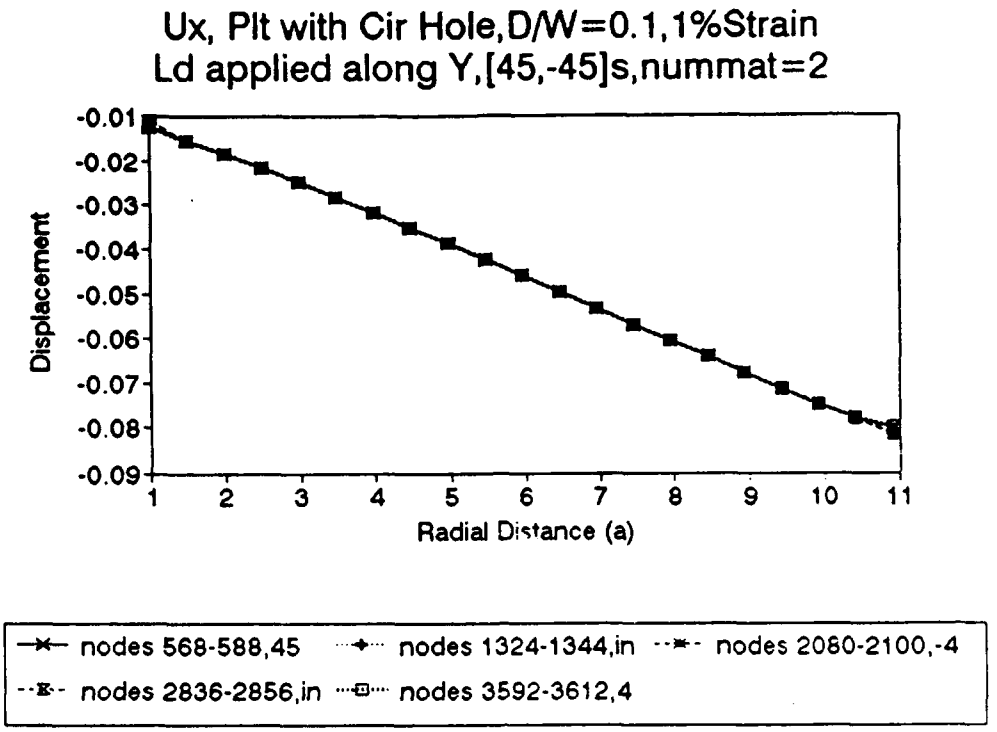

Figure 2.13

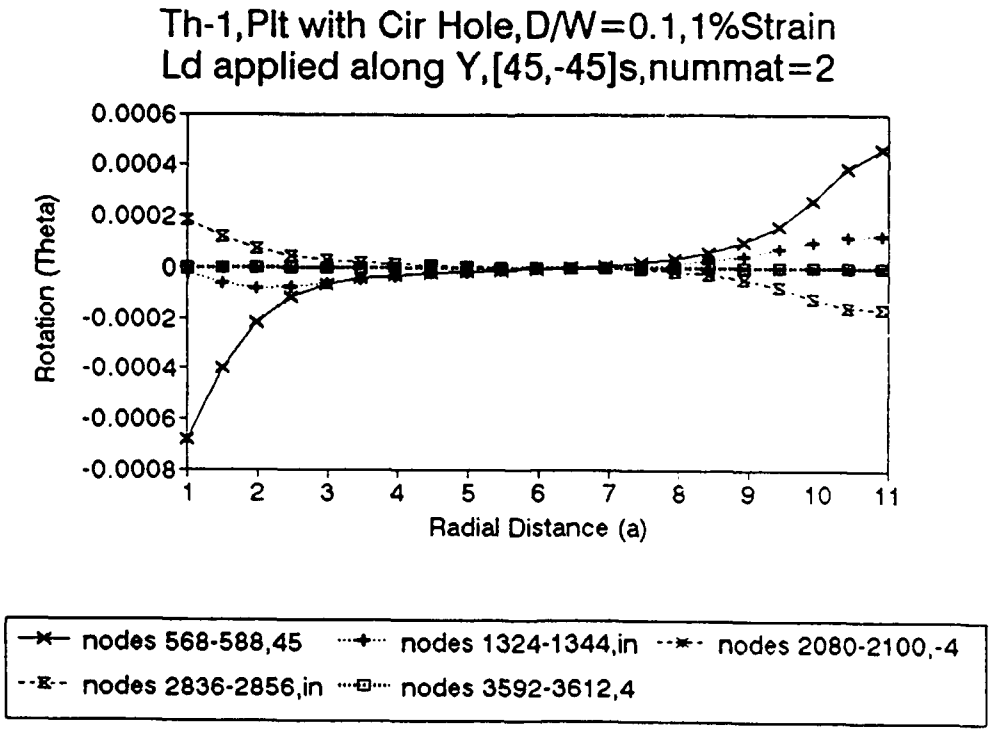

Figure 2.14

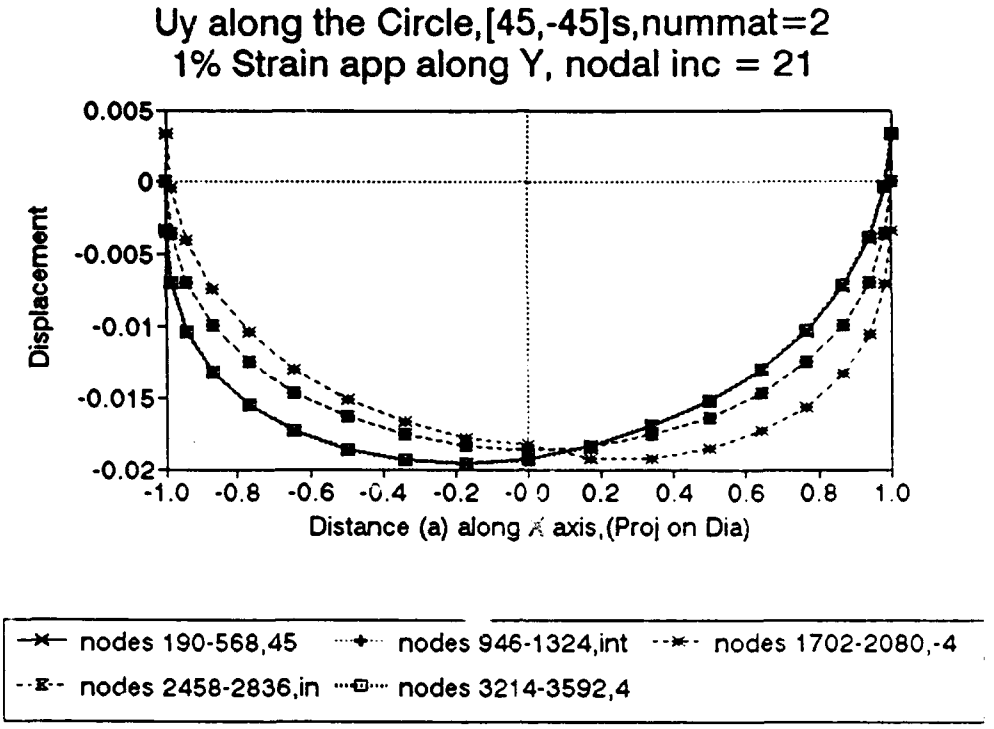

Figure 2.15

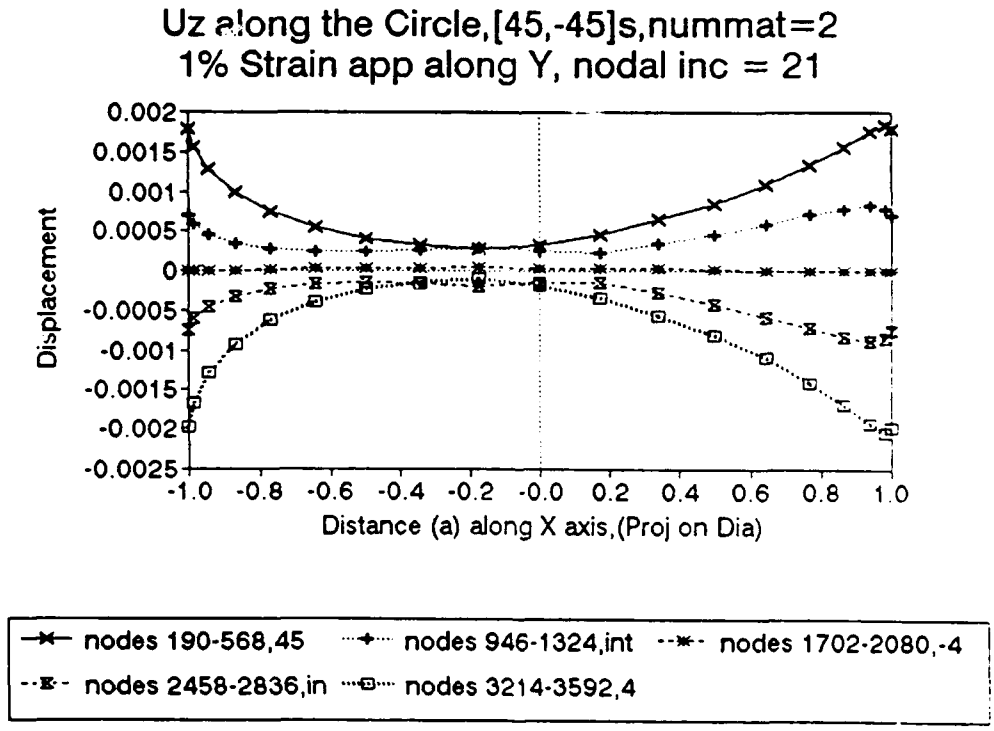

Figure 2.16

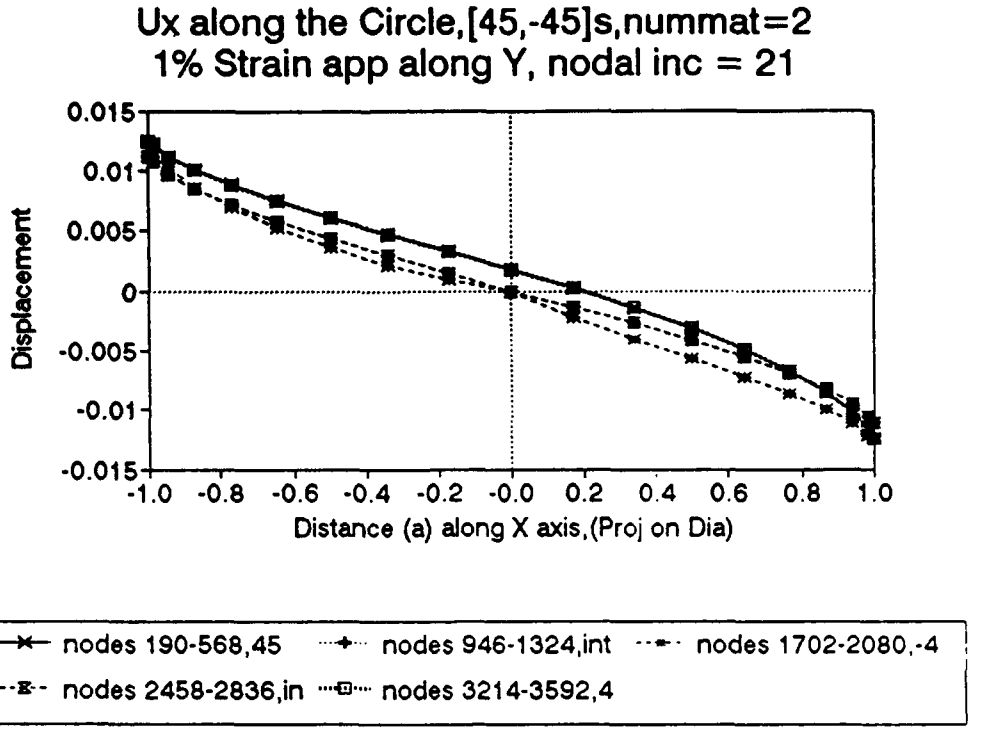

Figure 2.17

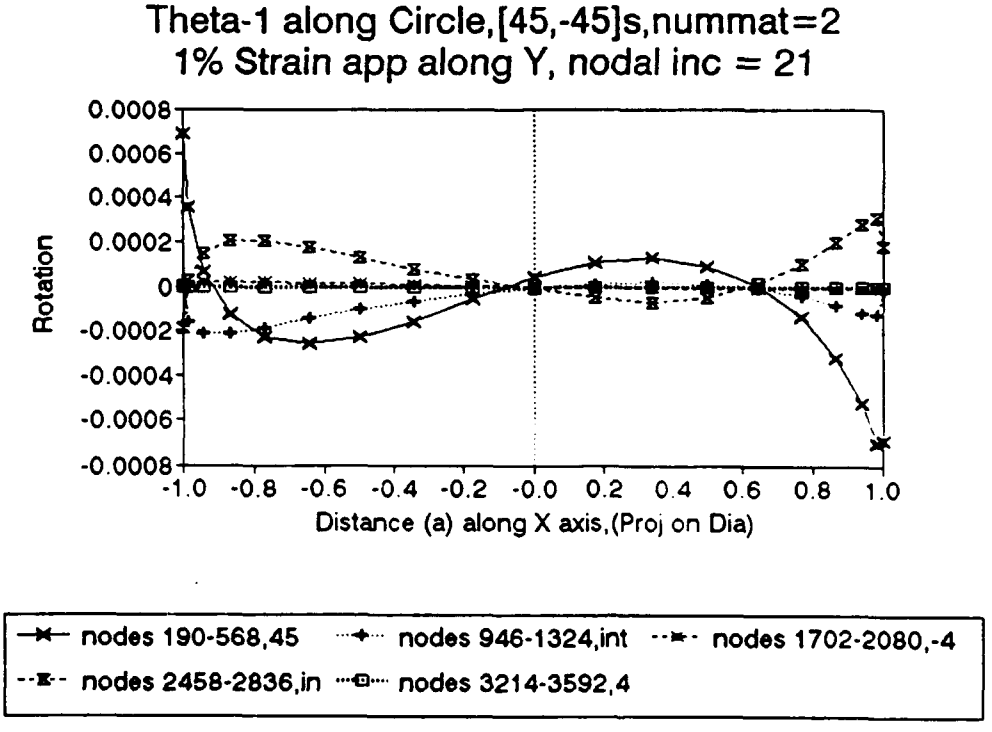

Figure 2.18

BASE

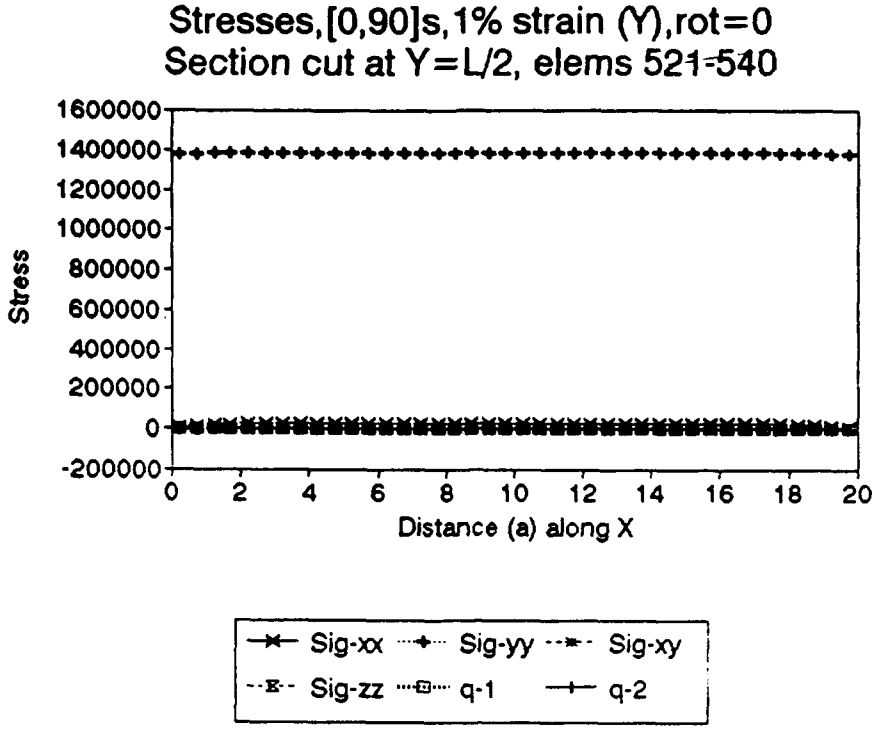

Figure 3.1

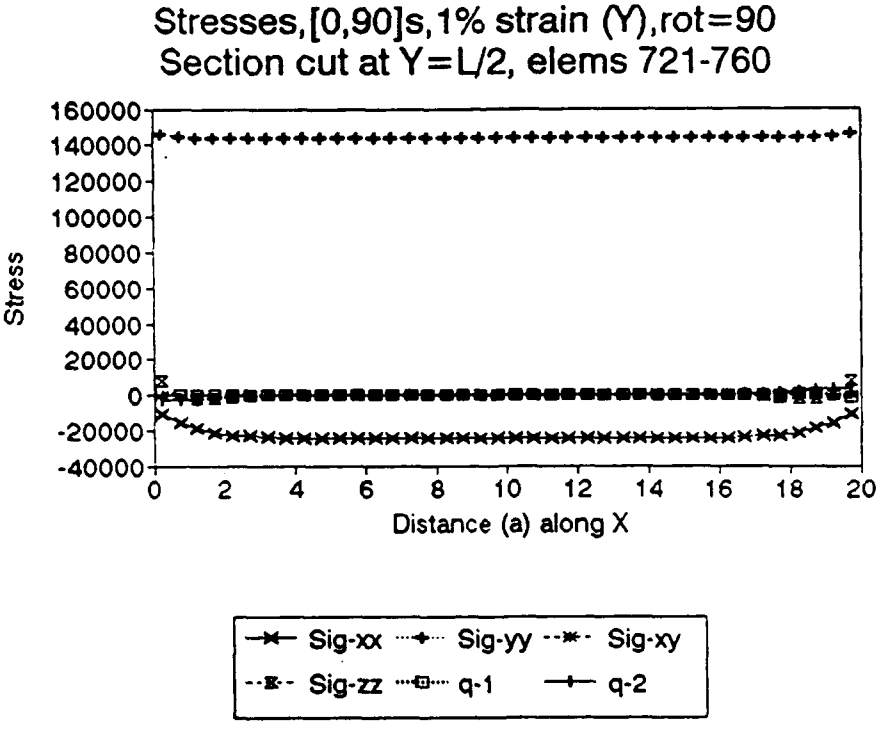

Figure 3.2

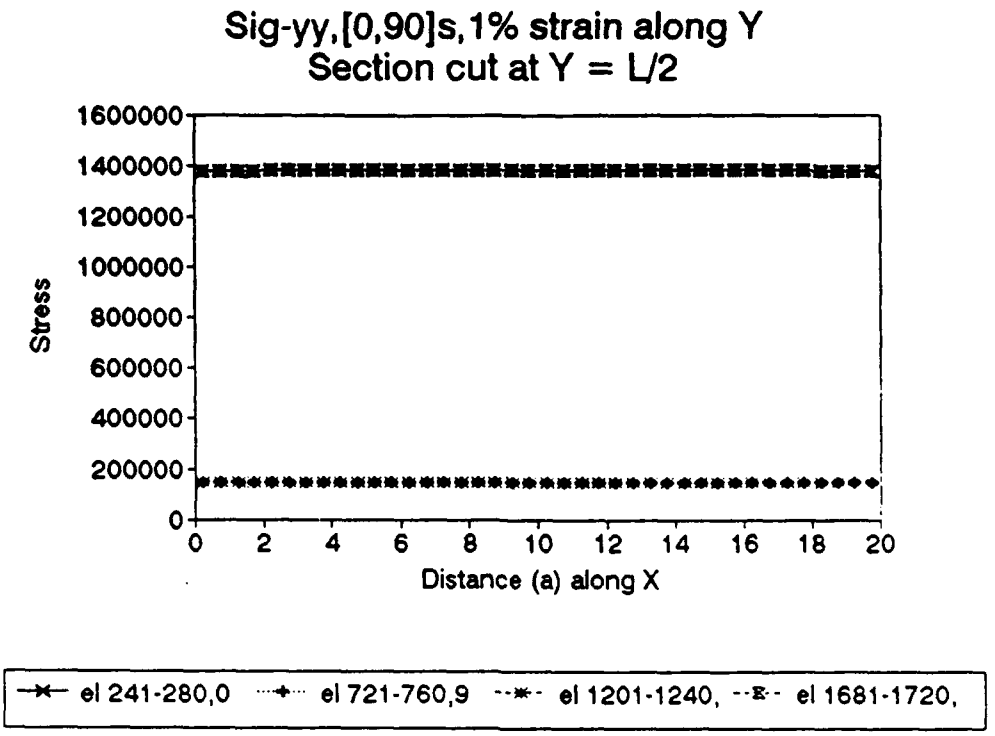

Figure 3.3

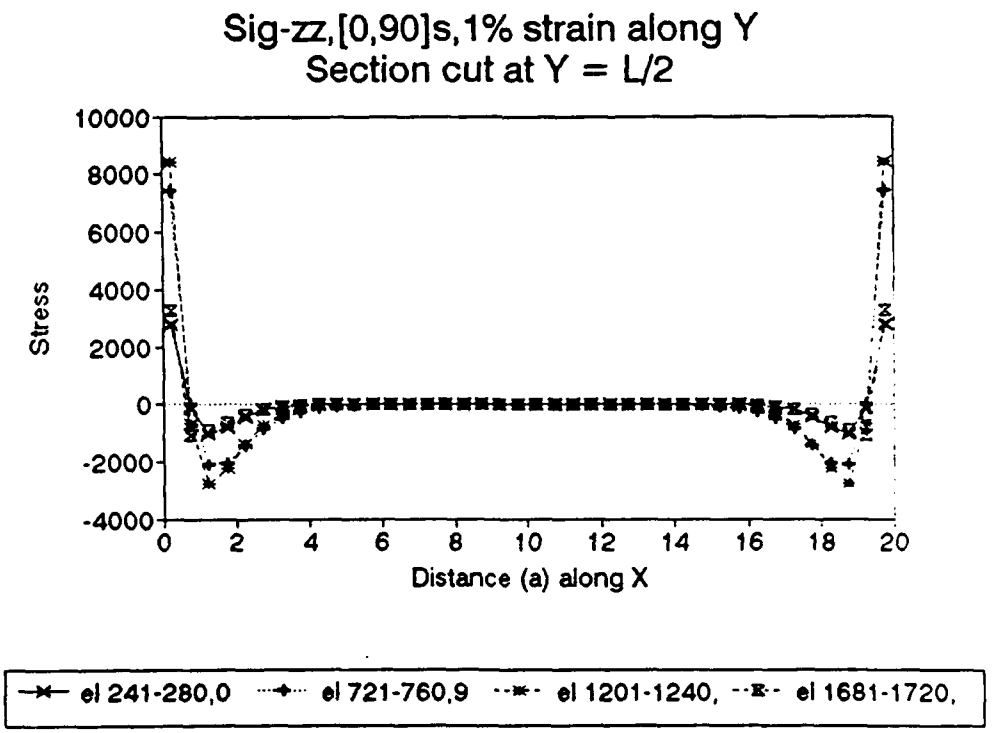

Figure 3.4

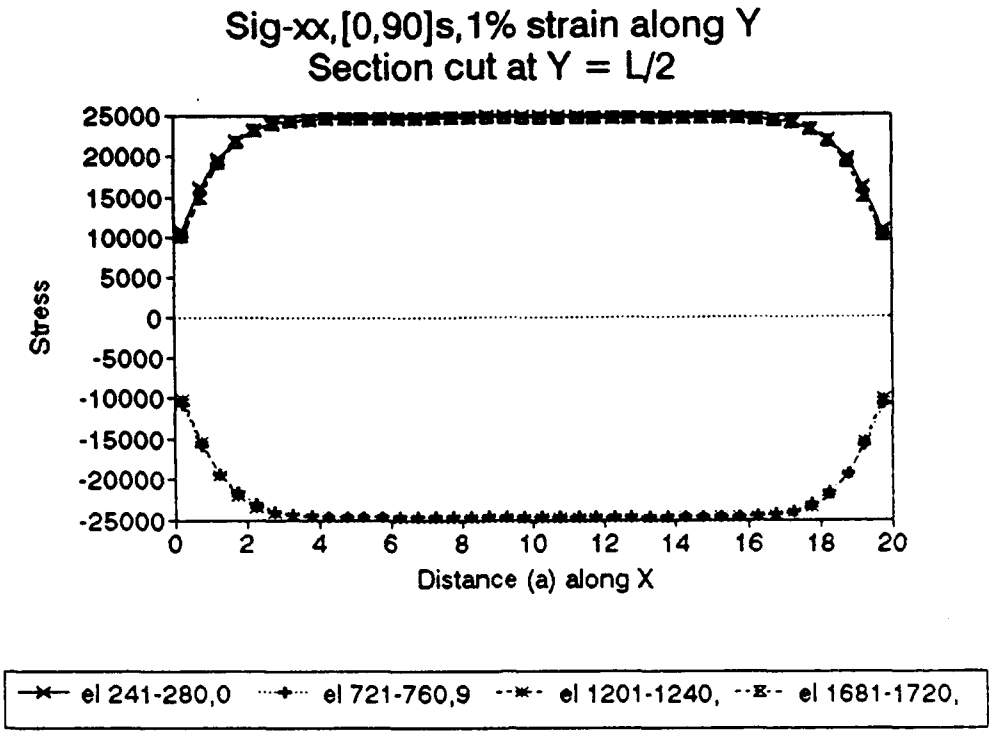

Figure 3.5

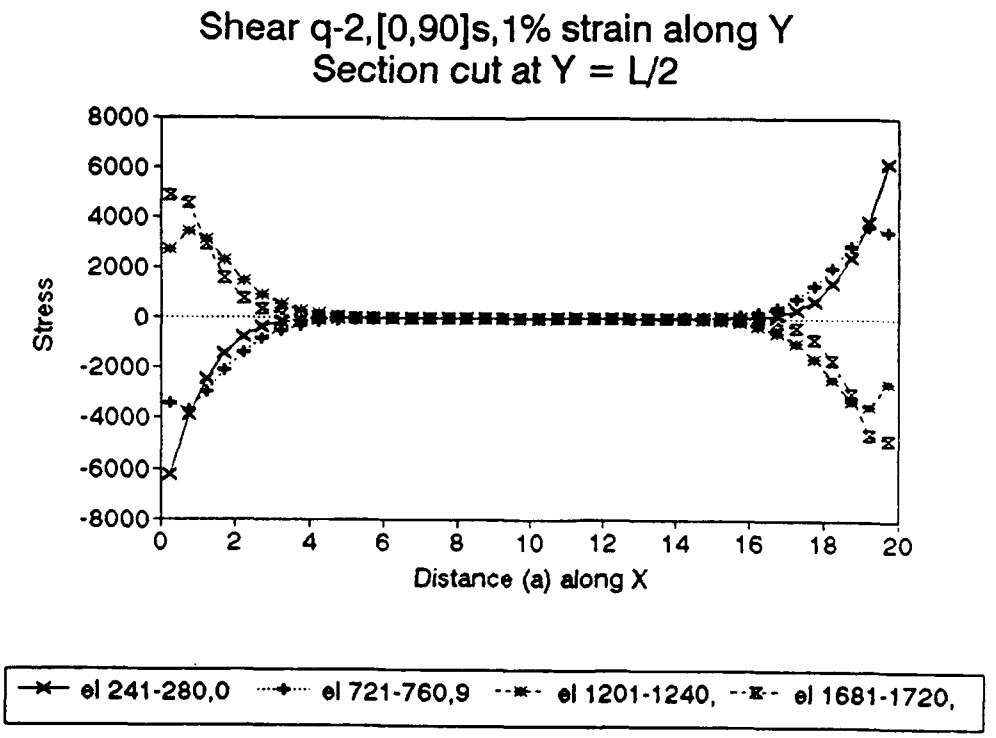

Figure 3.6

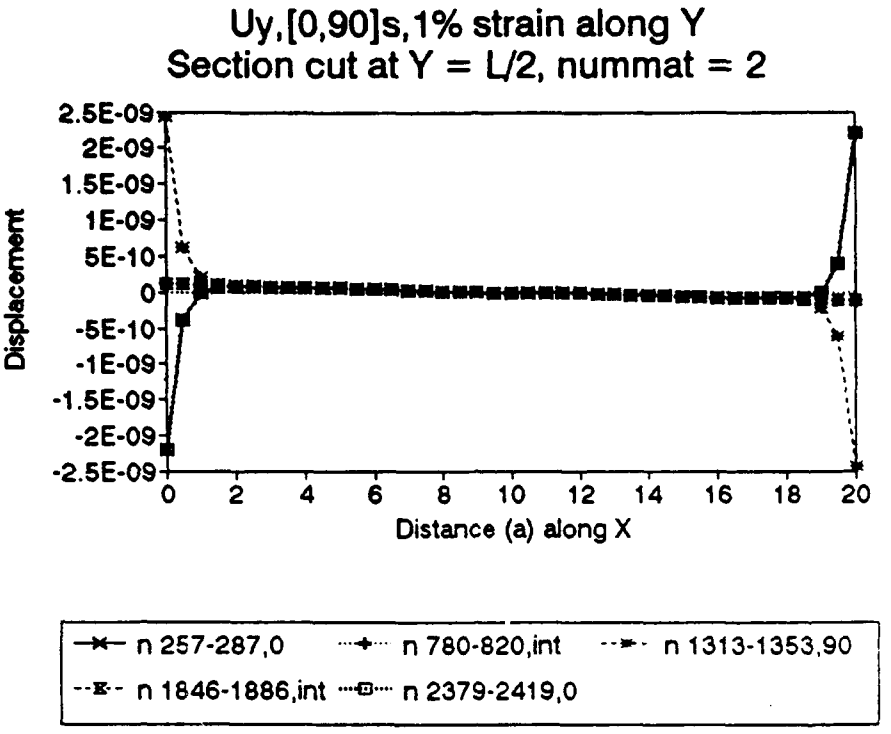

Figure 3.7

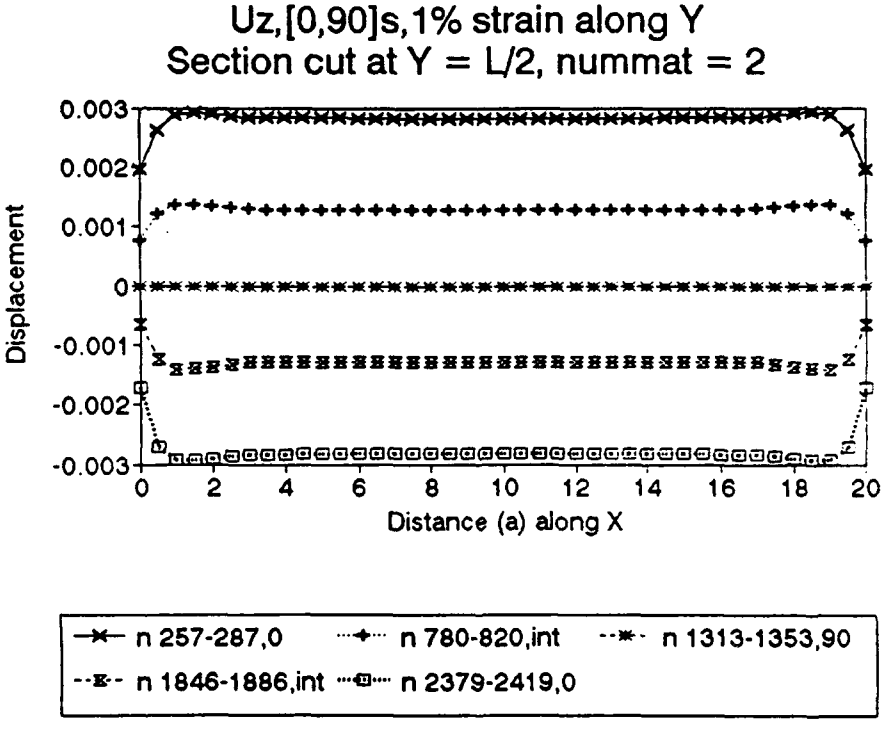

Figure 3.8

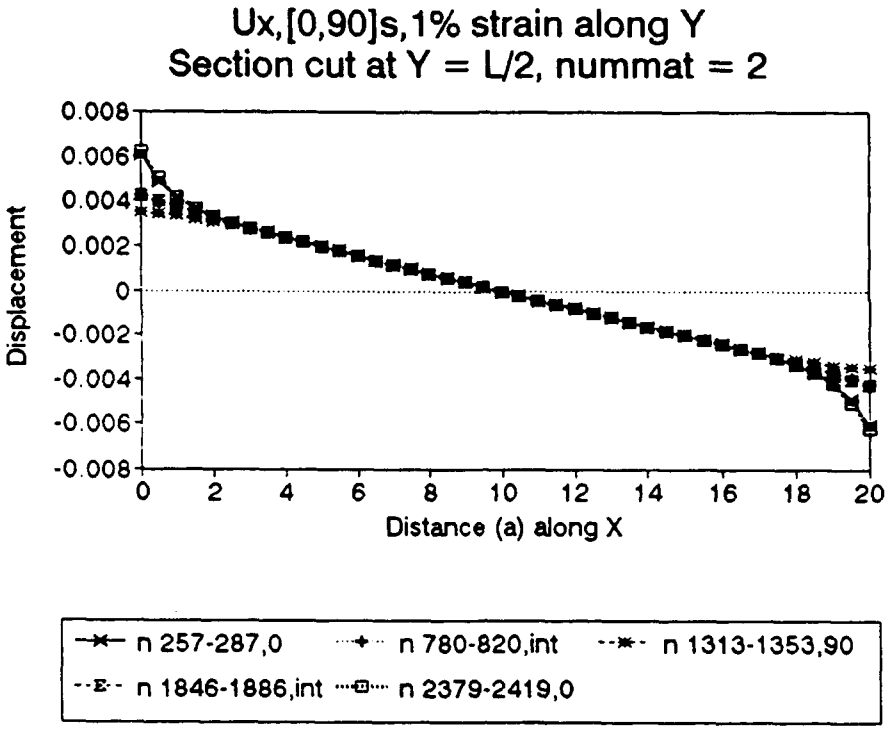

Figure 3.9

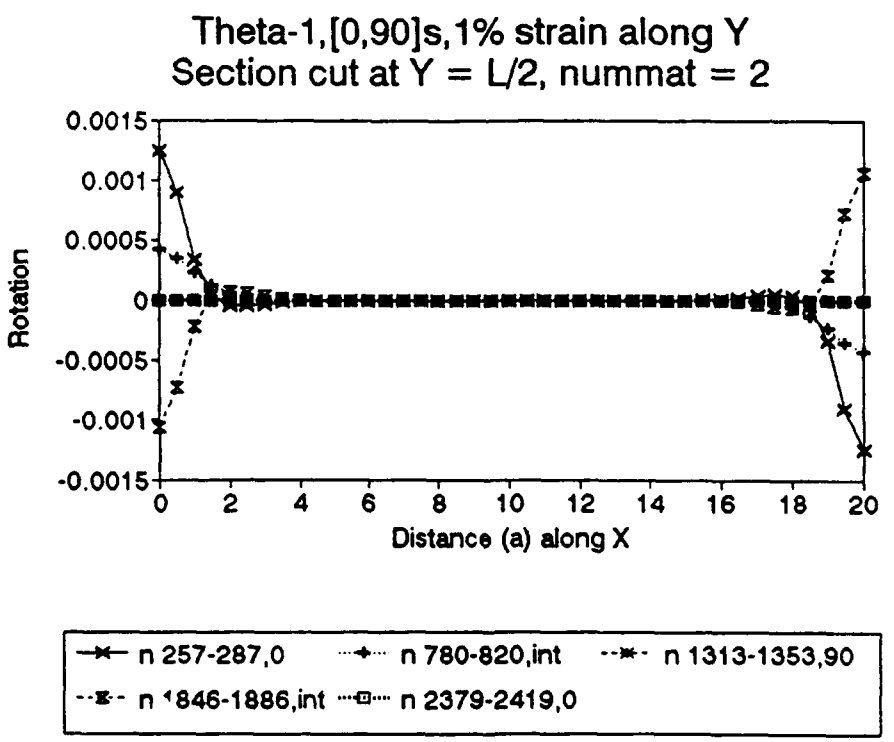

Figure 3.10

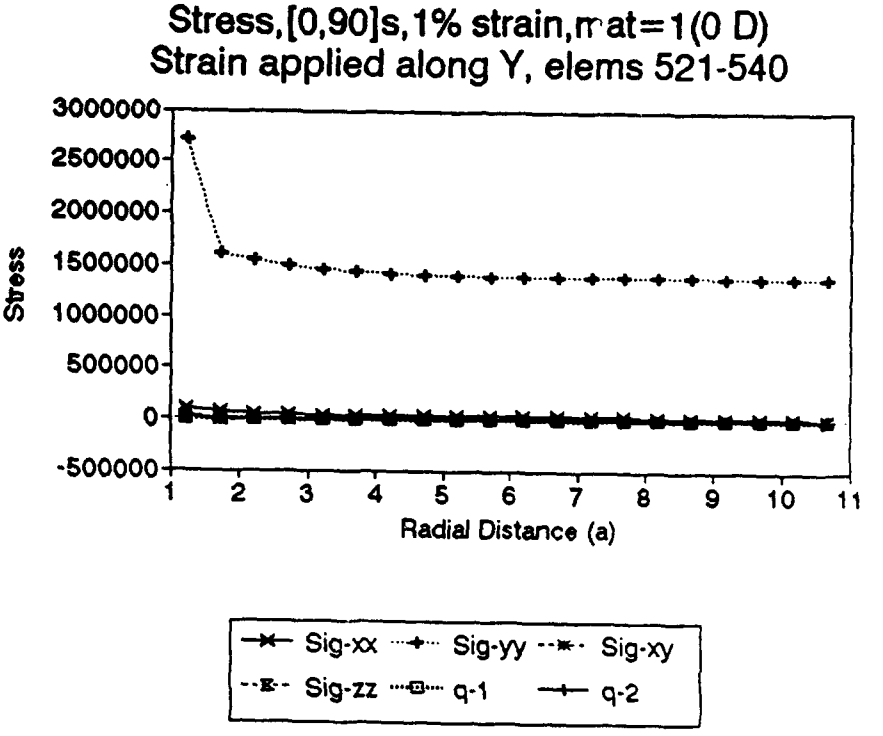

Figure 4.1

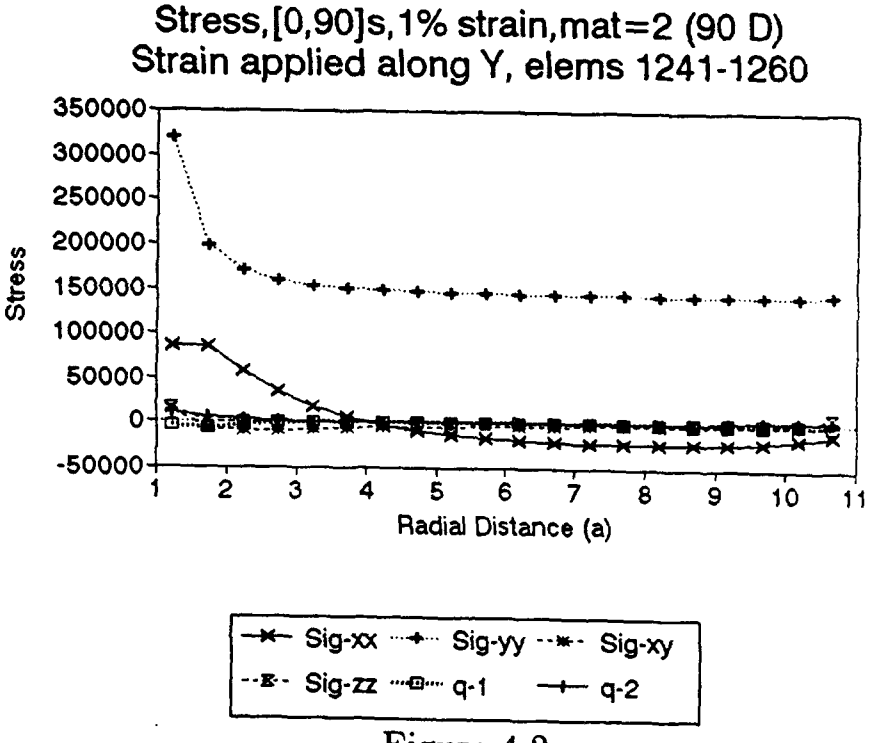

Figure 4.2

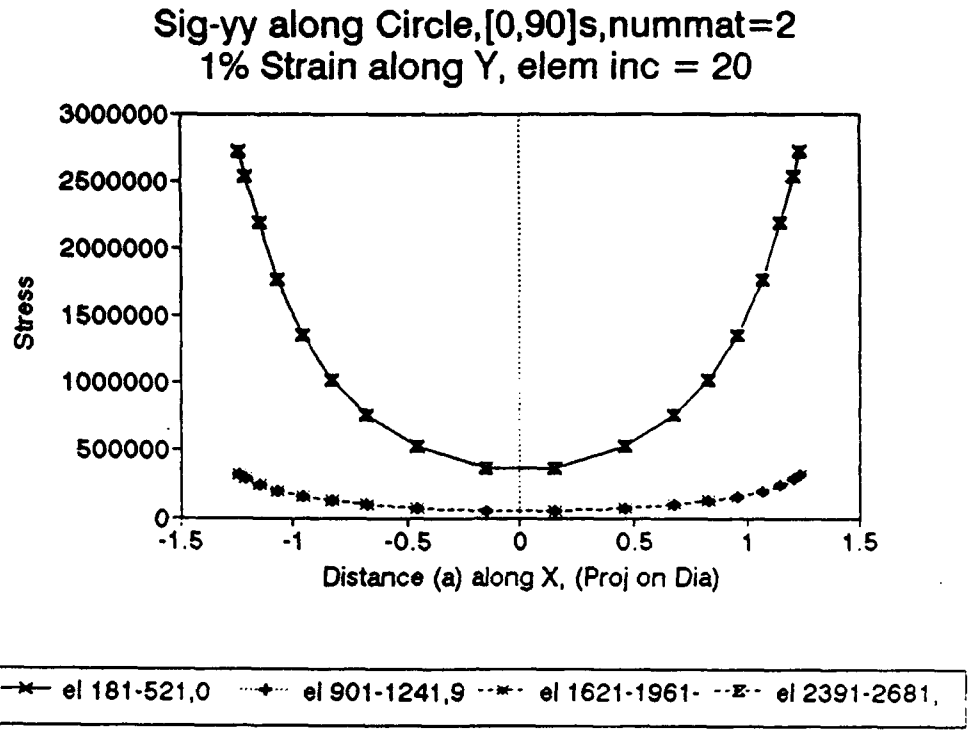

Figure 4.3

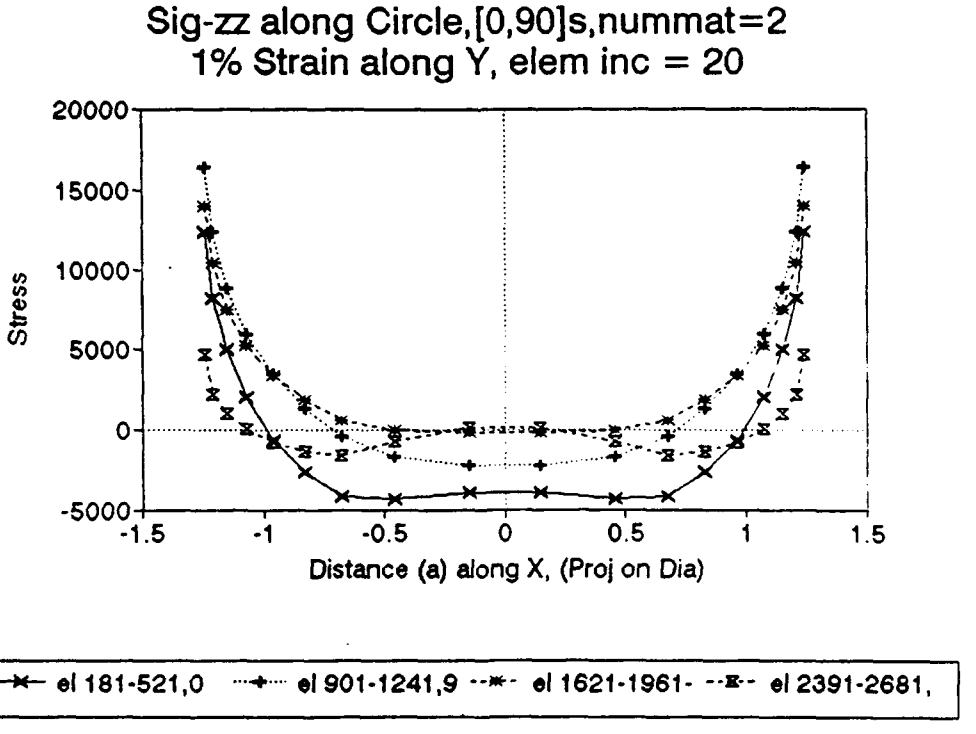

Figure 4.4

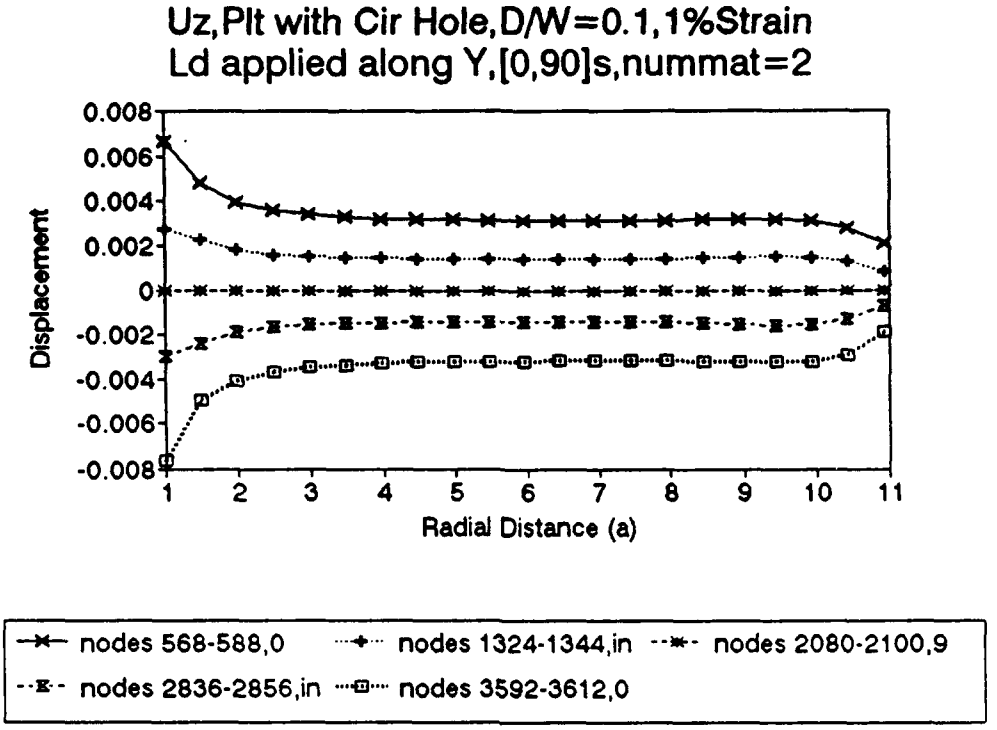

Figure 4.5

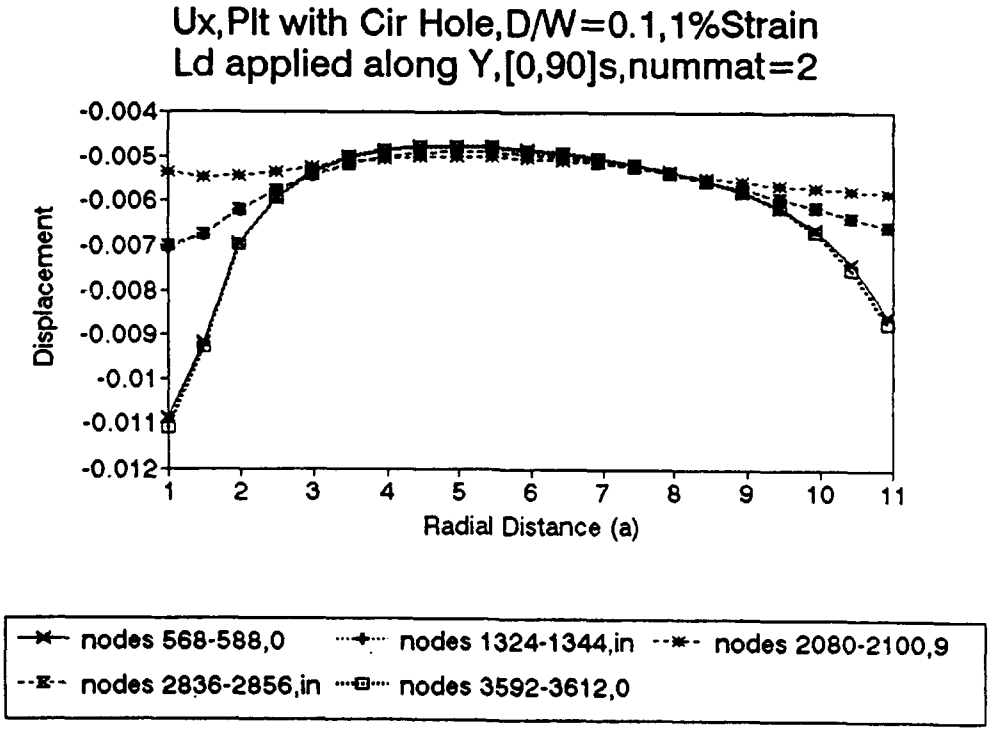

Figure 4.6

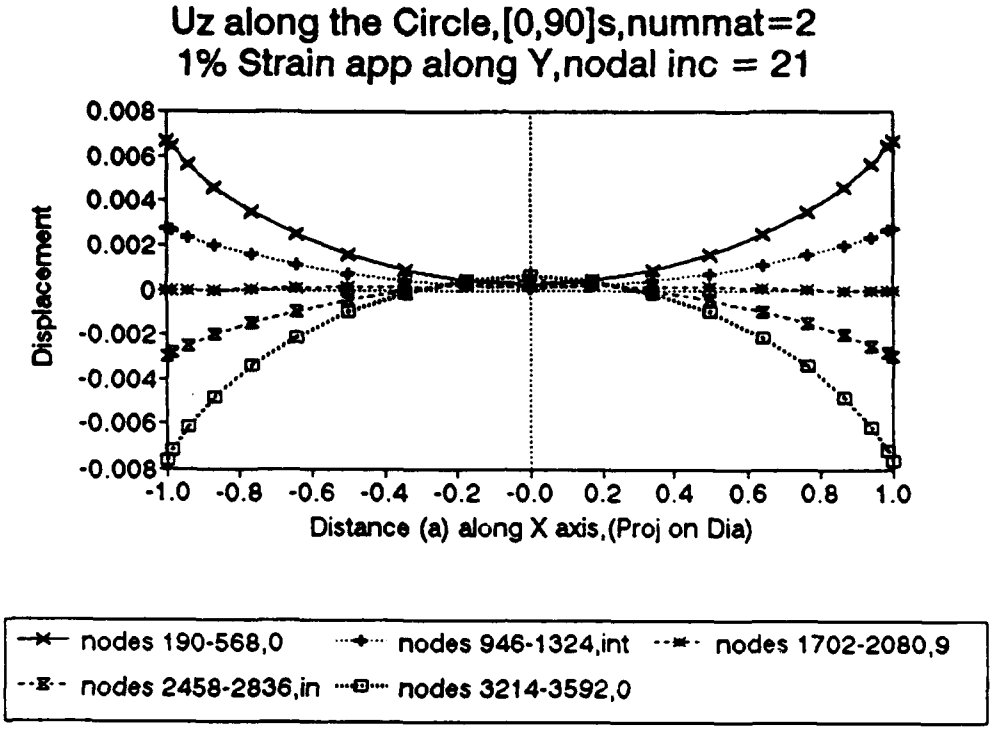

Figure 4.7

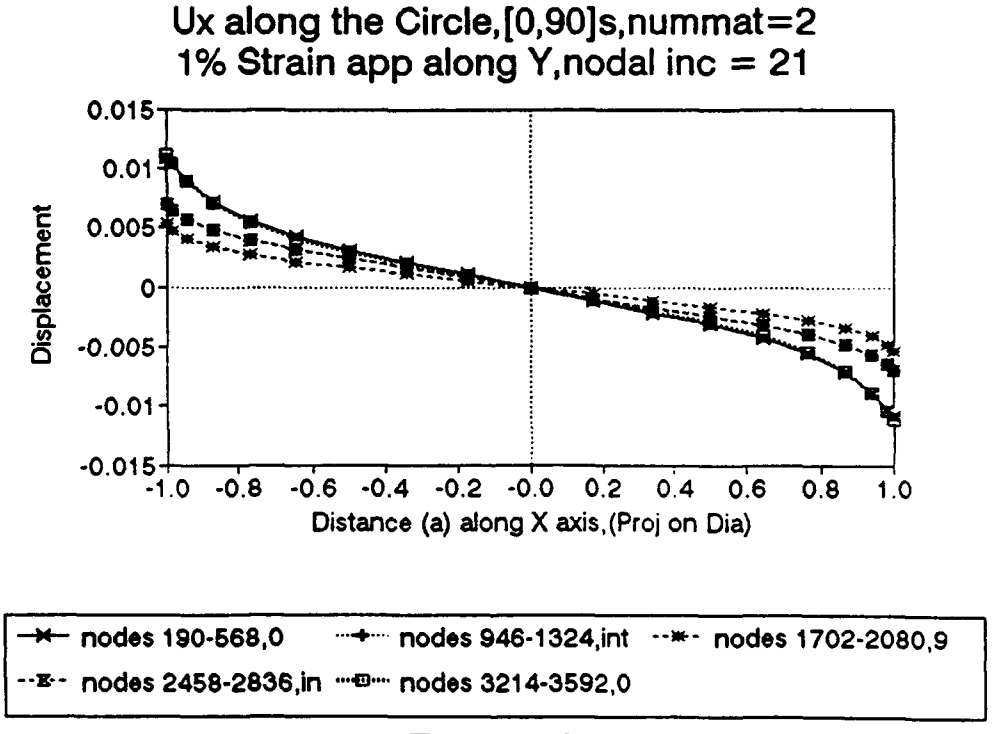

Figure 4.8

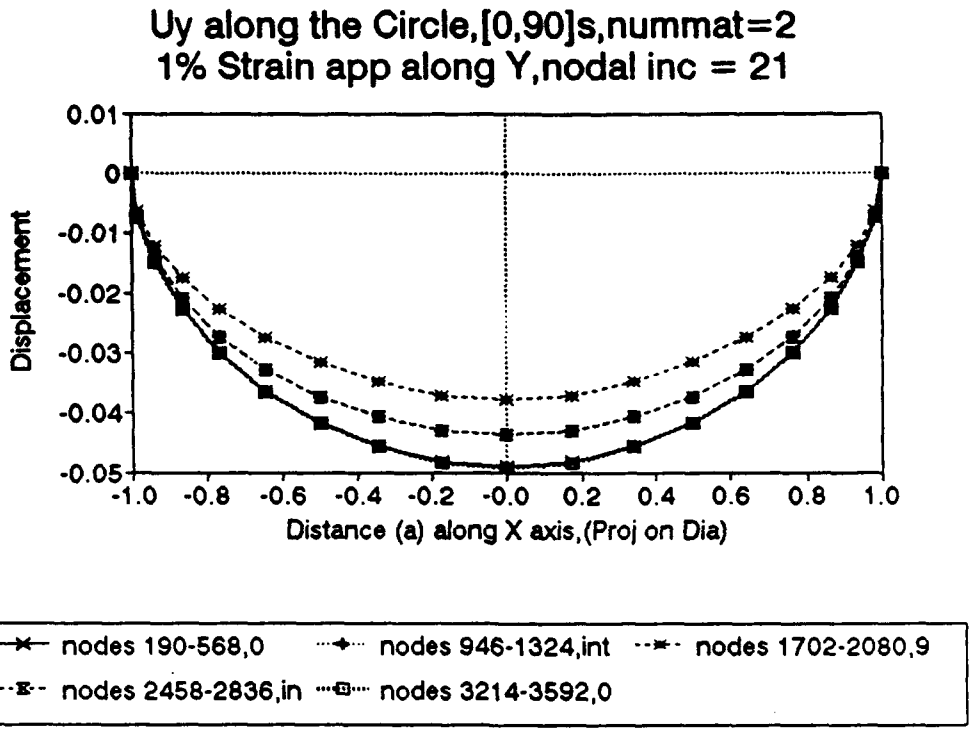
Uy along the Circle,[0,90]s,nummat=2
1% Strain app along Y,nodal inc = 21
Displacement
0.01
0
-0.01
-0.02
-0.03
-0.04
-0.05
-1.0
-0.8
-0.6
-0.4
-0.2
-0.0
0.2
0.4
0.6
0.8
1.0
Distance (a) along X axis,(Proj on Dia)
nodes 190-568,0
nodes 946-1324,int
nodes 1702-2080,9
nodes 2458-2836,in
nodes 3214-3592,0

Figure 4.9

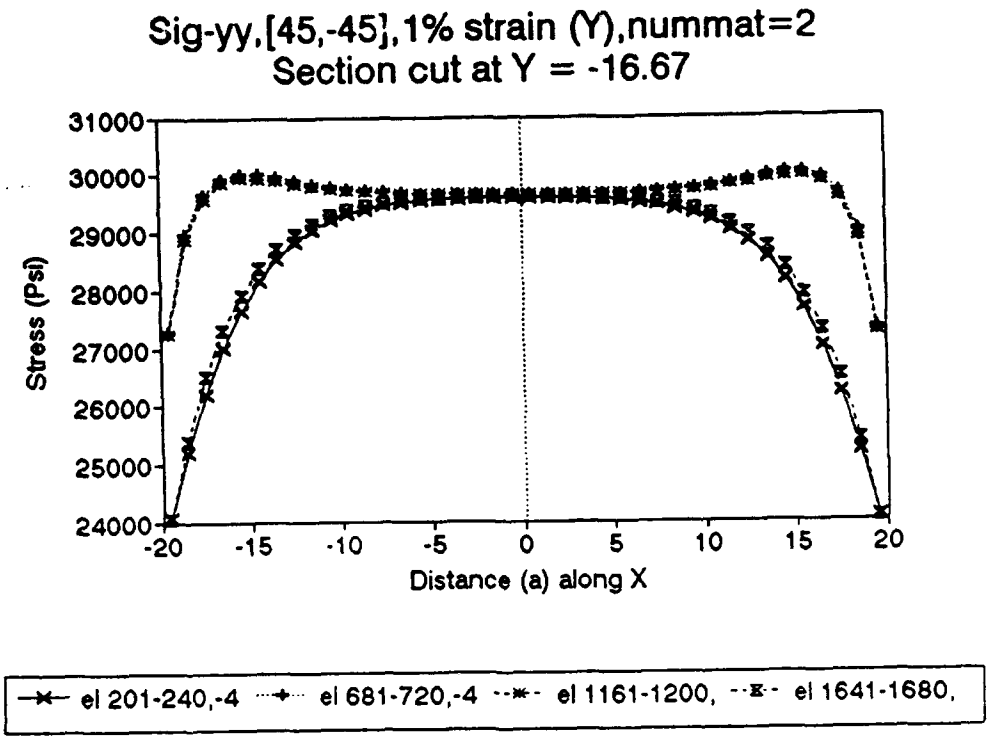

Figure 5.1

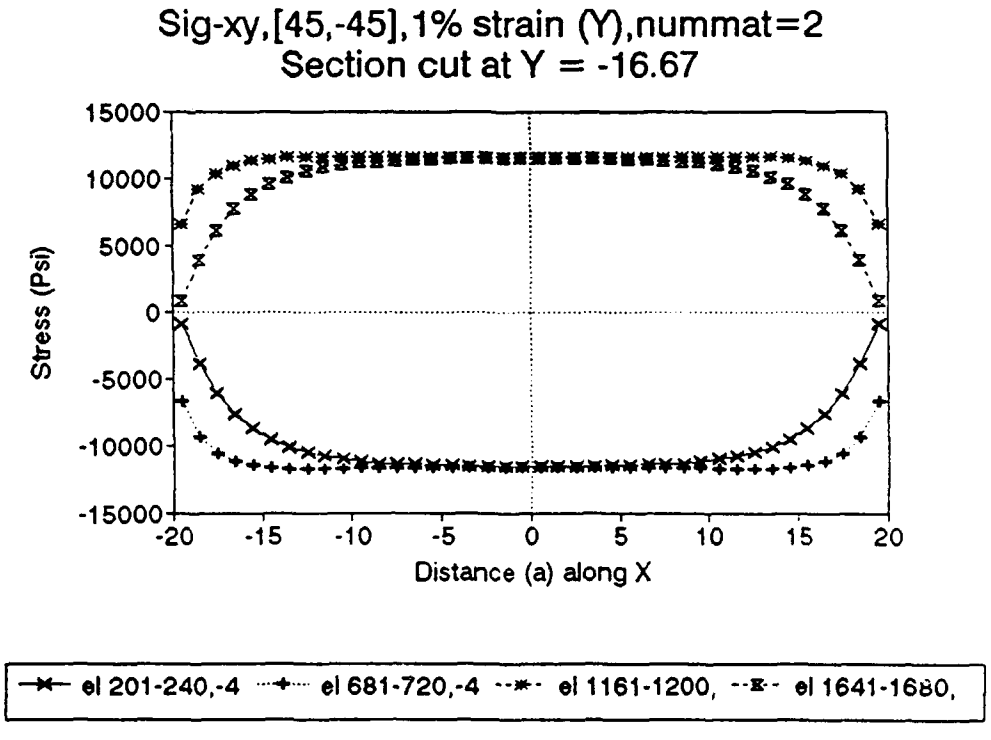

Figure 5.2

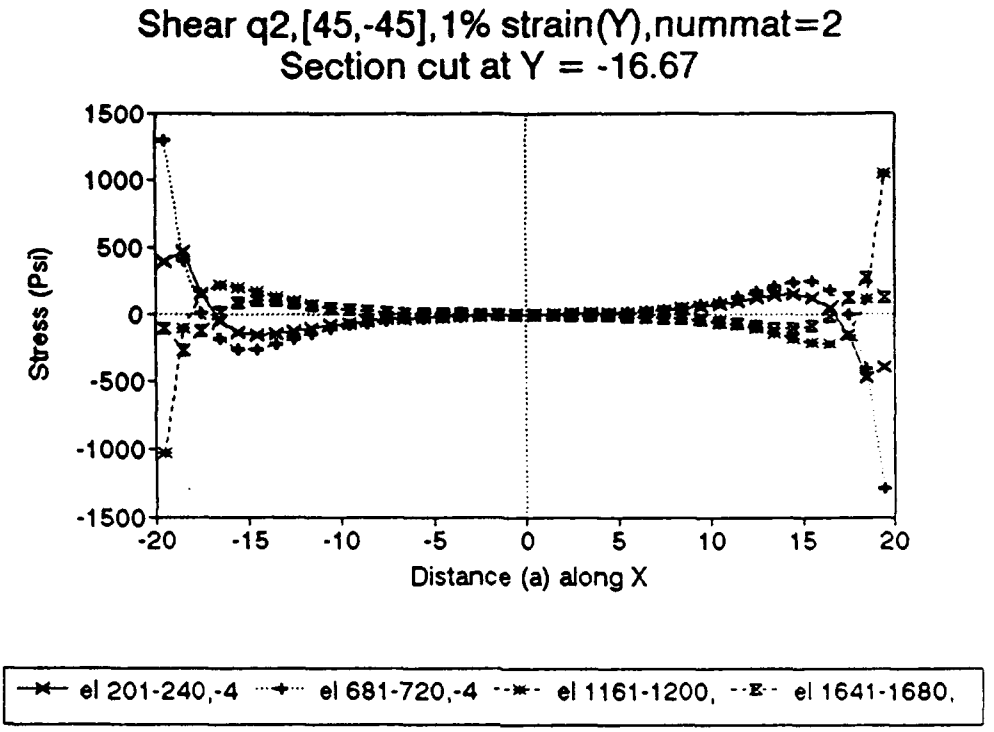

Figure 5.3

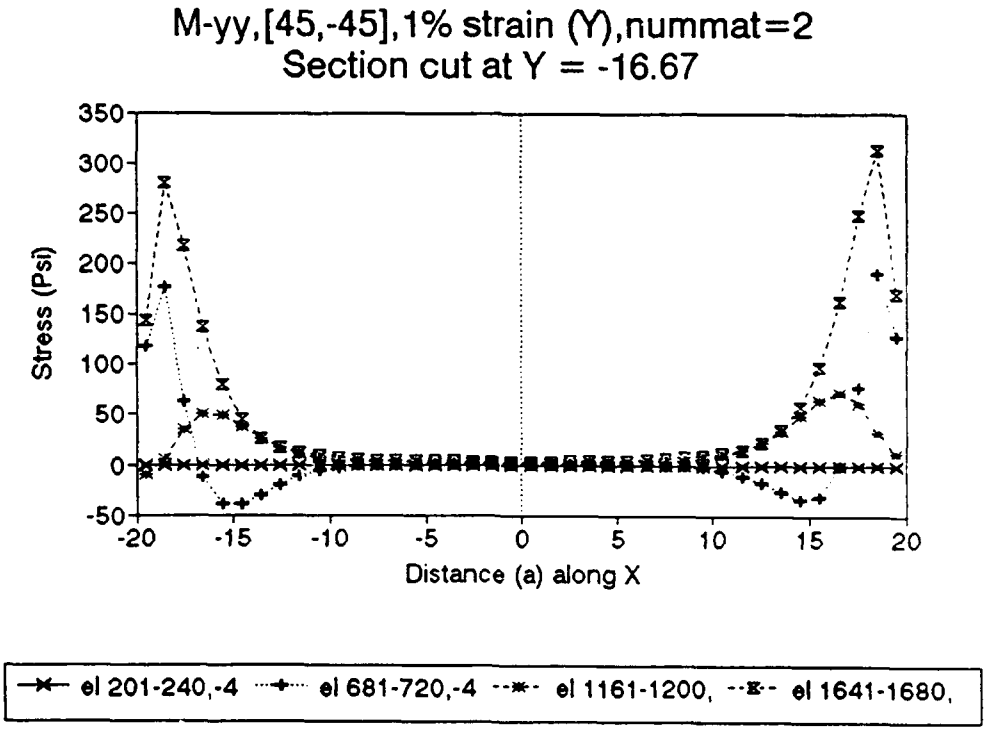

Figure 5.4

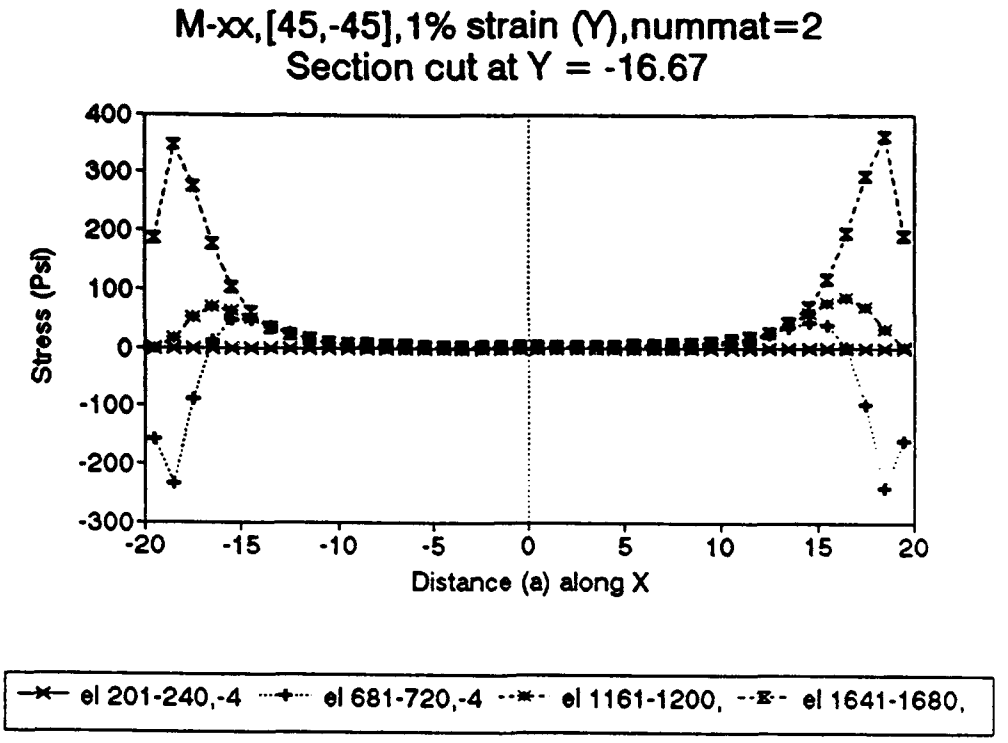

Figure 5.5

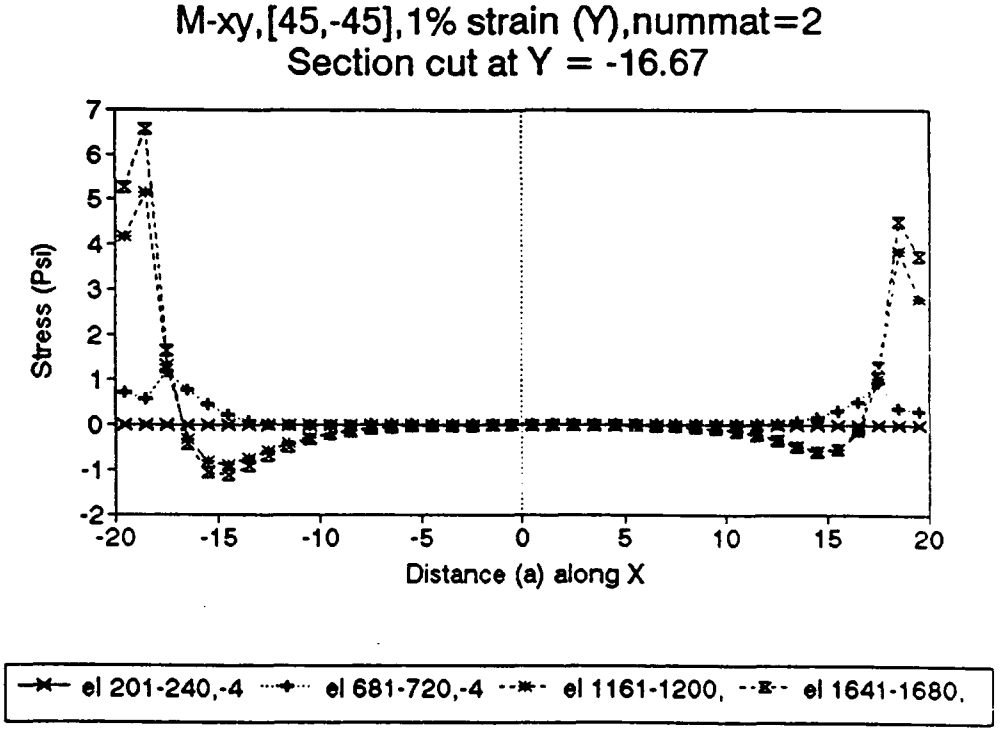

Figure 5.6

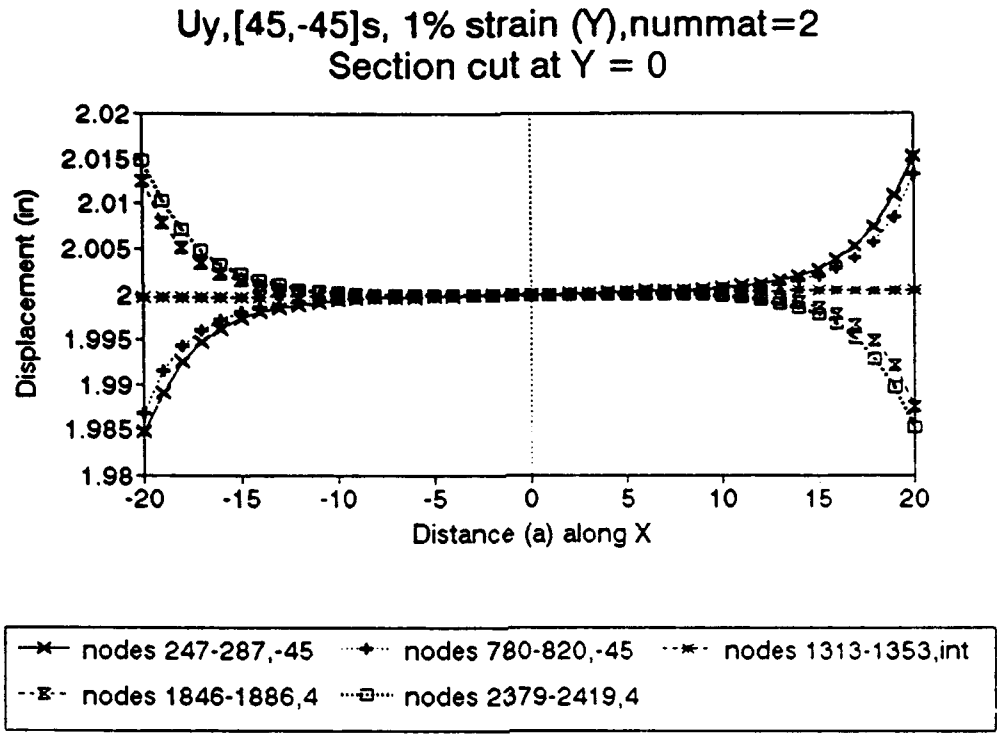

Figure 5.7

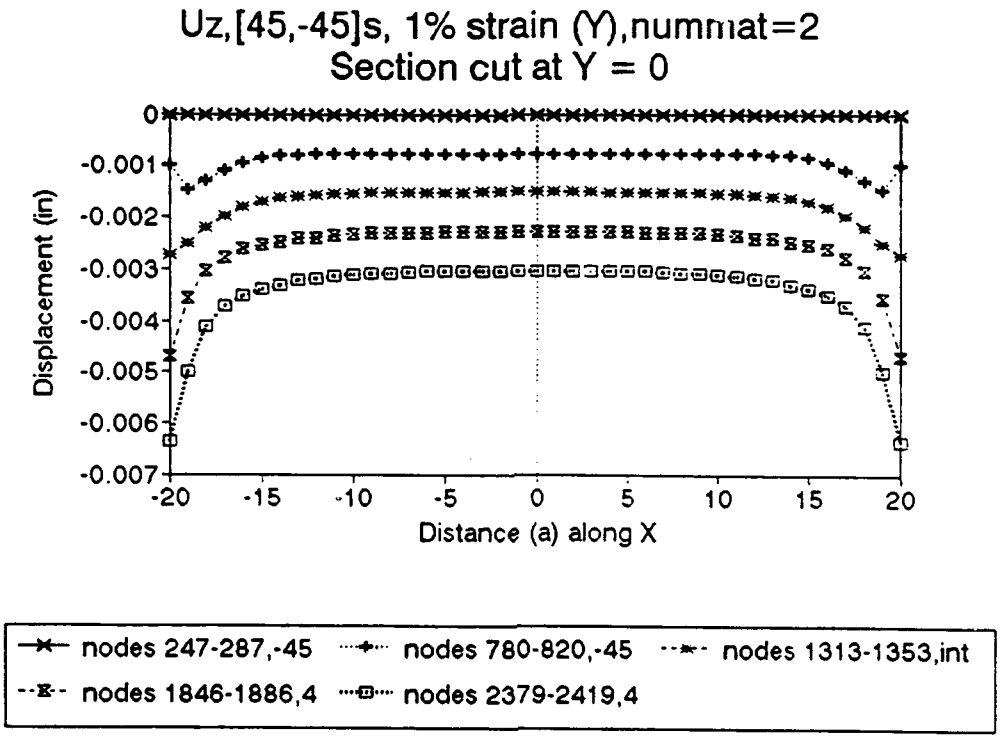

Figure 5.8

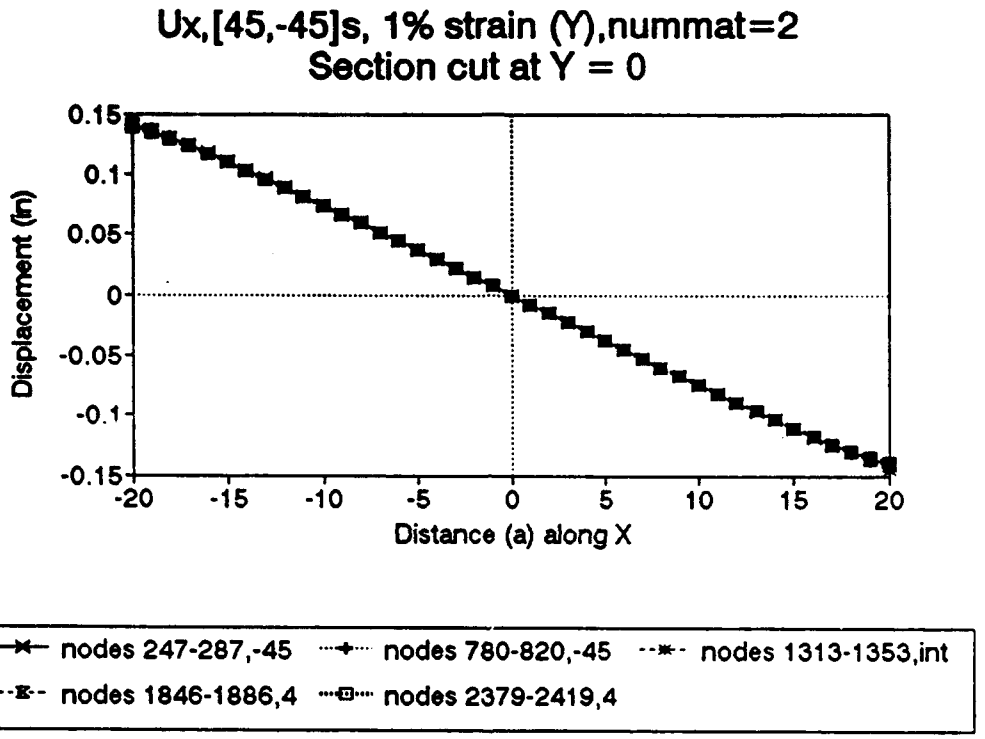
Ux,[45,-45]s, 1% strain (Y),nummat=2
Section cut at Y = 0
Displacement (in)
0.15
0.1
0.05
0
-0.05
-0.1
-0.15
-20
-15
-10
-5
0
5
10
15
20
Distance (a) along X
nodes 247-287,-45
nodes 780-820,-45
nodes 1313-1353,int
nodes 1846-1886,4
nodes 2379-2419,4

Figure 5.9

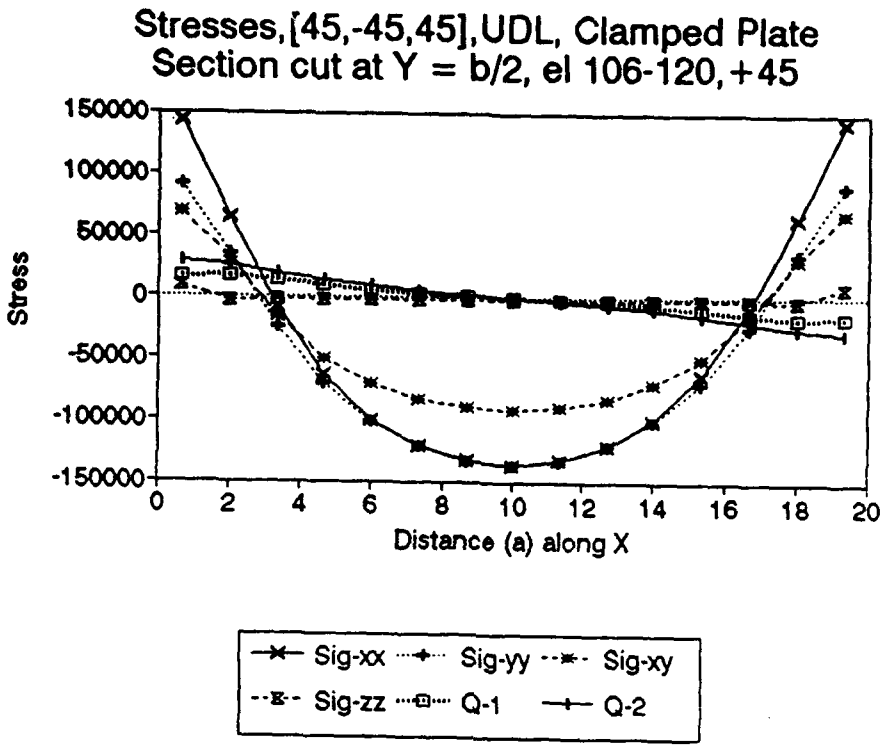

Figure 6.1

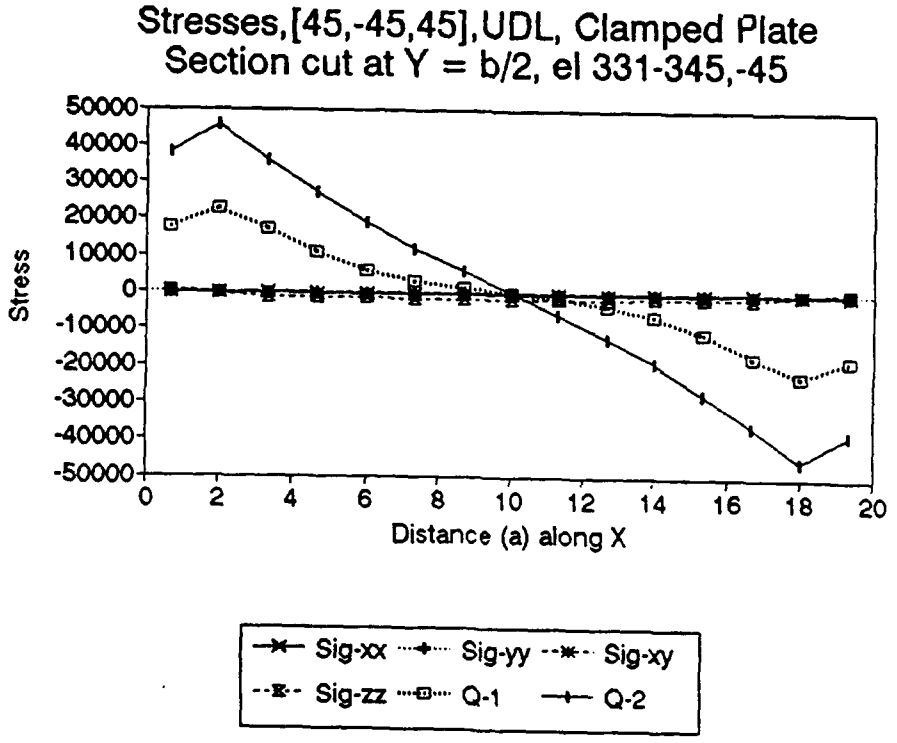

Figure 6.2

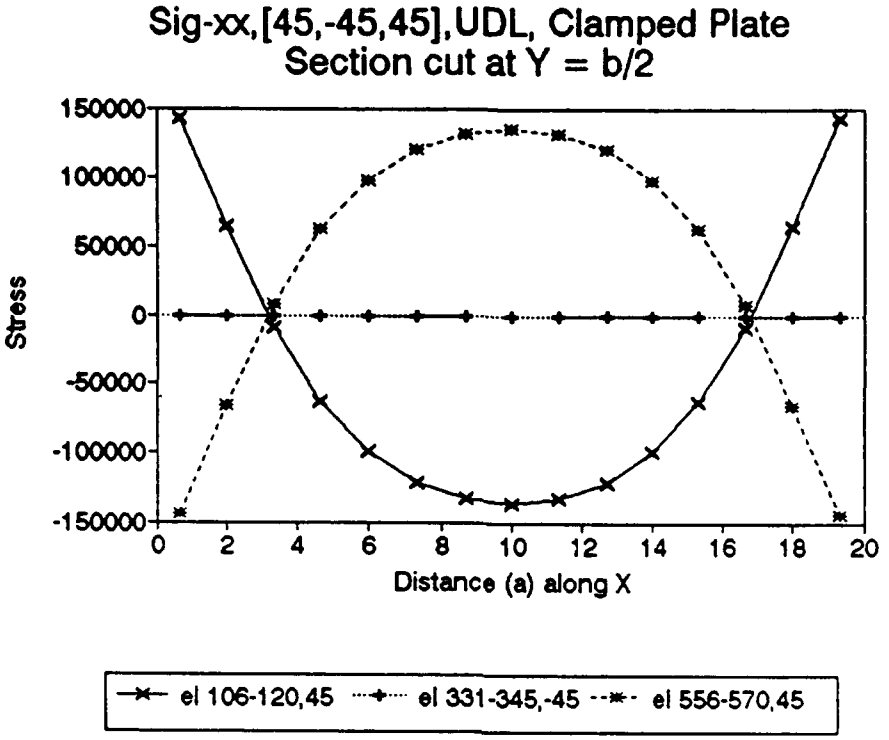

Figure 6.3

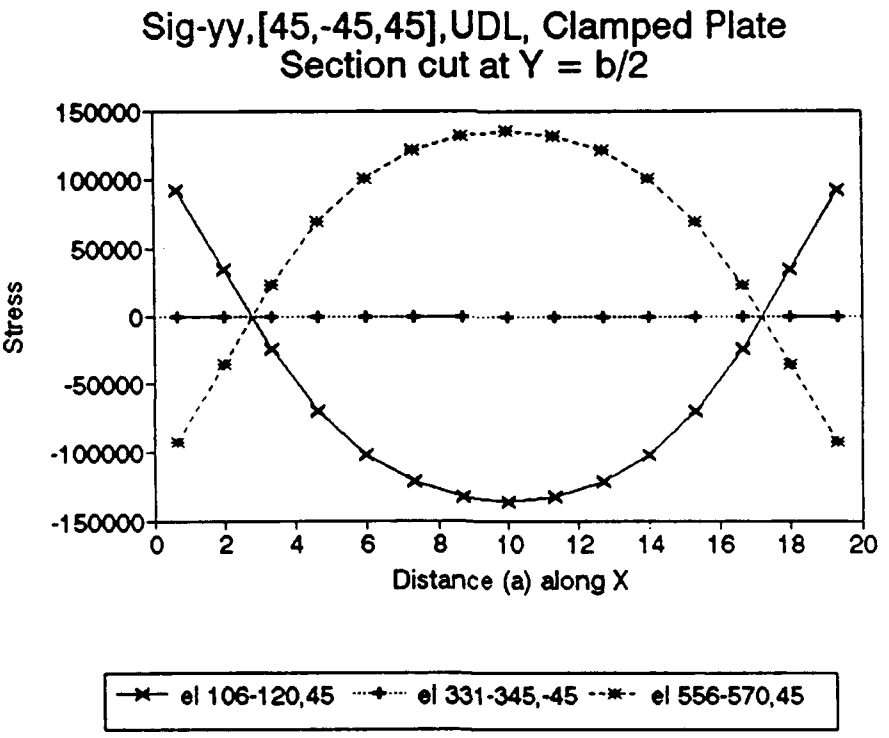

Figure 6.4

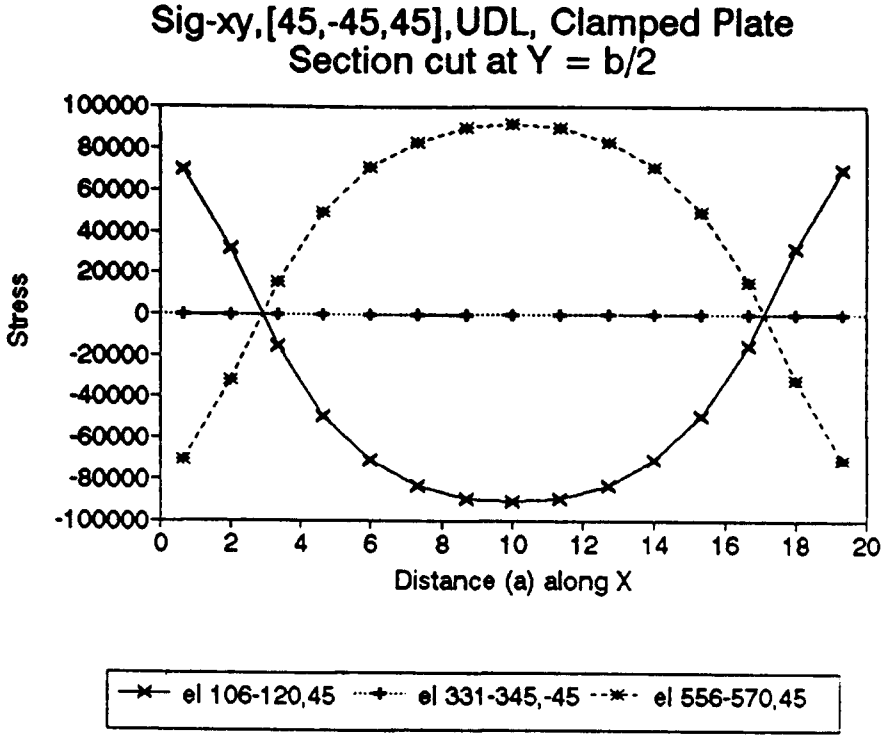

Figure 6.5

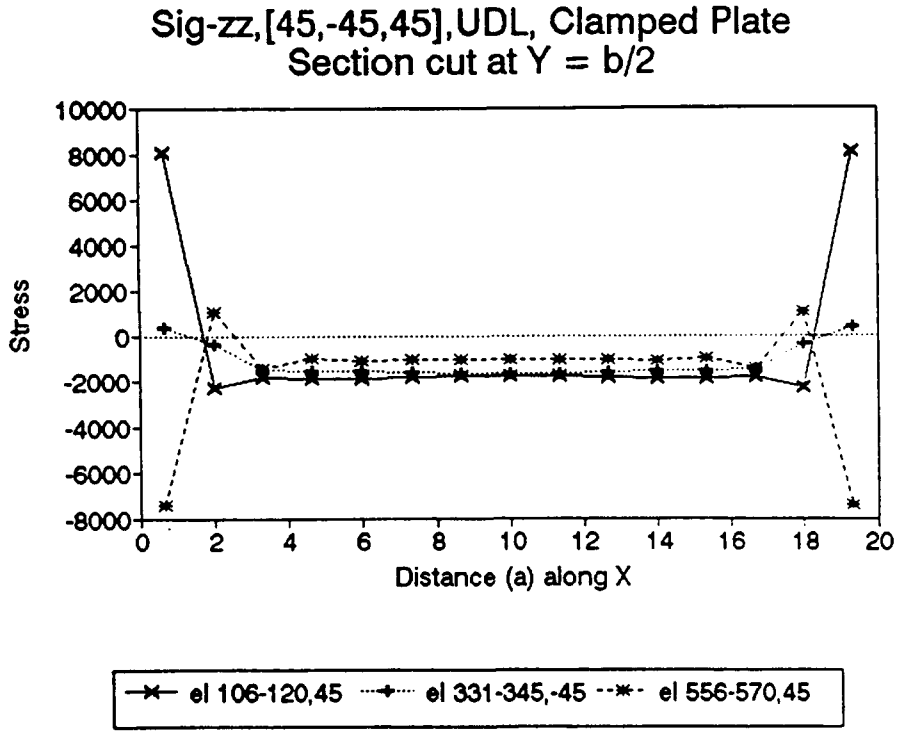

Figure 6.6

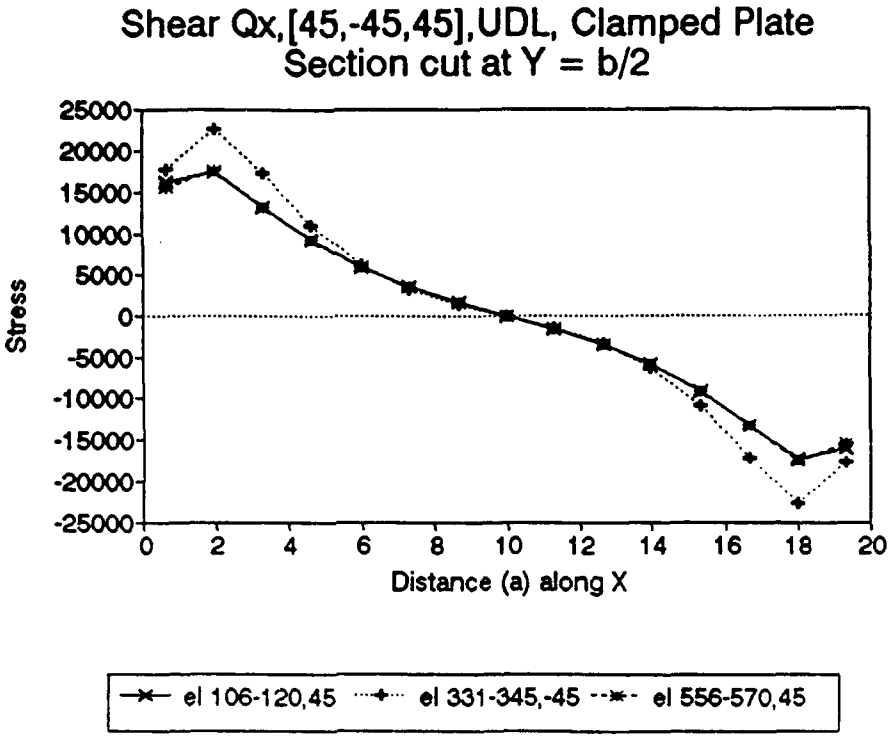

Figure 6.7

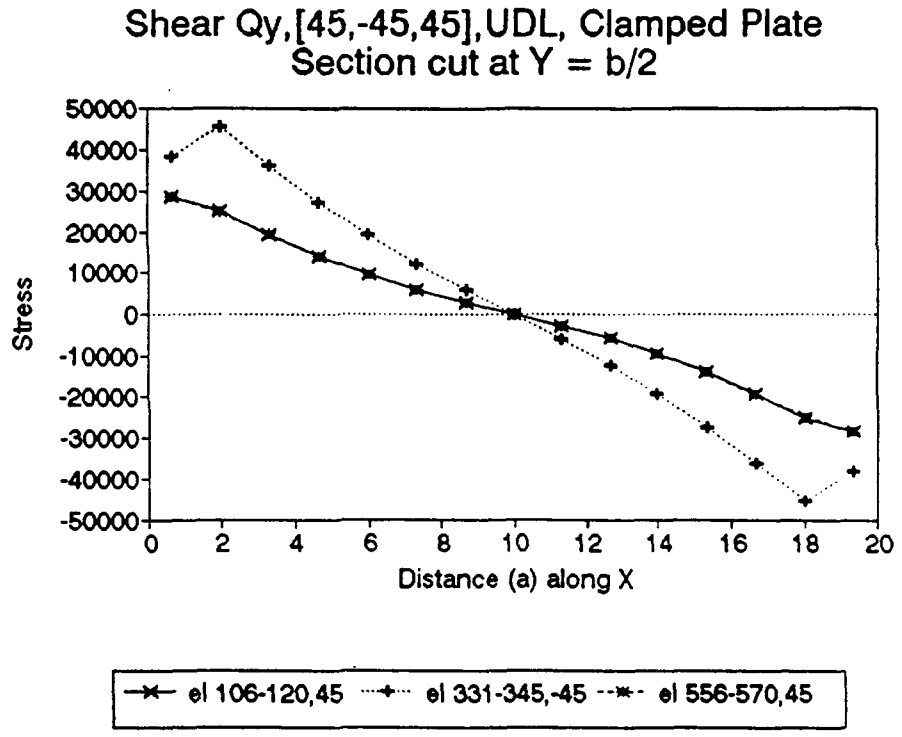

Figure 6.8

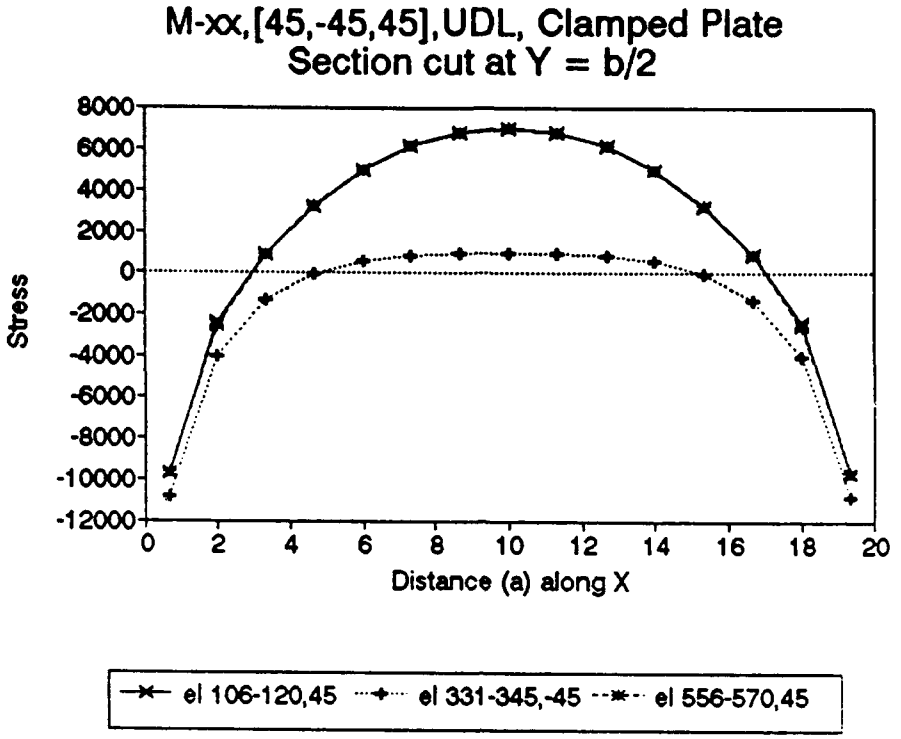

Figure 6.9

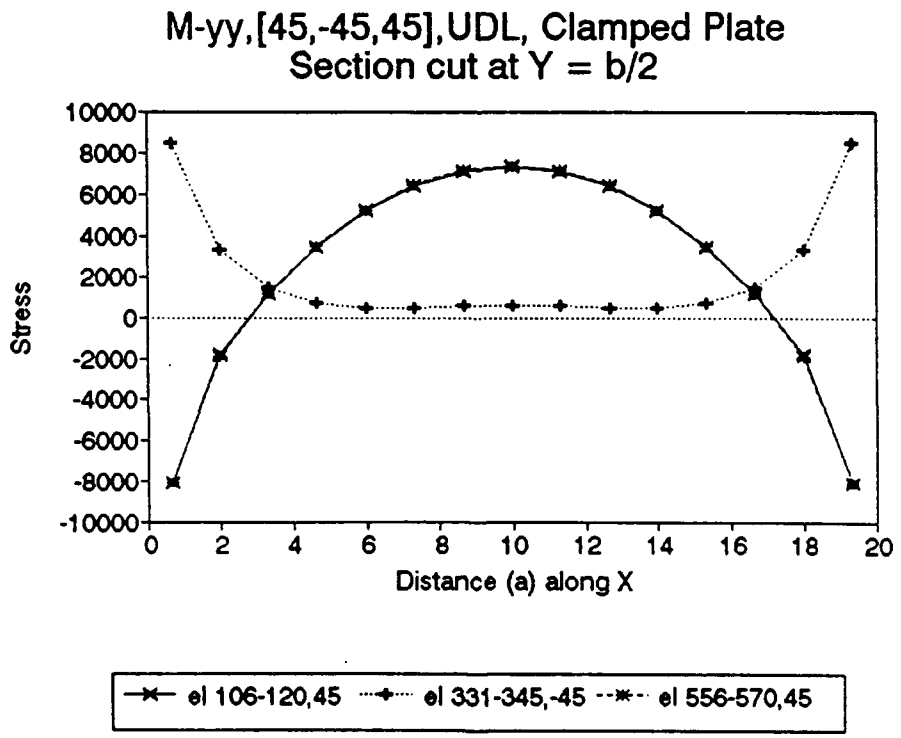

Figure 6.10

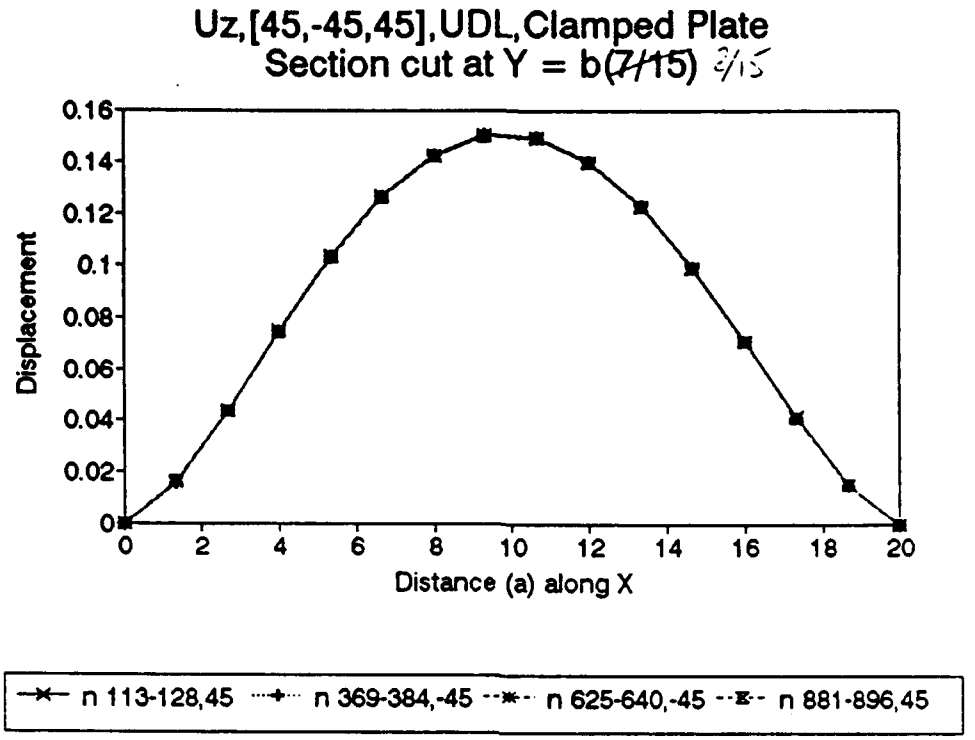

Figure 6.11

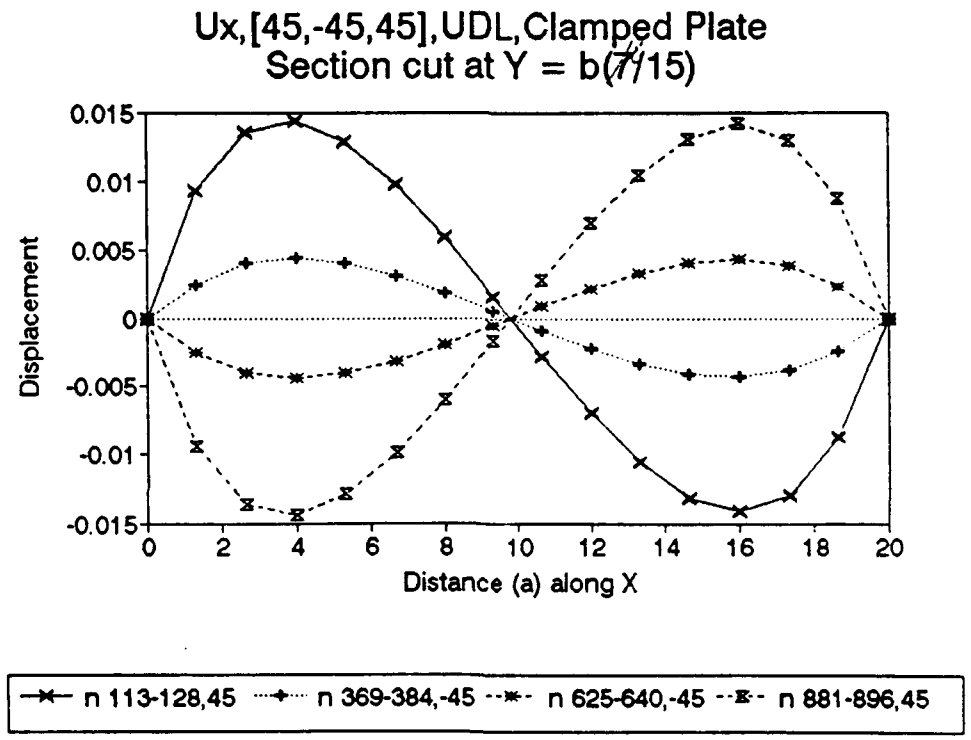

Figure 6.12

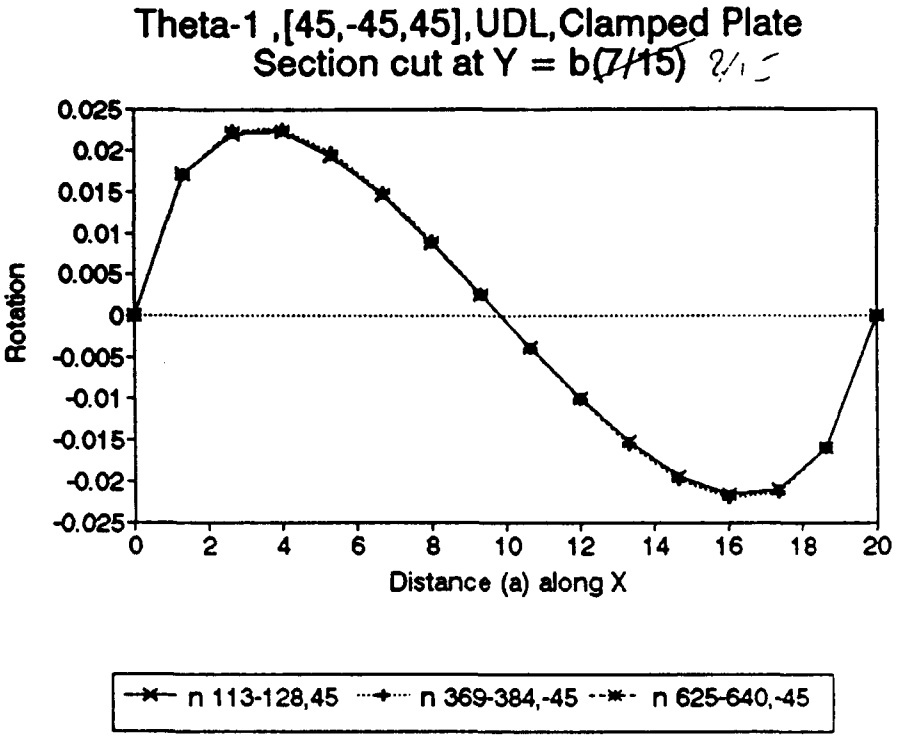
Theta-1 ,[45,-45,45],UDL,Clamped Plate
Section cut at Y = b(7/15) 2/15
Rotation
0.025
0.02
0.015
0.01
0.005
0
-0.005
-0.01
-0.015
-0.02
-0.025
0
2
4
6
8
10
12
14
16
18
20
Distance (a) along X
n 113-128,45
n 369-384,-45
n 625-640,-45

Figure 6.13

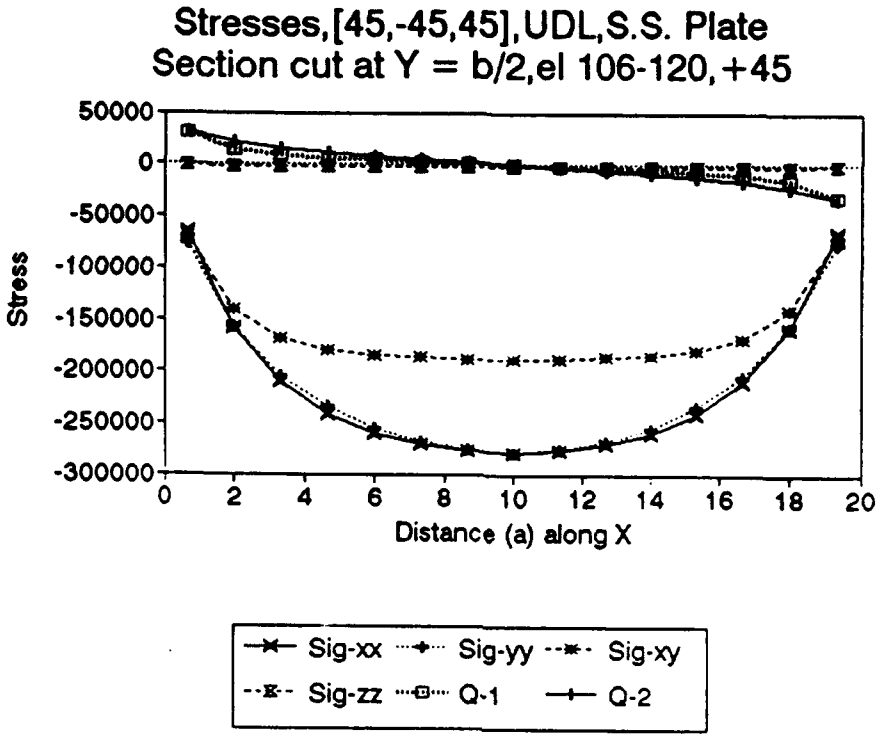

Figure 7.1

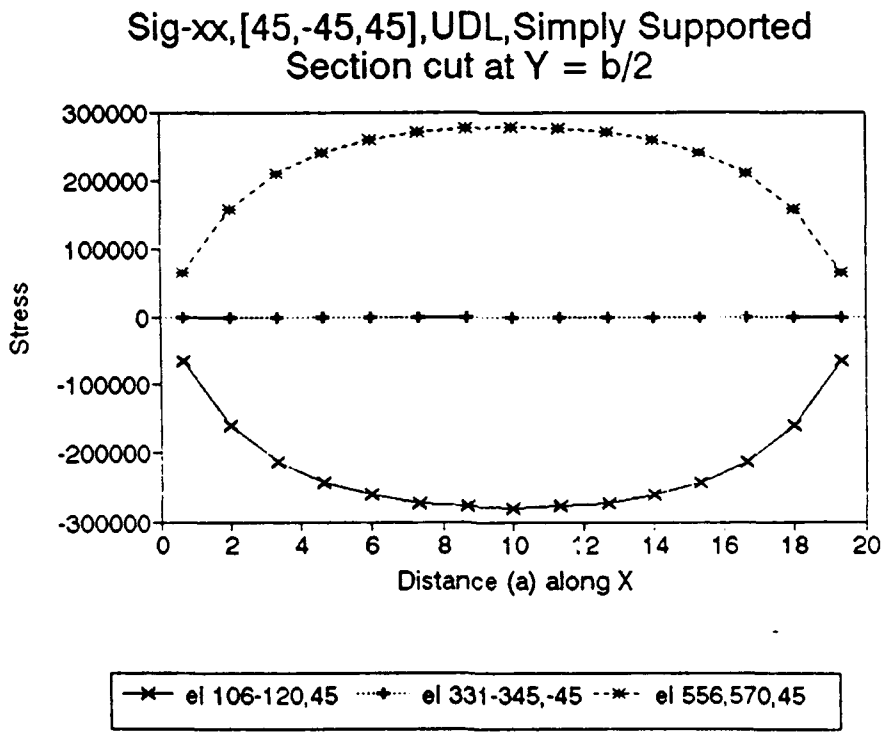

Figure 7.2

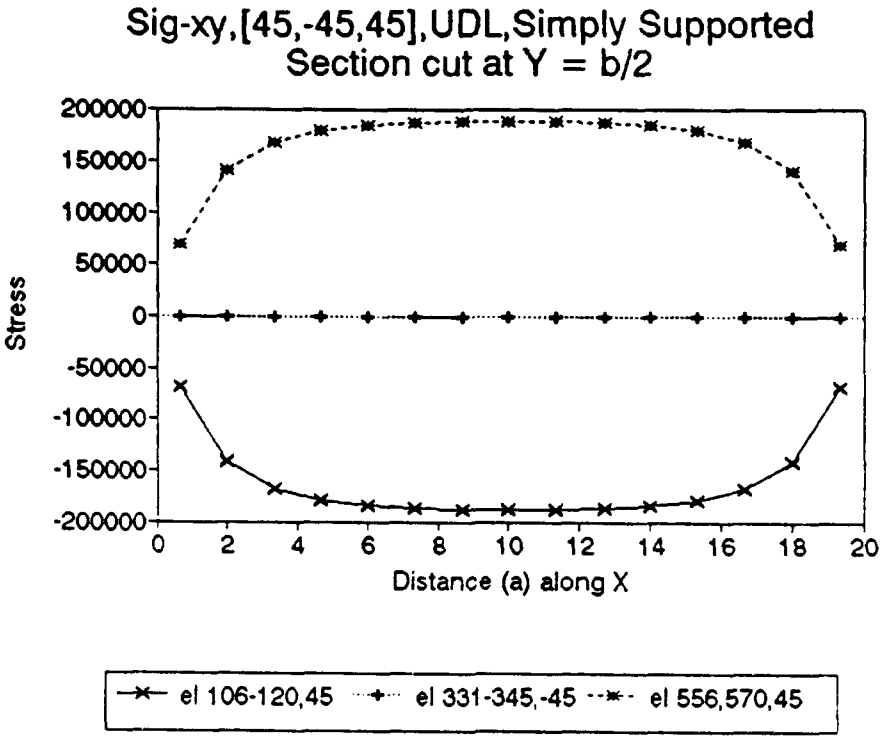

Figure 7.3

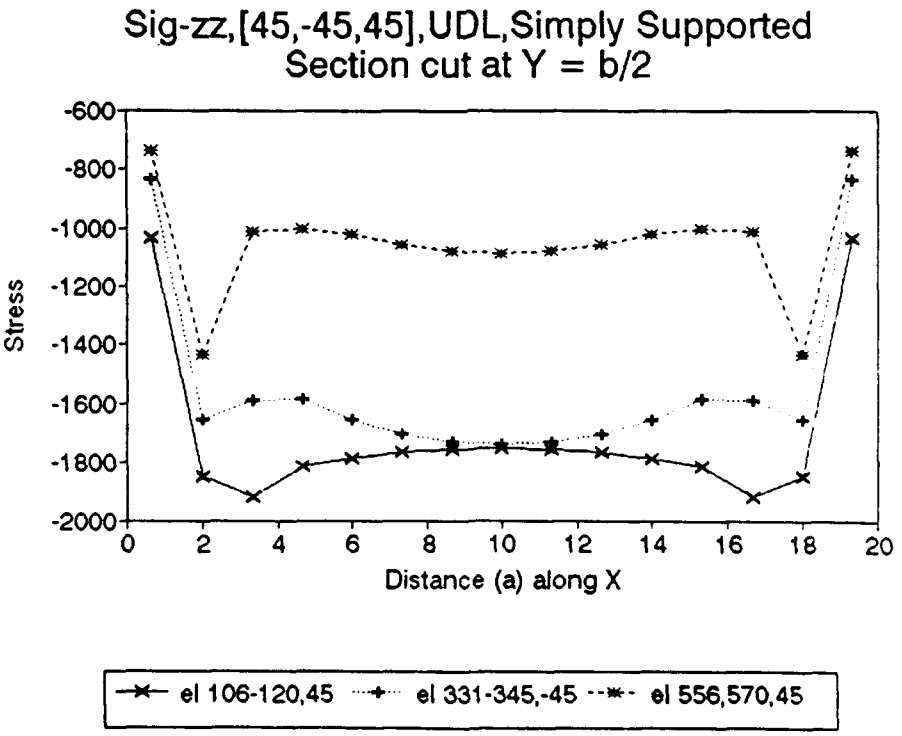

Figure 7.4

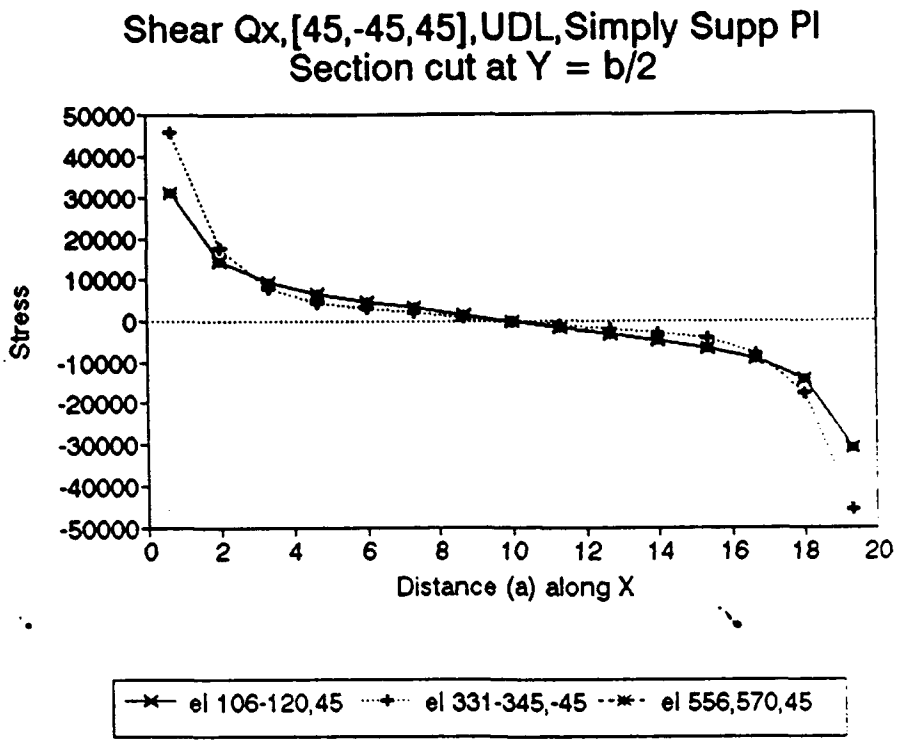

Figure 7.5

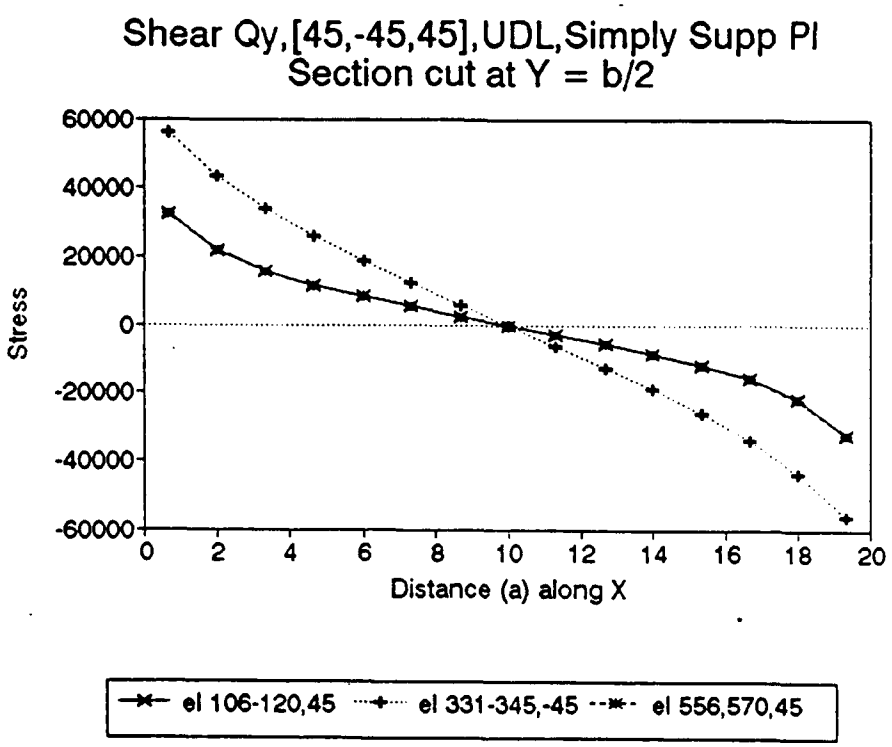

Figure 7.6

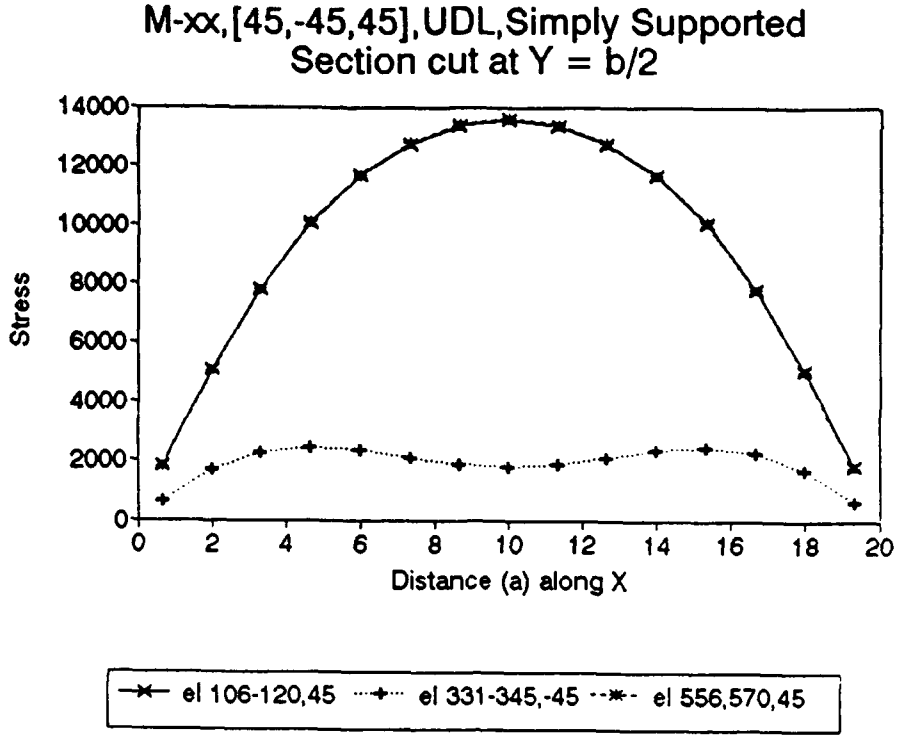

Figure 7.7

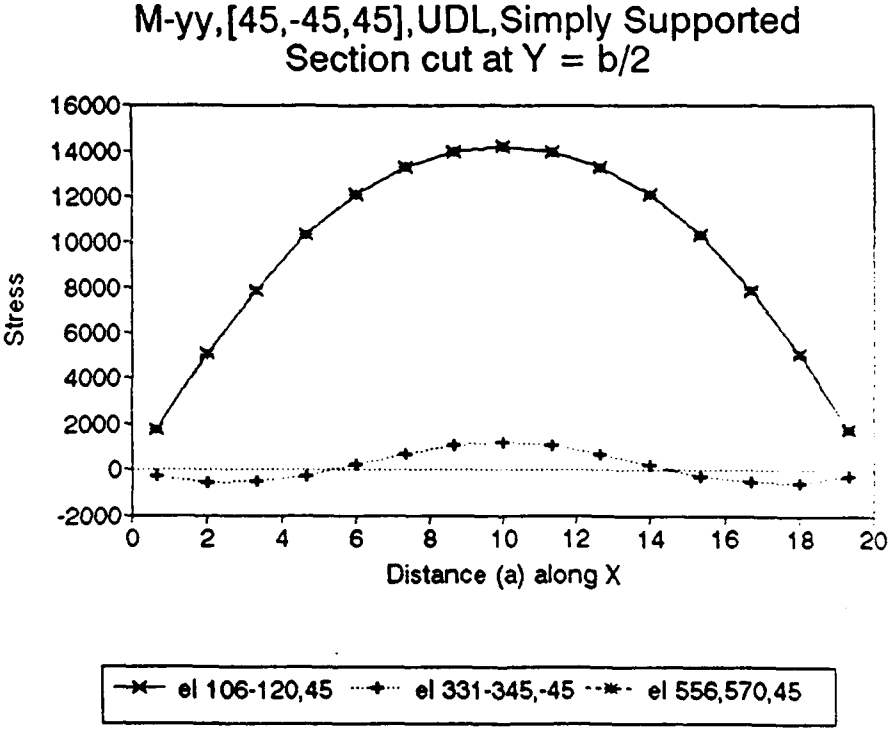

Figure 7.8

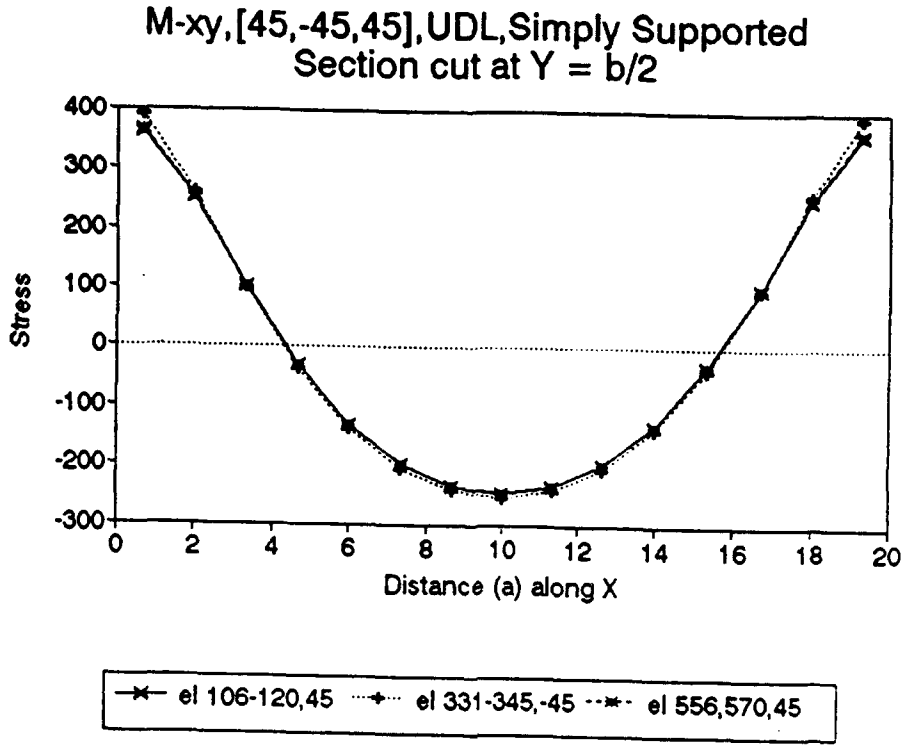

Figure 7.9

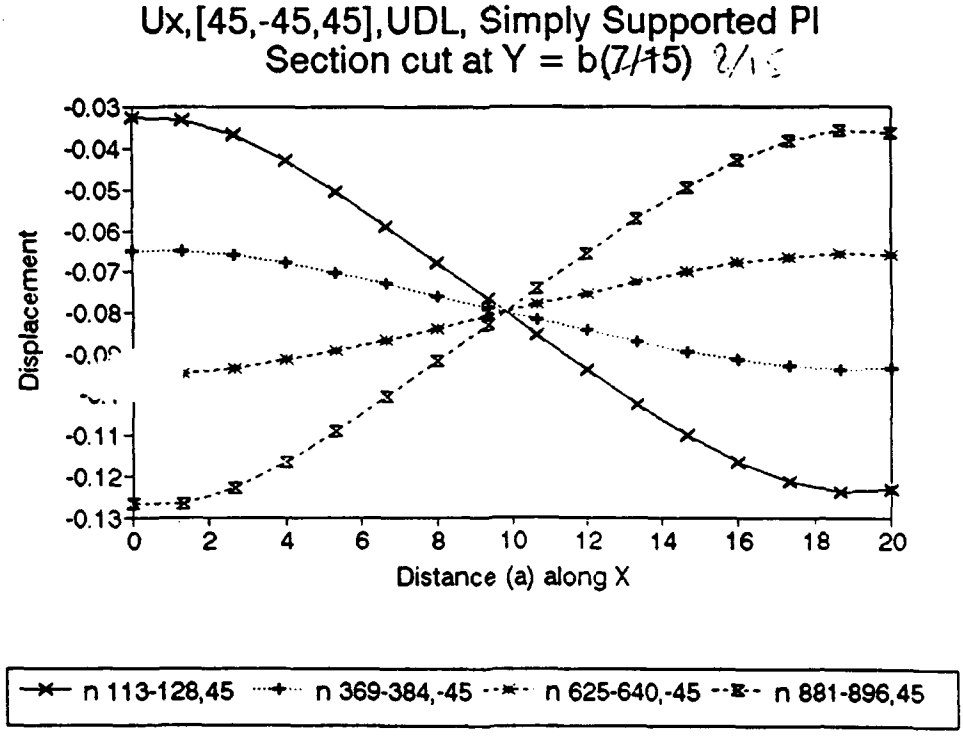

Figure 7.10

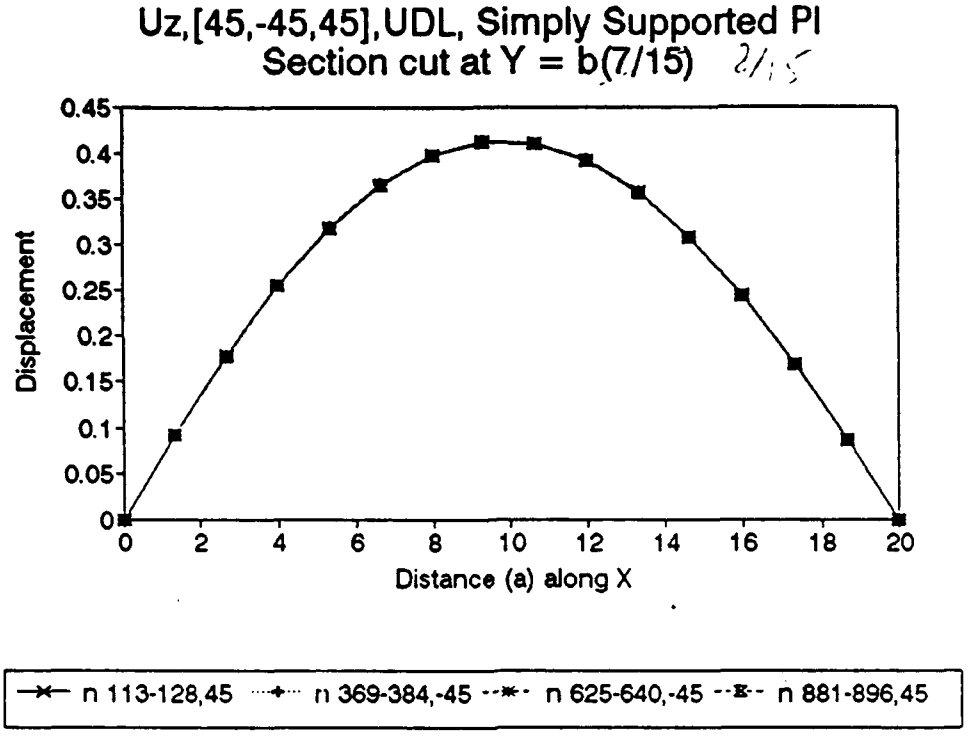

Figure 7.11

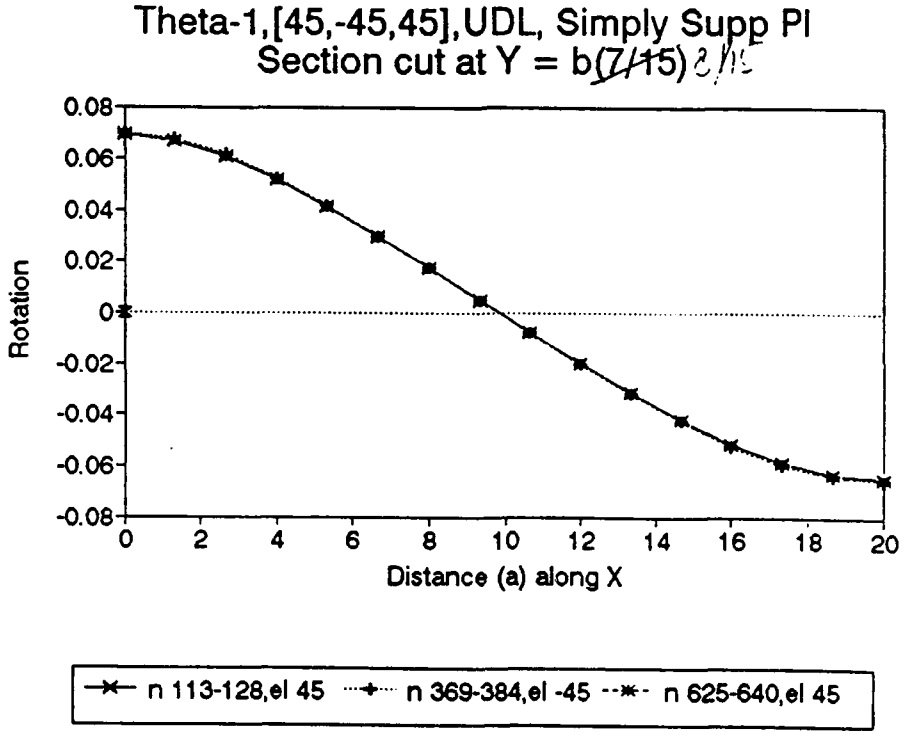

Figure 7.12

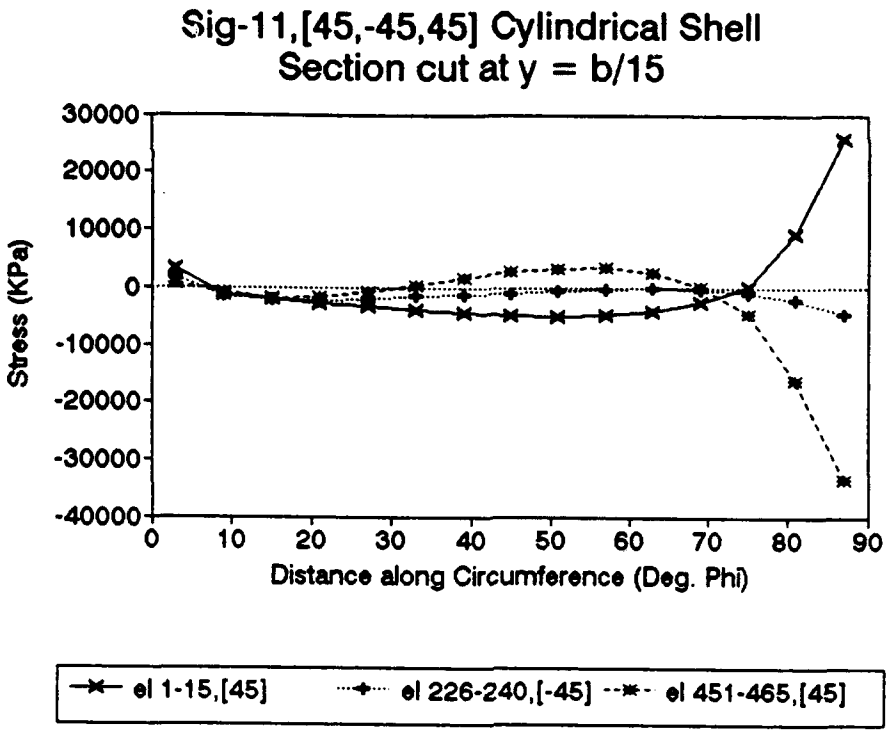

Figure 8.1

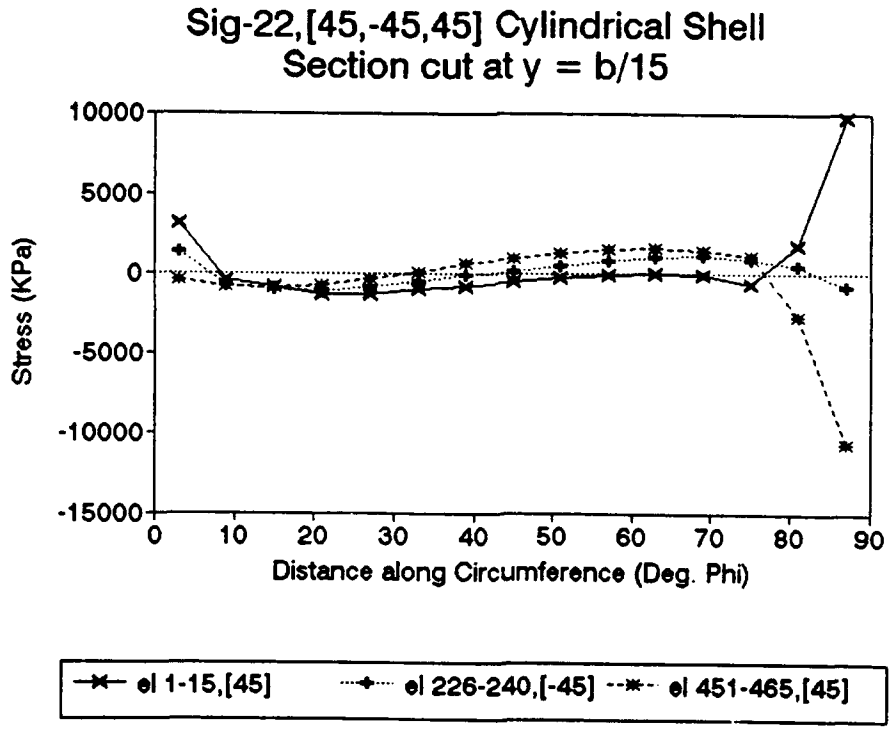

Figure 8.2

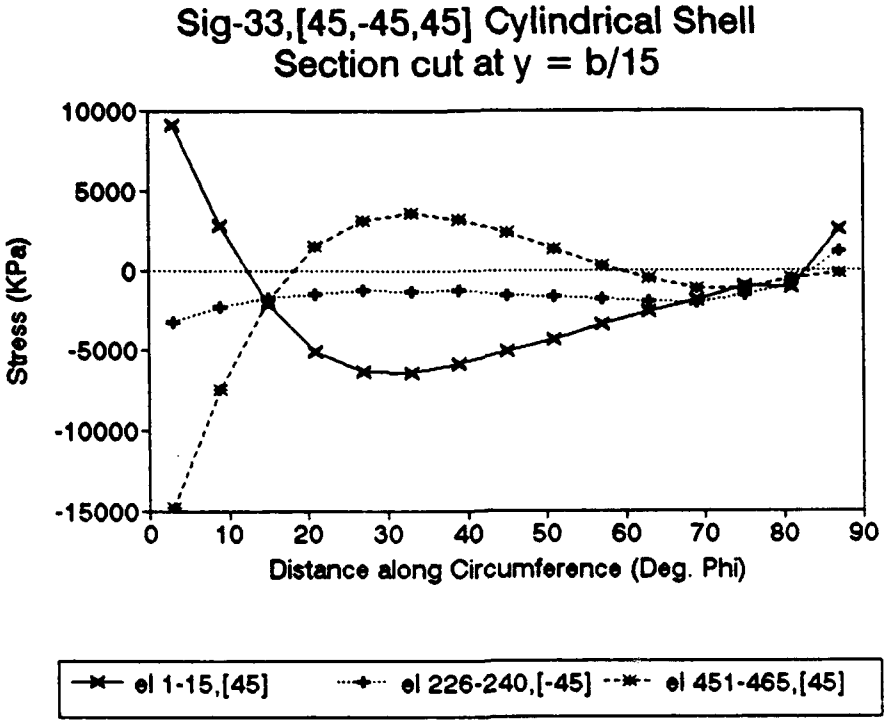

Figure 8.3

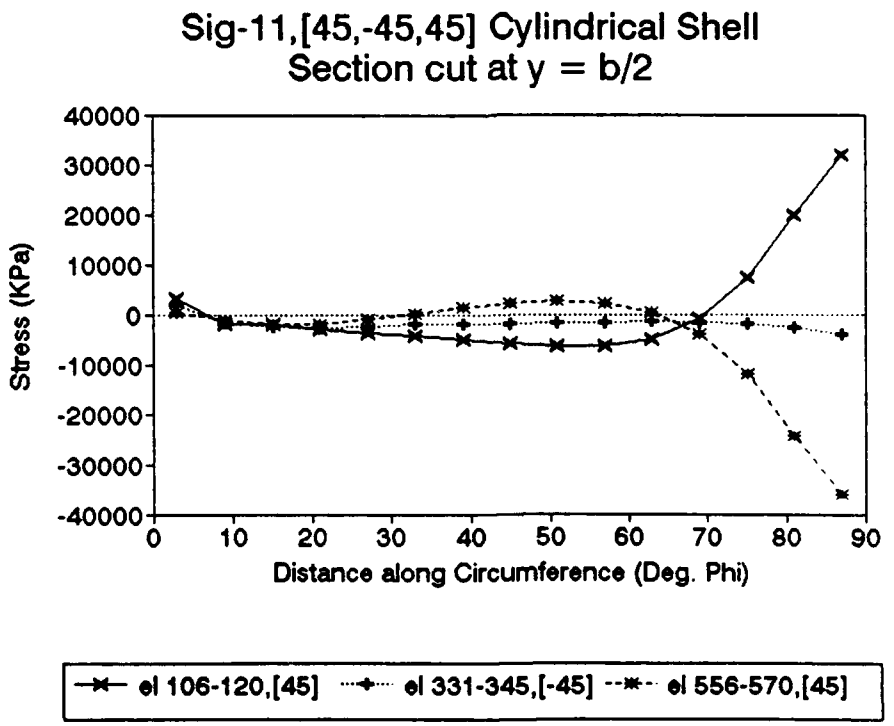

Figure 8.4

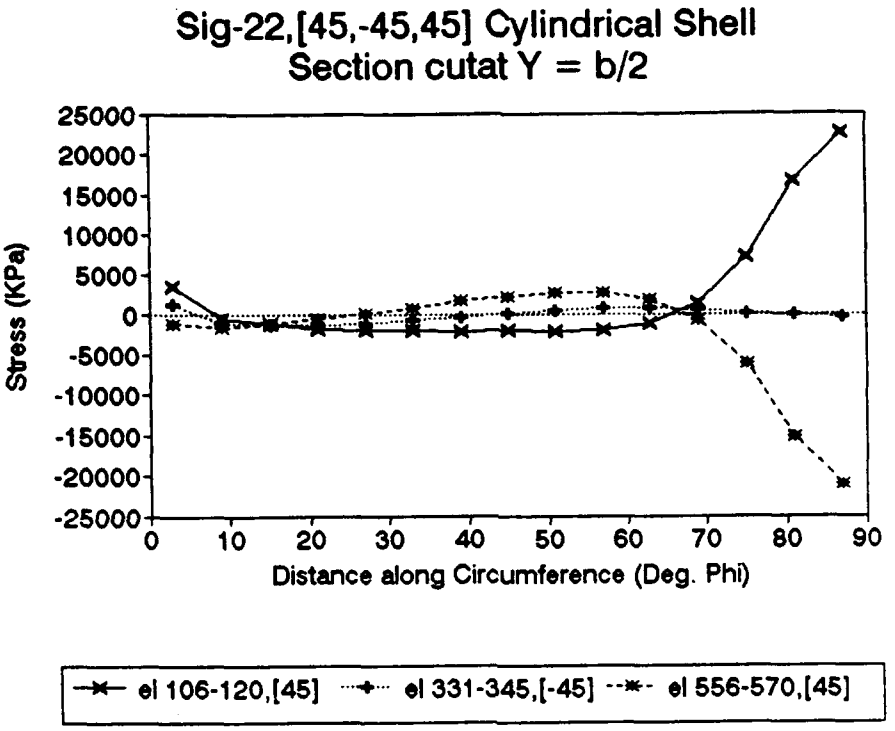

Figure 8.5

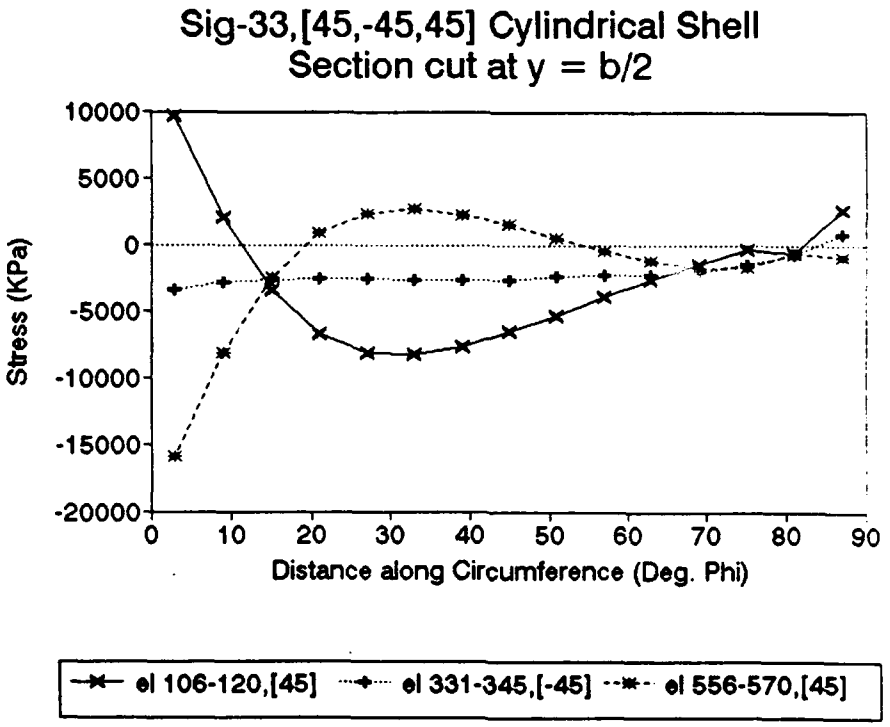

Figure 8.6

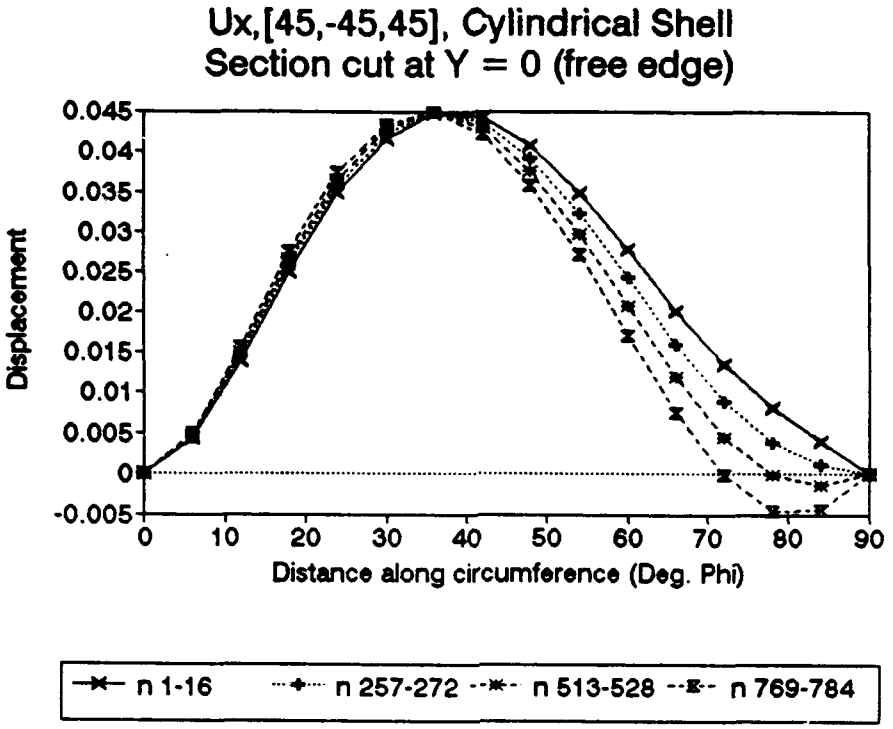

Figure 8.7

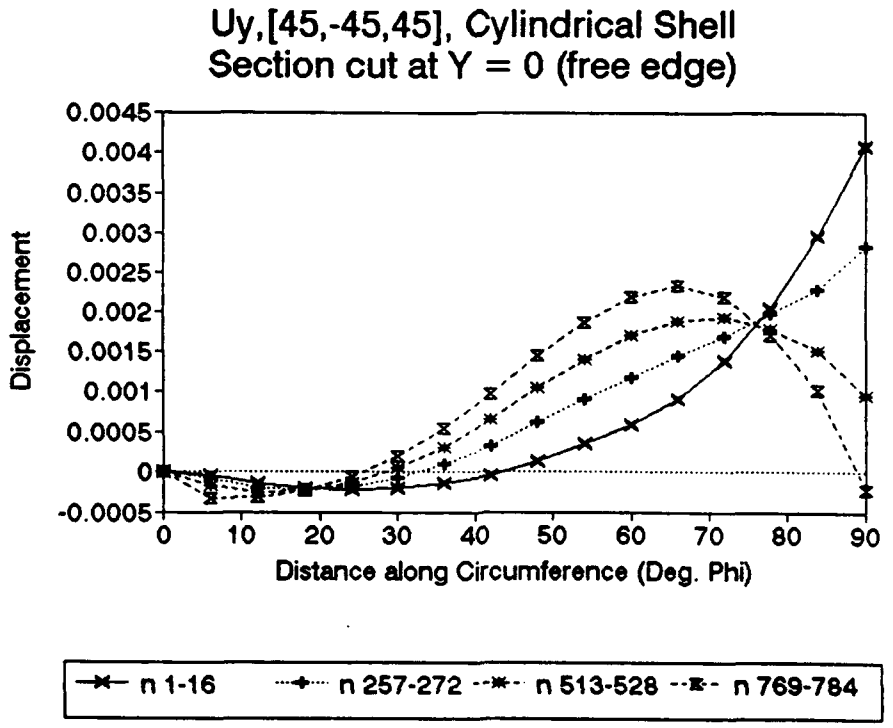

Figure 8.8

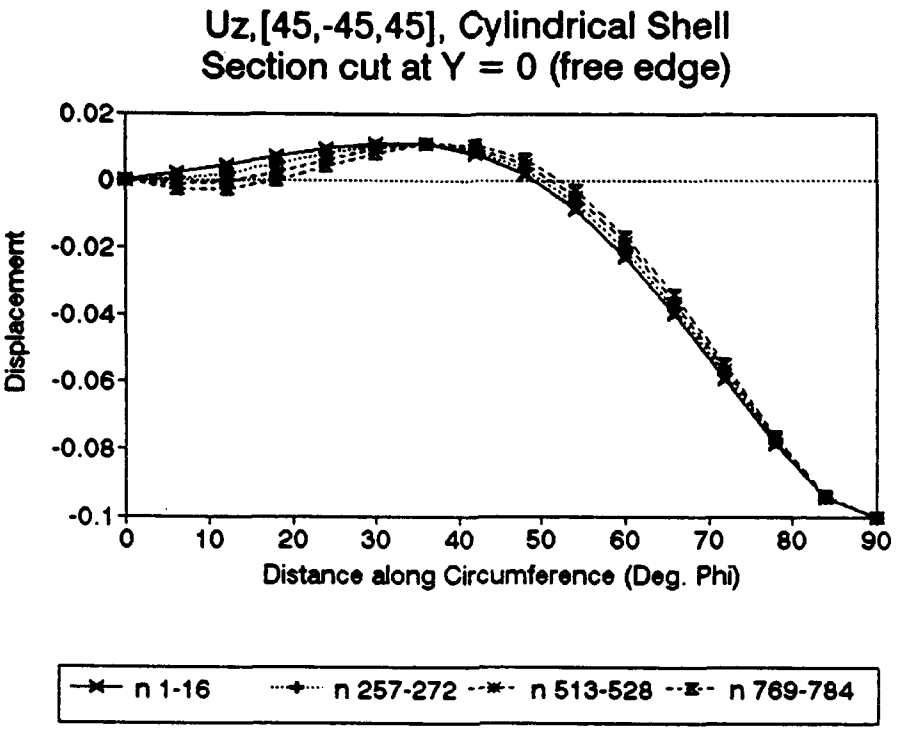

Figure 8.9

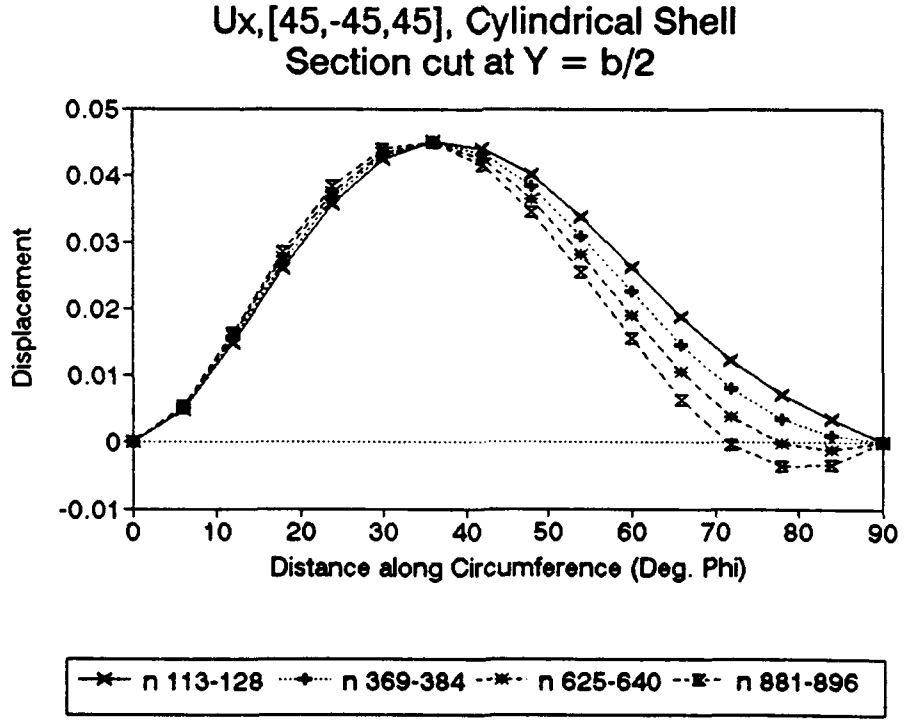

Figure 8.10

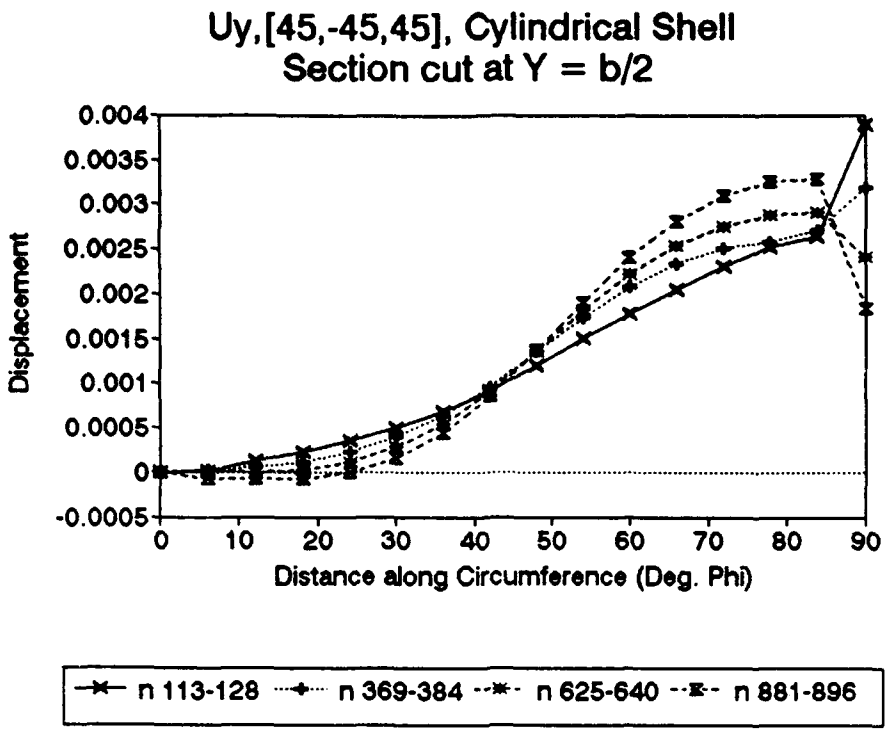

Figure 8.11

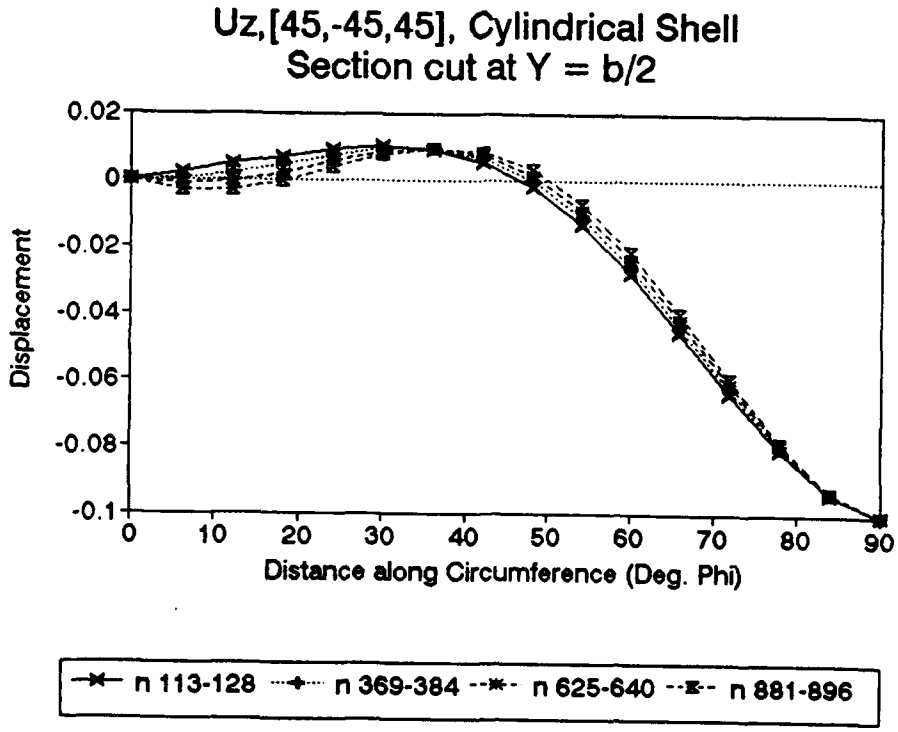

Figure 8.12

15. REFERENCES

Aboudi, J. [1989] "Micromechanical analysis of composites by the method of cells," *Appl. Mech. Rev.*, Vol. 42, No. 7, 193-221.

Aboudi, J. [1981a] "Generalized effective stiffness theory for the modeling of fiber-reinforced composites," *Int. J. Eng. Sci.*, Vol. 17, 1005-1018.

Aboudi, J. [1981b] "Generalized effective stiffness theory for nonelastic laminated composites," *Int. J. Eng. Sci.*, Vol. 19, 1269-1281.

Achenbach, J. D. [1976] "Generalized continuum theories for directionally reinforced solids," *Arch. Mech.*, Vol. 28, 257-278.

Achenbach, J. D. [1975] *A theory of elasticity with microstructure for directionally reinforced composites*, Springer-Verlag, New York.

Achenbach, J. D., Sun, C. T., and Herrmann, G. [1968] "On vibrations of laminated body," ASME paper 68-WA/APM-10.

Bedford, A., and Stern, M. [1971] "Toward a diffusing continuum theory of composite materials," *J. Appl Mech.*, Vol. 38, 8-14.

Bedford, A., and Stern, M. [1972] "A multi-continuum theory for composite elastic materials," *Acta Mechanica*, Vol. 14, 85.

Bedford, A., and Drumheller, D. S. [1974] "On a generalized effective stiffness theory," *J. Appl. Mech.*, Vol. 41, 305-307.

Blinowski, A. [1986] "Nonlinear microstructural continuous model of a laminated composite: I. Quasi-static phenomenological model," *Arch. Mech.*, Vol. 38, No. 5-6, 553-563.

Capriz, G. [1989] *Continua with microstructure*, Springer-Verlag, New York.

Chia, C. Y. [1988] "Geometrically nonlinear behavior of composite plates: A review," *Appl. Mech. Rev.*, Vol. 41, No. 12.

Christensen, R. M. [1979] *Mechanics of Composite Materials*, Wiley-Interscience, New York.

Dong, S. B., and Tso, F. K. W. [1972] "On a laminate orthotropic shell theory including transverse shear deformation," *J. Appl. Mech.*, 39.

Epstein, M., and Glockner, P. G. [1978] "Nonlinear analysis of multilayered shells," *Int. J. Solids Struct.* 13 (11), 1081-1089.

Epstein, M., and Glocker, P. G. [1979] "Multilayered shells and directed surfaces," *Int. J. Eng. Sci.* 17 (5), 553-562.

Ericksen, J. L., and Truesdell, C. [1958] "Exact theory of stress and strain in rods and shells," *Arch. Rat. Mech. Anal.*, Vol. 1, 295-323.

Eringen, A. C. [1975] "Continuum mechanics of single-substance bodies," in *Continuum Physics, Vol. II* (A. C. Eringen, Ed.), Academic Press, New York, 4-127.

Green, A. E., Naghdi, P. M., and Wenner, M. L. [1971] "Linear theory of Cosserat surface and elastic plates of variable thickness," *Proc. Camb. Phil. Soc.*, Vol. 69, 227-254.

Green, A. E., Naghdi, P. M., and Trapp, J. A. [1970] "Thermodynamics of a continuum with internal constraints," *Int. J. Eng. Sci.*, Vol. 1, 8, 891-908.

Green, A. E., and Naghdi, P. M. [1968] "Rods, plates and shells," *Proc. Camb. Phil. Soc.*, Vol. 64, 895-913.

Green, A. E., and Zerna, W. [1968] *Theoretical Elasticity*, 2nd ed., Oxford University Press.

Green, A. E., Naghdi, P. M., and Rivlin, R. S. [1965] "Directors and multipolar displacements in continuum mechanics," *Int. J. Eng. Sci.*, Vol. 2, 611-620.

Grot, R. A., and Achenbach, J. D. [1970] "Large deformations of a laminated composite," *Int. J. Solids Struc.*, Vol. 6, 641-659.

Hegemier, G. A., and Murakami, H. [1980] "On construction of mixture theories for composite materials by the method of multi-variable asymptotic expansion," in *Continuous models of discrete systems* (E. Kroner and K. H. Anthony, eds.) University of Waterloo Press, 423-441.

Hegemier, G. A., and Nayfeh, A. H. [1973] "A continuous theory for wave propagation in laminated composites," *J. Appl. Mech.*, Vol. 40, 503-510.

Hegemier, G. A., Gurtman, G. A., and Nayfeh, A. H. [1973] "A continuum mixture theory of wave propagation in laminated and fiber reinforced composites," *Int. J. Solids Struc.*, Vol. 9, 395-414.

Hughes, T. J. R. [1987] *The Finite Element Method*, Prentice Hall.

Jones, R. M. [1975] *Mechanics of Composite Materials*, McGraw-Hill Book Co., New York.

Koh, S. L. [1967] "Continuum theories for composite materials," in *Mechanics of Composite Materials* (F. W. Wendt, H. Liebowitz and N. Perrone, Eds.), Office of Naval Research, 387-402.

Minagawa, S., Nemat-Nasser, S., and Jamada, S. [1981] "Finite element analysis of harmonic waves in layered and fiber-reinforced composites," *Int. J. Num. Meth. Eng.*, Vol. 17, 1335-1353.

Mindlin, R. D. [1964] "Micro-structure in linear elasticity," *Arch. Rational Mech. Anal.*, Vol. 16, 51-78.

Murakami, H., and Hegemier, G. A. [1987] "A nonlinear constitutive model for metal-matrix composites," in *Design and Analysis of Composite Material Vessels,* (D. Hui and T. J. Kozik, eds.), ASME, 97-104.

Murakami, H., and Akiyama, A. [1985] "A mixture theory for wave propagation in single-ply laminates. Part 2: Application," *J. Appl. Mech.*, Vol. 52, 338-344.

Murakami, H. [1985] "A mixture theory for wave propagation in single-ply laminates. Part 1: Theory," *J. Appl. Mech.*, Vol. 52, 331-337.

Naghdi, P. M. [1982] "Finite deformation of elastic rods and shells," in *Proc. IUTAM Symposium on Finite Elasticity,* (D. E. Carlson, R. T. Shield, eds.), Matrinus Nijhoff Publishers, Boston, 47-103.

Naghdi, P. M. [1975] "On the formulation of contact problems of shells and plates," *J. Elasticity,* Vol. 5, 379-398.

Naghdi, P. M. [1974] "Direct formulation of some two-dimensional theories of mechanics," *Proc. 7th U.S. National Congr. Appl. Mech.*, ASME, 3-21.

Naghdi, P. M. [1972] "The theory of shells and plates," in S. Flugge's *Handbuch der Physik,* Vol. VIa/2, (C. Truesdell, ed.), Springer-Verlag, Berlin, 425-640.

Nayfeh, A. H., and Chimenti, D. E. [1987] "Mechanical modeling and measurements of fibrous composite," in *Solid Mechanics Research for Quantitative Non-Destructive Evaluation,*" (J. D. Achenbach and Y. Rajapakse, eds.), Martinus Nijhoff Publishers, Boston, 397-409.

Nayfeh, A. H., and Nemat-Nasser, S. [1972] "Elastic waves in inhomogeneous elastic media," *J. Appl. Mech.*, Vol. 9, 690-702.

Nemat-Nasser, S., Fu, F. C. L., and Minagawa, S. [1975] "Harmonic waves in one-, two- and three-dimensional composites; Bounds for eigenfrequencies," *Int. J. Eng. Sci.*, Vol. 11, 617-642.

Noor, A. K., and Burton, W. S. [1989] "Assessment of shear deformation theories for multi-layered composite plates," *Appl. Mech. Rev.*, 42(1), 1-13.

Noor, A. K. and Burton, W. S. [1990] "Assessment of computational models for multilayered composite shells," *Appl. Mech. Rev.*, Vol. 43, No. 4.

Ochoa, O. O., Reddy, J. N. [1992] *Finite Element Analysis of Composite Laminates*, Kluwer Academic Publishers.

Pagano, N. J. [1970] "Exact solutions for rectangular bidirectional composites and sandwich plates," *J. Comp. Mater.*, 4, 20-34.

Pagano, N. J., and Pipes, R. B. [1973] "Some observations on the interlaminar strength of composite laminates," *Int. J. Mech. Sci.*, Vol. 15, p. 679.

Pagano, N. J. [1989] "Interlaminar response of composite materials," *Composite Material Series*, Vol. 5.

Pipes, R. B., and Pagano, N. J. [1970] "Interlaminar stresses in composite laminates under uniform axial extension," *J. Comp. Materials*, Vol. 4, p. 538.

Reddy, J. N. [1984] "A refined nonlinear theory of plates with transverse shear deformation," *Int. J. Solids Struct.*, 20 (9/10), 881-896.

Reddy, J. N. [1988] "Mechanics of laminated composite structures: Theory and analysis," Lecture Notes, VPI/SU.

Reddy, J. N. [1993] "An evaluation of equivalent-single-layer and layerwise theories of composite laminates," *Composite Structures,* 25, 21-35.

Sun, C. T., Achenbach, J. D., and Herrmann, G. [1968] "Continuum theory for a laminated medium," *J. Appl. Mech.,* Vol. 35, 467-475.

Tiersten, H. F., and Jahanmir, M. [1977] "A theory of composites modeled as interpenetrating solid continua," *Arch. Rational Mech. Anal.,* Vol. 65, 153-192.

Truesdell, C., and Toupin, R. A. [1960] The Classical Field Theories, in S. Flugge's *Handbuch der Physik,* Vol. III/1 (S. Flugge, ed.), Springer-Verlag, Berlin, 226-793.

Wang, A. S. D., and Crossman, F. W. [1977] "Some new results on edge effect in symmetric composite laminates," *J. Comp. Mater.,* Vol. 11.

Wang. S. S., and Choi, I. [1982] "Boundary-layer effects in composite laminates: Part 1 — Free-edge singularities," *J. Appl. Mech.,* Vol. 49, p. 541.

Wang. S. S., and Choi, I. [1982] "Boundary-layer effects in composite laminates: Part 2 — Free-edge stress solutions and basic characteristics," *J. Appl. Mech.,* Vol. 49/549.

Whitney, J. M. [1987] *Structural Analysis of laminated anisotropic plates,* Technion Publishing Co., Lancaster.

Whitney, J. M., Pagano, N. J. [1970] "Shear deformation in heterogeneous anisotropic plates," *J. Appl. Mech. 37,* 1031.

Yancey, R. N., and Pindera, M. J. [1988] "Micromechanical analysis of time-dependent

response of unidirectional composites," in *Recent Advances in the Macro- and Micro-Mechanics of Composite Materials Structures* (D. Hui and J. R. Vinson, eds.), ASME, New York.